CERN-TH.7011/93
DTP/93/74

On Colour Rearrangement in Hadronic W^+W^- Events

Torbjörn Sjöstrand

Theory Division, CERN
CH-1211 Geneva 23, Switzerland

and

Valery A. Khoze

Department of Physics, University of Durham
Durham DH1 3LE, England

Abstract

We discuss the possibility of colour rearrangement in $e^+e^- \to W^+W^- \to q_1\overline{q}_2q_3\overline{q}_4$ events, i.e. that the original colour singlets $q_1\overline{q}_2$ and $q_3\overline{q}_4$ may be transmuted, for instance, into new singlets $q_1\overline{q}_4$ and $q_3\overline{q}_2$. The effects on event properties could be quite large if such a rearrangement would occur instantaneously, so that gluon emission would be restricted to each of the new singlets separately. We argue that such a scenario is unlikely for two reasons. Firstly, the W^+ and W^- usually decay at separate times after the W^+W^- production, which leads to large relative phases for energetic radiation off the two constituents of a rearranged system, and a corresponding dampening of the QCD cascades. Secondly, within the perturbative scenario the colour transmutation appears only in order α_s^2 and is colour-suppressed. Colour reconnection at longer time scales is quite feasible, however, and may affect the fragmentation phase. If so, the nature of non-perturbative QCD can be probed in a new way. We formulate several alternative toy models and use these to estimate the colour reconnection probability as a function of the event kinematics. Possible consequences for LEP 2 events are illustrated, with special attention to systematic errors in W mass determinations.

CERN-TH.7011/93
October 1993

1 Introduction

Consider the production of several colour singlet particles, which decay to coloured partons close to each other in space and time. A topical example, which will be used as a basis for the continued discussion, is

$$e^+e^- \to W^+W^- \to q_1\overline{q}_2\, q_3\overline{q}_4 \tag{1}$$

at LEP 2. The outgoing partons first undergo a perturbative phase, in which showers of additional partons develop, and subsequently a non-perturbative phase, in which the partons fragment into a hadronic final state. In this paper we will study the extent to which the showering and fragmentation of one singlet can 'interfere' with that of the other, in such a way that observable event properties are affected. This is a topic about which little is known today, but which has the potential to provide new insights, as we shall try to show.

Since perturbative QCD is reasonably well understood, it is possible to predict with some confidence what to expect on the partonic level. We will here demonstrate that within the purely perturbative scenario these interference effects should be negligibly small. However, non-perturbative QCD is not yet well understood, and there is no obvious reason why interference effects should be small in the fragmentation process. It is therefore in this area that process (1) can be a very useful probe. We will develop and compare the predictions of two main alternative models, which correspond to two different hypotheses on the structure of the QCD vacuum and of the confinement mechanism. With a lot of hard work and some luck, LEP 2 could be in a position to provide some discrimination.

To illustrate what we mean by 'interference', consider process (1) above. The standard point of view is to assume the W^+ and W^- decays to be independent of each other. Apart from some spin-related correlations in the angular distribution of the W-decay products, each W system can then shower and fragment without any reference to what is happening to the other. In particular, the perturbative parton emission is initiated by two separate colour dipoles, $q_1\overline{q}_2$ and $q_3\overline{q}_4$. This picture should be valid if the W's are long-lived, so that the two W decays occur at well-separated points. In the other extreme, the W's are assumed to decay 'instantaneously', so that the process really involves the production of a $q_1\overline{q}_2q_3\overline{q}_4$ state in a single point. This state forms one single colour quadrupole, and it is the quadrupole as a whole that can emit additional partons and eventually fragment to hadrons. No trace is left of the individual identities of the W^+ and W^- decay products.

It is very difficult to obtain a complete description along the latter lines — all the standard methods of dealing with the showering and fragmentation processes would be of little use. (The matrix element calculation approach would still be valid, but more difficult to apply.) However, our experience with perturbative QCD in $q\overline{q}g$ events has taught us that a colour quadrupole can be well approximated by the sum of two separate colour dipoles, each of which is a net colour singlet. (There may also be contributions from non-singlet dipoles, see below.) The new aspect is that we here have two sets of such potential dipoles, the original one, i.e. $q_1\overline{q}_2$ and $q_3\overline{q}_4$, and a colour rearranged set, $q_1\overline{q}_4$ and $q_3\overline{q}_2$.

The possibility of having events with rearranged colour dipoles was first studied by Gustafson, Pettersson and Zerwas (GPZ) [1]. Since they assume that the dipole mass sets the scale for the amount of energetic gluon radiation and multiple soft particle production to be expected, event properties may change a lot if the original dipoles are replaced by the rearranged ones. The original dipoles each have the W mass, while the rearranged

ones may have much lower masses, if the kinematics is selected suitably. GPZ could therefore present large differences in the total multiplicity, the energy flow, the rapidity distribution, and so on.

Unfortunately, this is not a very likely scenario. As we will show, the separation between the W^+ and W^- decay vertices is large enough that energetic QCD radiation will occur independently within each original dipole, to a good first approximation. However, the fragmentation process is extending much further in space and time, and thus colour reconnection in this phase is a possibility. Observable event properties are less affected by a reconnection that comes only after the perturbative phase [2], but this does not necessarily mean that effects are negligibly small. Detailed studies of event shapes should help reveal the nature and size of colour rearrangement phenomena.

While interference effects are interesting in their own right, if there, they may also provide a serious source of uncertainty. One of the main objectives of LEP 2 will be to determine the W mass. This could either be done by a threshold scan of the cross section, or by a reconstruction of W masses event by event for some fixed energy above the W^+W^- threshold. Currently the latter approach is the favoured one [3]. Fully hadronic decays, i.e. process (1), would seem to be preferable: jet energies need not be so well measured in the calorimeters, since already a knowledge of the four jet directions would be enough to constrain the kinematics and therefore the W masses. Electroweak effects, including initial state radiation, and effects of semileptonic c decays would be under control. By contrast, purely leptonic or mixed leptonic–hadronic decays suffer from a large missing momentum vector given by the neutrino(s).

The main problem is that the assignment of hadrons to either of the two W's is not unique. If only an experimental issue, the smearing could be estimated and corrected for. However, to this we now add an uncertainty in the colour structure of the event. So long as the original $q_1\overline{q}_2$ and $q_3\overline{q}_4$ dipoles shower and fragment independently of each other, the invariant masses of the hadrons belonging to these two systems, if separated correctly, add up to give the original W^+ and W^- masses, respectively. But if a reconnection occurs, e.g. to the alternative colour singlets $q_1\overline{q}_4$ and $q_3\overline{q}_2$ (or even more complicated systems), there is no concept of a conserved W mass in the fragmentation. This introduces an additional element of smearing and, more dangerously, the potentiality for a systematic bias in the W mass determination. Clearly, such effects must be studied and understood, in order to be corrected for.

The possibility of colour rearrangements is not restricted to $e^+e^- \to W^+W^-$ events. Other examples could have been found: $pp/p\overline{p} \to W^+W^-$, $e^+e^- \to Z^0Z^0$, $e^+e^- \to Z^0H^0$, $pp/p\overline{p} \to W^\pm H^0$, $H^0 \to W^+W^-$, $t\overline{t} \to bW^+\overline{b}W^-$, etc. One could also add processes that involve a single colour singlet particle interfering with the beam jets of a pp event, such as $pp \to W^\pm$, or even interactions among beam jets themselves, such as in multiple parton–parton interaction events or in heavy ion collisions. The problem with the latter processes is that there are so many other uncertainties that any chance of systematic studies would be excluded. By contrast, in $e^+e^- \to W^+W^-$ events, the decay of a non-interfering W pair is very well understood, thanks to our experience with Z^0 decays at LEP 1.

The hadronic decay of a B meson is another typical example of a colour quadrupole structure. J/ψ production in such decays is the one place where colour reconnection has already been observed (see discussion and additional references in ref. [1]): in a $b \to c + W^- \to c + \overline{c} + s$ decay the c and $\overline{c}$ belong to separate colour singlets, but appear almost simultaneously and can therefore coherently form a colour singlet state such as the J/ψ. Of course, the number of colours not being infinite, there is a finite chance

of $1/N_C^2 = 1/9$ that the c and $\overline{\mathrm{c}}$ are in a colour singlet configuration. However, this kind of accidental colour ambiguities is not what we imply by colour rearrangement — after all, had the W been a long-lived particle, so that the c and $\overline{\mathrm{c}}$ were produced far away, the question of whether they are in a relative octet or singlet state would have been moot. (Accidental ambiguities do not spoil the original colour singlet combinations, such as $\overline{\mathrm{c}} + \mathrm{s}$, but only add more.) Further, while difficult to estimate, it seems that the colour reconnection probability in B decay is more like 20%, i.e. higher than the above maximum. In this paper we will therefore concentrate on dynamical models for colour rearrangement, and leave aside the accidental possibility. Anyway, one should not use the details of $\mathrm{B} \to \mathrm{J}/\psi$ phenomenology to provide any specific input for $\mathrm{W}^+\mathrm{W}^-$ production, since the space–time evolution and the capability to radiate energetic gluons are rather different in the two processes.

To summarize, there are two main reasons to study the phenomenon of colour rearrangement:

1. In its own right, since it provides a laboratory for a better understanding of the space–time structure of perturbative and non-perturbative QCD.
2. As a potential source of error to W mass determinations and other measurements. (In the end, the precision of the theoretical predictions has to match the experimental accuracy, or even exceed it.)

We cannot today predict what will come out of experimental studies at LEP 2, but want to provide here some comments on what one could plausibly expect under some simplified alternative scenarios. This might form a reasonable starting point for more refined theoretical and experimental studies in the future.

The plan of the paper is therefore as follows. In section 2 we show what maximal effects could be expected if colour rearrangement always took place, either 'instantaneously' or only later, between the parton shower and the fragmentation phases. These 'worst case' or 'best case' scenarios, depending on the point of view, are subsequently rejected in favour of more realistic ones. In Section 3 we show why one would not expect sizeable effects on the perturbative level, based on the time separation between the W^+ and W^- decays, and on colour algebra. The subsequent discussion is therefore concentrated on effects in the fragmentation process: in Section 4 we describe different ways of estimating the colour rearrangement probability as a function of event topology, and in Section 5 some experimental consequences are discussed. Finally, Section 6 contains a summary and outlook.

2 Maximal effects of colour reconnection

The objective of this section is purely didactic: to familiarize readers with possible experimental consequences of colour rearrangements. Our 'best bet' estimates of such effects will be presented in Section 5. The current section is here mainly because it is needed to appreciate the significance of Sections 3 and 4. The naïve scenarios we introduce here should be taken for what they are: extremely simple recipes for colour reconnection, in which a number of known complications are swept under the carpet. In particular, the W^+ and W^- are assumed to decay instantaneously, so that there is no space or time separation between the two decay vertices.

In order to stay as close as possible to the studies of GPZ, we first consider two W bosons produced at rest, each with the nominal mass $m_{\mathrm{W}} = 80$ GeV, decaying into the

final state $u\overline{d} + d\overline{u}$, with an opening angle of 30° between u and $\overline{u}$, Fig. 1a. To first approximation, one may then entertain three alternatives:

1. In the no-reconnection scenario, the $u\overline{d}$ and $d\overline{u}$ systems shower and fragment independently of each other, Fig. 1b. The event therefore looks like two overlayed e^+e^- annihilation events at rest, each with 80 GeV c.m. energy. This scenario is just what one expects from an extreme perturbative point of view.
2. In the GPZ 'instantaneous' reconnection scenario, two colour singlets $u\overline{u}$ and $d\overline{d}$ are immediately formed, each then having an invariant mass of 20.7 GeV and a net motion away from the origin. These systems subsequently shower and fragment independently of each other, Fig. 1c. There is only little radiation, since the maximum scale for that radiation is 20 GeV rather than 80 GeV. The final event looks like two strongly boosted 20 GeV e^+e^- annihilation events. We do not know of any physics mechanism that would lead to this scenario (except maybe as a rare fluctuation), but include it since it was advocated by GPZ and since it gives maximal effects.
3. In the intermediate reconnection scenario, a reconnection occurs between the shower and fragmentation steps. Therefore the original $u\overline{d}$ and $d\overline{u}$ colour singlet systems shower, each with maximum virtuality 80 GeV, just as in the no-reconnection scenario. Stricty speaking, the gluons emitted in the $u\overline{d}$ system are not uniquely associated to either the u or the $\overline{d}$. However, in practice, the shower algorithm used [4] does allow a pragmatic subdivision of the radiation into two subsets, essentially (but not quite) by hemisphere. For instance, if partons are ordered in colour/string/dipole order, a W^+ (W^-) branching to $ug_1^+g_2^+g_3^+\overline{d}$ ($dg_1^-g_2^-g_3^-g_4^-\overline{u}$) may be split into two subsets ug_1^+ and $g_2^+g_3^+\overline{d}$ ($dg_1^-g_2^-g_3^-$ and $g_4^-\overline{u}$). After the showers, the partons can therefore be reconnected into two new colour singlets, $ug_1^+g_4^-\overline{u}$ and $dg_1^-g_2^-g_3^-g_2^+g_3^+\overline{d}$. Each of these systems then fragments separately, Fig. 1d. In the limit $\alpha_s \to 0$, i.e. when energetic QCD radiation is switched off, this coincides with the instantaneous scenario. In practice, however, QCD radiation is profuse, and the masses of the two fragmenting systems is substantially above the 20 GeV nominal value.

Fragmentation is assumed to be given according to the Lund string model [5] (see also Section 4.1). Events are generated with the JETSET 7.3 program [6], which is known to well describe the $e^+e^- \to q\overline{q}$ events in the 10–100 GeV mass range.

Some simple results are presented in Fig. 2. The event axis (with respect to which e.g. rapidity is defined) is here the theoretical one, i.e. intermediate between the original u and $\overline{u}$ directions. The total multiplicity is about a factor of 2 lower for the instantaneous reconnection scenario: $\langle n_{\mathrm{ch}} \rangle = 21.8$ versus 40.0 for no reconnection and 37.8 for the intermediate one. The first number reflects the lower invariant mass of the colour singlet systems. The instantaneous scenario contains two strongly boosted systems with nothing in between; therefore the rapidity distribution has a very strong dip in the middle, Fig. 2b, which is reflected in the multiplicity distribution for the central rapidity region, $|y| < 1$, Fig. 2c. It is also visible in the charged particle flow in the event plane, Fig. 2d, where particle production at around 90° to the event axis is suppressed. It is maybe a bit more surprising that the instantaneous scenario does not have more particle production than the no-reconnection one at 0°; after all, this is the region where a string connects the u (d) and $\overline{u}$ ($\overline{d}$) partons of the instantaneous events, while no such string is present in the no-reconnection ones. Our interpretation is that this shows how large the effects of QCD radiation are, i.e. that radiation with an 80 GeV maximum virtuality scale leads to an overwhelmingly large broadening of jet profiles.

In all the distributions, the intermediate scenario deviates much less from the standard one than does the instantaneous. This means that the particle flow is to a large extent dominated by the perturbative gluon emission phase, at least when this phase is assumed to be valid down to a cut-off scale of $Q_0 \approx 1$ GeV and gluon emission is therefore profuse. However, the effects of the intermediate scenario seem puny only when compared with the instantaneous one: the differences between the no- and intermediate-reconnection distributions of Fig. 2b (e.g.) would be easily distinguishable experimentally.

The problem is that the kinematics we have considered so far is totally unrealistic. While effects are largest when the two W's are produced at rest, this is the point where the phase space for production is vanishing. Next we therefore have to introduce some semi-realistic experimental conditions.

In order to generate complete $\mathrm{e^+e^-} \to \mathrm{W^+W^-} \to \mathrm{q_1\overline{q}_2q_3\overline{q}_4}$ events, we use the PYTHIA 5.6 event generator [7]. The $\mathrm{W^+W^-}$ pair is here distributed according to the product of three terms: a Breit-Wigner for each W, and a basic $\mathrm{e^+e^-} \to \mathrm{W^+W^-}$ matrix element (which is a function of the actual $\mathrm{W^\pm}$ masses) [8]. Subsequently each W decays to a $\mathrm{q\overline{q}}$ pair, $\mathrm{u\overline{d}}$, $\mathrm{u\overline{s}}$, $\mathrm{c\overline{d}}$, $\mathrm{c\overline{s}}$ or their charge conjugates. The decay angles are properly correlated [9]. This is followed by perturbative parton shower evolution and non-perturbative fragmentation, as above. Initial state photon radiation can and should also be included for detailed experimental studies, but is omitted for most of the studies below.

To illustrate the size of the effects, consider a c.m. energy of 170 GeV, i.e. some distance above the threshold. The nominal input W mass is 80 GeV; the average generated m_{W} is somewhat lower, predominantly because of phase-space effects.The charged multiplicity distribution is shown in Fig. 3a for the scenarios 1–3 above. Clearly differences are nowhere as drastic as in Fig. 2a: the average values are 36.6 without recoupling, 36.2 with intermediate, and 33.7 with instantaneous recoupling. In part this is related to an averaging over various event topologies in Fig. 3, where Fig. 2 was only for one particularly favourable configuration. In part one also expects smaller differences further away above threshold, since the difference in mass between original and reconnected colour systems is reduced. The latter effect is particularly easy to understand if one considers the region far above threshold, where the two W's and their respective decay products are strongly boosted away from each other, and a reconnection between the two widely separated systems in fact leads to an increase in system masses, i.e. opposite to the threshold behaviour.

The charged rapidity distribution with respect to the thrust axis, Fig. 3b, and the number of charged particles in $|y| < 1$, Fig. 3c, also show much lesser differences than those observed in Figs. 2b and 2c. In particular, the change in kinematics leads to a much narrower central rapidity dip. Qualitatively, however, differences are still there. This is particularly obvious in the low-multiplicity part of Fig. 3c. Differences can be enhanced by various cuts, e.g. by requiring a large thrust value.

As a final exercise, we study the task of W mass determination. This is an important topic in itself [3], and it is not our intention here to optimize an algorithm so as to minimize statistical errors. Rather, the objective is to find whether any systematic effects arise from reconnections.

The details of our W mass reconstruction algorithm will be presented in Section 5.3. For the moment, suffice it to say that four jets are reconstructed per event (events without a clear four-jet structure are rejected), assuming that particle four-momenta are fully known. The jets are paired to give two W masses, which are then averaged to give one $\overline{m}_{\mathrm{W}} = (m_{\mathrm{W^+}} + m_{\mathrm{W^-}})/2$ number per event. The difference between the reconstructed

and the generated $\overline{m}_{\mathrm{W}}$ is shown in Fig. 3d. By the procedure adopted, the distributions thus do not contain any spread from the intrinsic Breit-Wigner shape of the W's or from detector imperfections. Any spread comes from misassignments of particles to jets. Large deviations may occur when entire subjets are incorrectly clustered.

If one considers the range ± 10 GeV of difference between reconstructed and generated masses, the average and spread is -0.28 ± 1.57 GeV for the no-reconnection scenario, -0.14 ± 1.60 GeV for the intermediate one, and 0.30 ± 1.55 GeV for the instantaneous one. The fraction of W's with deviations larger than ± 10 GeV is 1.5%, 1.5% and 1.7%, respectively. Compared with the no-reconnection scenario, the intermediate (instantaneous) one gives a systematic shift of over 100 (500) MeV. The aimed-for statistical error on the W mass is roughly 50 MeV. It is therefore of importance to understand whether these colour reconnection numbers above have to be included as a systematical uncertainty, or whether reconnection effects are only a small fraction of this.

3 The perturbative picture of colour rearrangement

In this section we want to discuss the colour dynamics of particle flow in $\mathrm{W}^+\mathrm{W}^-$ events from a purely perturbative point of view. The non-perturbative standpoint will follow in Section 4.

3.1 Introduction to the perturbative approach

During the last years experiments, especially at the Z^0 pole, have provided an exceedingly rich source of information on the jet structure of final states in hard processes (see e.g. ref. [10]). These data have shown that, at high energies, the main characteristics of multihadronic events are determined by the perturbative stage of the process evolution. Analytical perturbation theory — the perturbative approach [11] — provides a quantitative description of inclusive particle production in jets. In the perturbative approach the resummation of the perturbative series is performed, and the terms of relative order $\sqrt{\alpha_s}$ are taken into account in a systematic way — the modified leading logarithmic approximation (MLLA). Under the key assumption that the non-perturbative hadronization process is local in the configuration space of partons, the infrared singularities can be factorized out of hadron distributions. If so, the asymptotic shapes of these distributions are fully predicted — the hypothesis of local parton–hadron duality (LPHD). Data agree remarkably well with the predictions of the MLLA–LPHD framework [12].

Until now, the perturbative approach was applied only to systems of partons produced almost simultaneously, with a short time scale

$$t_{\mathrm{prod}} \sim \frac{1}{E} \ll \frac{1}{\mu} \, , \tag{2}$$

where E is the hard scale of the production process and $\mu^{-1} \approx 1$ fm is the characteristic strong interaction time scale. The radiation accompanying such a system can be represented as a superposition of gauge invariant terms, in which each external quark line is uniquely connected to an external antiquark line of the same colour. The description of gluons is straightforward: remember that a gluon has both a quark and an antiquark colour index. The system is thus decomposed into a set of colourless $\mathrm{q\overline{q}}$ antennae (dipoles). One of the simplest examples is the celebrated $\mathrm{q\overline{q}g}$ system, which (to

leading order in $1/N_C^2$) is well approximated by the sum of two separate antennae/dipoles. The perturbative treatment of the $q\overline{q}$ antennae is based on the following key ideas:

1. The principal source of multiple hadroproduction is gluon bremsstrahlung caused by conserved colour currents. Therefore the flow of colour quantum numbers, reflecting the dynamics at short distances, controls the particle distributions in the final state.
2. The evolution of a quark jet is viewed as a sequence of coherent parton branchings. In the final state, an original quark jet is enshrouded by secondary partons resulting from radiation of quasi-collinear and/or soft gluons with momenta k and transverse momenta $k_\perp$ in the range
$$\mu \lesssim k_\perp \ll k \ll E \ . \tag{3}$$
It is the large probability for such emissions,
$$\mathcal{W} \sim \frac{\alpha_s}{\pi} \ln^2 E \sim 1 \tag{4}$$
that leads to the well-known double logarithmic phenomena in jet development.

In this approach, the particle multiplicity is obtained as the convolution of the probability of primary gluon bremstrahlung off the parent quarks with the multiplicity initiated by such a gluon [11].

Any restriction on the primary gluon energy to be well below E
$$k \lesssim k_{\max} \ll E \tag{5}$$
drastically reduces the perturbatively induced multiplicity and makes the $q\overline{q}$ antenna practically inactive [11, 13]. As we shall see, this is of relevance for colour rearranged systems in W^+W^- events.

3.2 W-pair decays in the perturbative approach

Encouraged by the successes of the perturbative approach, one could be tempted to apply the same quark–gluon dynamics to the description of the final state in process (1). In particular, each individual $W^\pm$ decay corresponds to a parton shower at almost the same scale as the well-studied $Z^0 \to q\overline{q}$ case.

As we shall show, the emission of a single primary gluon (which subsequently initiates a coherent parton shower) corresponds to the no-reconnection scenario. Within the perturbative approach, colour transmutations can result only from the interferences between gluons (virtual as well as real) radiated in the two decays. Rearrangements of the colour flows should lead to a dependence of the structure of final particle distributions on the relative angles between the jets originating from the different W's (on top of what may be there from trivial kinematics).

It is the goal of this section to demonstrate why the colour reconnection effects, viewed perturbatively, are strongly suppressed. Our argumentation below is based on two main reasons, which are deeply rooted in the basic structure of QCD:

1. Because of the group structure of QCD, at least two gluons should be emitted to generate the colour rearrangement. Moreover the interference piece proves to be suppressed by $1/N_C^2$ as compared to the $\mathcal{O}(\alpha_s^2)$ no-reconnection emissions.
2. The effects of the W width Γ_W strongly restrict the energy range of primary gluons generated by the alternative systems of type $q_1\overline{q}_4$ and $q_3\overline{q}_2$. Not so far from the W^+W^- threshold one expects
$$k \lesssim k_{\max}^{\text{recon}} \sim \Gamma_W \ . \tag{6}$$

Therefore the would-be parton showers initiated by such systems are terminated at a virtuality scale of $\mathcal{O}(\Gamma_{\rm W})$, and can hardly lead to sizeable fluctuations in the structure of the hadronic final state.

3.3 Single-gluon emission in W pair decays

Let us first consider the emission of a single primary soft gluon of four-momentum k, see Fig. 4. The momenta of the final state quarks are labelled by $\mathrm{e^+e^-} \to \mathrm{q_1}(p_1)\,\overline{\mathrm{q}}_2(p_2)\,\mathrm{q_3}(p_3)\,\overline{\mathrm{q}}_4(p_4)$, with $Q_1 = p_1 + p_2$ and $Q_2 = p_3 + p_4$. Denote by $\widehat{M}^{(0)}$ the non-radiative Feynman amplitude with the W propagators removed and introduce the conserved currents $J^\mu(k)$, $J'^\mu(k)$ generated by the individual W decays. In the limit $k \ll p_i$ the amplitude $M^{(1)}$ for gluon radiation accompanying process (1) is then

$$M^{(1)} \equiv (M^{(1)})^{in}_{jm} = g_s\,\widehat{M}^{(0)}\,\left[(T^a)^i_j\,\delta^n_m\,(J(k)\cdot\epsilon_\lambda) + \delta^i_j\,(T^a)^n_m\,(J'(k)\cdot\epsilon_\lambda)\right]\ , \tag{7}$$

where g_s is related to the strong coupling constant by $\alpha_s = g_s^2/4\pi$, ϵ_λ is the gluon polarization vector, T^a are the **SU(3)** colour matrices, and $a = 1,\ldots,8$ and $i,j,m,n = 1,2,3$ are colour labels.

The $\mathrm{W}^\pm$ propagator functions D are absorbed into the definition of the currents $J^\mu(k)$, $J'^\mu(k)$ [14]

$$\begin{aligned} J^\mu(k) &= j^\mu(k)\,D(Q_1+k)\,D(Q_2)\ , \\ J'^\mu(k) &= j'^\mu(k)\,D(Q_1)\,D(Q_2+k)\ , \end{aligned} \tag{8}$$

where

$$\begin{aligned} j^\mu(k) &= \frac{p_1^\mu}{p_1\cdot k} - \frac{p_2^\mu}{p_2\cdot k}\ , \\ j'^\mu(k) &= \frac{p_3^\mu}{p_3\cdot k} - \frac{p_4^\mu}{p_4\cdot k} \end{aligned} \tag{9}$$

describe the gauge-invariant soft gluon emission from two colour charges of momenta p_1, p_2 (p_3, p_4). The expression for the propagator function is

$$D(Q) = \frac{1}{Q^2 - m_{\rm W}^2 + i m_{\rm W}\Gamma_{\rm W}}\ . \tag{10}$$

To emphasize that the emission is generated primarily by the conserved currents j^μ, j'^μ we have introduced the 'radiative blobs' in Fig. 4 and in what follows.

In order to obtain the differential distribution for gluon emission we have to square the matrix element, sum over colours and spins, and integrate over the Q_1^2 and Q_2^2 virtualities. We find (see also [13, 14])

$$\frac{1}{\sigma^{(0)}}\,\mathrm{d}\sigma^{(1)} = \frac{\mathrm{d}^3k}{\omega}\,\frac{C_F\,\alpha_s}{4\pi^2}\,\mathcal{F}^{(1)}\ , \tag{11}$$

$$\mathcal{F}^{(1)} = \left(\frac{m_{\rm W}\Gamma_{\rm W}}{\pi}\right)^2 \int \mathrm{d}Q_1^2\,\mathrm{d}Q_2^2\,\left[-J\cdot J^\dagger - J'\cdot J'^\dagger\right]\ , \tag{12}$$

where $\omega = k^0$ is the gluon energy and $C_F = (N_C^2-1)/2N_C = 4/3$.

In the massless quark limit the radiation pattern $\mathcal{F}^{(1)}$ is given by

$$\mathcal{F}^{(1)} = 2\,(\widehat{12} + \widehat{34})\ , \tag{13}$$

where the $\mathrm{q\overline{q}}$ 'antennae' are defined by [11]

$$\widehat{ij} = \frac{(p_i \cdot p_j)}{(p_i \cdot k)(p_j \cdot k)}\ . \tag{14}$$

Near threshold, where the decay products of a W are almost back-to-back,

$$\begin{aligned}\mathcal{F}^{(1)} &= \frac{2}{\omega^2}\,\left(\frac{1-\cos\theta_{12}}{(1-\cos\theta_1)(1-\cos\theta_2)} + \frac{1-\cos\theta_{34}}{(1-\cos\theta_3)(1-\cos\theta_4)}\right) \\ &\approx \frac{4}{\omega^2}\,\left(\frac{1}{\sin^2\theta_1} + \frac{1}{\sin^2\theta_3}\right)\ ,\end{aligned} \tag{15}$$

where θ_i is the angle between parton i and the gluon, and θ_{ij} the angle between partons i and j.

Let us emphasize that on the level of single gluon emission, real as well as virtual, the two antennae $\mathrm{q_1\overline{q}_2}$ and $\mathrm{q_3\overline{q}_4}$ do not interact and the colour flows are not rearranged. The absence of such an interaction is easily seen from the diagram of Fig. 5, which represents the decay–decay radiative interference contribution to the cross section of process (1). At the position of the vertical dashed line, both the $\mathrm{q_1\overline{q}_2}$ and the $\mathrm{q_3\overline{q}_4}$ subsystems have to be in colour singlet states (in order to couple to the W's), so the gluon octet charge is uncompensated.

3.4 Double-gluon interference effects in W-pair decays

At least two primary gluons, real or virtual, should be emitted to generate a colour flow rearrangement, see Figs. 6–8. Note that the diagrams of Figs. 6a and 6b do not interfere with each other, and that the diagrams of Fig. 7 could interfere with those of Fig. 4, thus inducing a colour transmutation. The infrared divergences in the virtual pieces are cancelled by the corresponding real emissions. For the case of decay–decay radiative interference the soft emissions are cancelled in the inclusive cross section up to at least $\mathcal{O}(\Gamma_{\mathrm{W}}/m_{\mathrm{W}})$ (see [15, 16] and below).

The main qualitative results for the reconnection effects appearing in $\mathcal{O}(\alpha_s^2)$ are not much different for various decay–decay interference samples. We shall examine below one example corresponding to the diagrams of Fig. 6a. In the limit $k_1, k_2 \ll p_i$ the matrix element can be written as

$$\begin{aligned}M_a^{(2)} = g_s^2\,\widehat{M}^{(0)}\ \Big[&(T^a)^i_j\,(T^b)^n_m\,(j(k_1)\cdot\epsilon^{(1)}_\lambda)\,(j'(k_2)\cdot\epsilon^{(2)}_{\lambda'})\,D(Q_1+k_1)\,D(Q_2+k_2) \\ &+ \left\{a \leftrightarrow b, k_1 \leftrightarrow k_2, \epsilon^{(1)}_\lambda \leftrightarrow \epsilon^{(2)}_{\lambda'}\right\}\Big]\ ,\end{aligned} \tag{16}$$

where $k_{1,2}$ are the momenta of the soft gluons and $\epsilon^{(1)}_\lambda$, $\epsilon^{(2)}_{\lambda'}$ are their polarization vectors.

After summing over colours and spins, the interference term may be presented in the form

$$\frac{1}{\sigma_0}\,\mathrm{d}\sigma_a^{\mathrm{int}} \simeq \frac{\mathrm{d}^3k_1}{\omega_1}\,\frac{\mathrm{d}^3k_2}{\omega_2}\,\left(\frac{C_F\,\alpha_s}{4\pi^2}\right)^2\,\frac{1}{N_C^2-1}\,\frac{1}{2}\,\mathcal{F}_a^{\mathrm{int}}\ , \tag{17}$$

$$\mathcal{F}_a^{\mathrm{int}} = 2\,\chi_{12}\,(j(k_1)\cdot j'(k_1))\,(j(k_2)\cdot j'(k_2))\ , \tag{18}$$

with

$$-(j(k)\cdot j'(k)) = \widehat{14} + \widehat{23} - \widehat{13} - \widehat{24} \ . \tag{19}$$

Here χ_{12} is the so-called profile function [13, 14], which controls the decay–decay interferences:

$$\chi_{12} = \left(\frac{m_{\rm W}\Gamma_{\rm W}}{\pi}\right)^2 \ \Re \int {\rm d}Q_1^2\, {\rm d}Q_2^2\, D(Q_1+k_1)\, D^*(Q_1+k_2)\, D(Q_2+k_2)\, D^*(Q_2+k_1) \ , \tag{20}$$

where D^* is the complex conjugate of D and $\Re$ represents the real part. The profile function has the formal property that $\chi_{12} \to 0$ as $\Gamma_{\rm W} \to 0$ and $\chi_{12} \to 1$ as $\Gamma \to \infty$.

The interference is suppressed by $1/(N_C^2-1) = 1/8$ as compared to the total rate of double primary gluon emissions (related to the square of diagrams of the type of Fig. 6), see eq. (17). This is a result of the ratio of the corresponding colour traces,

$$\frac{{\rm Tr}(T^aT^b)\cdot{\rm Tr}(T^aT^b)}{{\rm Tr}(T^aT^a)\cdot{\rm Tr}(T^bT^b)} = \frac{(C_F\,N_C)/2}{(C_F\,N_C)^2} = \frac{1}{N_C^2-1}. \tag{21}$$

Such a suppression takes place for any decay–decay radiative interference piece, real as well as virtual, as is clear from Fig. 8.

Near threshold and in the limit of massless quarks the interference contribution to the radiation pattern is

$$\mathcal{F}_a^{\rm int} = \frac{2\,\chi_{12}}{\omega_1^2\,\omega_2^2}\ \frac{16\,\cos\phi_{13}\,\cos\tilde{\phi}_{13}}{\sin\theta_1\,\sin\theta_3\,\sin\tilde{\theta}_1\,\sin\tilde{\theta}_3} \ , \tag{22}$$

where θ_i ($\tilde{\theta}_i$) is the angle between the q_i and the gluon k_1 (k_2), and ϕ_{13} ($\tilde{\phi}_{13}$) is the relative azimuth between q_1 and q_3 around the direction of the k_1 (k_2). The expression in eq. (22) evidently contains a dependence on the relative orientation of the decay products of the two W's. (The interference is maximal when all the partons lie in the same plane, $\phi_{13} = \tilde{\phi}_{13} = 0$, cf. eqs. (15) and (22).) Therefore one might expect that the decay–decay interferences would induce some colour-suppressed reconnection effects in the structure of final states in process (1).

3.5 W width effects

It is the profile function χ_{12} that cuts down the phase space available for gluon emissions by the alternative quark pairs (or by any accidental colour singlets) and thus eliminates the very possibility for the reconnected systems to develop QCD cascades. That the W width does control the radiative interferences can be easily understood by considering the extreme cases.

If the W-boson lifetime could be considered as very short, $1/\Gamma_{\rm W} \to 0$, both the $\mathrm{q}_1\overline{\mathrm{q}}_2$ and $\mathrm{q}_3\overline{\mathrm{q}}_4$ pairs appear almost instantaneously, and they radiate coherently, as though produced at the same vertex. In the other extreme, $\Gamma_{\rm W} \to 0$, the $\mathrm{q}_1\overline{\mathrm{q}}_2$ and $\mathrm{q}_3\overline{\mathrm{q}}_4$ pairs appear at very different times t_1, t_2 after the $\mathrm{W}^+\mathrm{W}^-$ production,

$$t_{\rm prod} \sim \frac{1}{m_{\rm W}} \ll \Delta t = |t_1 - t_2| \sim \frac{1}{\Gamma_{\rm W}} \ . \tag{23}$$

The two dipoles therefore radiate gluons and produce hadrons according to the no-reconnection scenario.

The crucial point is the proper choice of the scale the W width should be compared with. That scale is set by the energies of primary emissions, real or virtual [13, 14, 15]. Let us clarify this supposing, for simplicity, that we are in the W^+W^- threshold region. The relative phases of radiation accompanying two W decays are then given by the quantity

$$\omega_i \, \Delta t \sim \frac{\omega_i}{\Gamma_W} \ . \tag{24}$$

When $\omega_i/\Gamma_W \gg 1$ the phases fluctuate wildly and the interference terms vanish. This is a direct consequence of the radiophysics of the colour flows [11] reflecting the wave dynamics of QCD. The argumentation remains valid for energies above the W^+W^- threshold as well. Suppression of the interference in the case of radiation with $\omega_i \gg \Gamma_W$ can be demonstrated also in a more formal way.

One can perform the integration over dQ_1^2 and dQ_2^2 in eq. (20) by taking the residues of the poles in the propagators. This gives

$$\chi_{12} = \frac{m_W^2 \Gamma_W^2 \, (\kappa_1 \kappa_2 + m_W^2 \Gamma_W^2)}{(\kappa_1^2 + m_W^2 \Gamma_W^2) \, (\kappa_2^2 + m_W^2 \Gamma_W^2)} \ , \tag{25}$$

with

$$\kappa_{1,2} = Q_{1,2} \cdot (k_1 - k_2) \ . \tag{26}$$

For the interference between the diagrams of Fig. 6b, the corresponding profile function is given by the same formula with $k_2 \to -k_2$. Near the W^+W^- pair threshold eq. (25) is reduced to

$$\chi_{12} = \frac{\Gamma_W^2}{\Gamma_W^2 + (\omega_1 - \omega_2)^2} \ . \tag{27}$$

From eq. (27) it is clear that only primary emissions with $\omega_{1,2} \lesssim \Gamma_W$ can induce significant rearrangement effects: the radiation of energetic gluons (real or virtual) with $\omega_{1,2} \gg \Gamma_W$ pushes the W propagators far off their non-radiative resonant positions, so that the propagator functions $D(Q_1 + k_1)$ and $D(Q_1 + k_2)$ ($D(Q_2 + k_1)$ and $D(Q_2 + k_2)$) corresponding to the same W practically do not overlap. We can neglect the contribution to the inclusive cross section from kinematical configurations with $\omega_1, \omega_2 \gg \Gamma_W$, $|\omega_1 - \omega_2| \lesssim \Gamma_W$ since the corresponding phase-space volume is negligibly small.

Equation (25) clearly shows that χ_{12} vanishes if any of the scalar products $Q_i \cdot k_j$ ($i, j = 1, 2$) well exceeds $m_W \Gamma_W$. Again accidental kinematics with $\kappa_1, \kappa_2 \ll m_W \Gamma_W$ is suppressed because of phase space reasons. Hence all our arguments concerning cutting down the QCD cascades induced by the alternative systems remain valid above the threshold as well. The smallness of the decay–decay radiative interference for energetic emission in the production of a heavy unstable particle pair, at the threshold and far above it, proves to be of a general nature. For the case of $e^+e^- \to bW^+\overline{b}W^-$ this was explicitly demonstrated in ref. [14].

At very high energies $E \gg m_W$ the energy scale of the would-be QCD showers generated by the alternative systems is restricted more strongly,

$$k_{\max}^{\mathrm{recon}} \sim \frac{\Gamma_W \, m_W}{E_W} \ . \tag{28}$$

Within the framework of a perturbative analysis such a restriction makes sense only if

$$\eta = \mu \, \frac{E_W}{m_W \, \Gamma_W} \lesssim 1 \ . \tag{29}$$

Remembering that the lifetime of a W in the laboratory frame is

$$t_{\rm dec} \sim \frac{E_{\rm W}}{m_{\rm W}} \frac{1}{\Gamma_{\rm W}} \tag{30}$$

one can easily see that as long as $\eta < 1$, the requirement of perturbative soft gluons $\omega > \mu$ automatically implies that a W decays before the formation of the first light hadrons from the QCD cascades.

In the extreme ultrarelativistic limit, when $\eta = \mu\, t_{\rm dec} \gg 1$, the energy of primary perturbative gluons becomes limited from below, $\omega > \mu\, \eta$. This restriction arises from the relationship between $t_{\rm dec}$ and the gluon hadronization time,

$$t_{\rm dec} < t_{\rm had} \sim \frac{\omega}{\mu^2} \ . \tag{31}$$

The profile function χ_{12} in such an extreme case decreases with increasing energy and the decay–decay radiative interference is strongly suppressed. For instance,

$$\begin{aligned} \chi_{12} \sim \left(\frac{\mu}{\omega}\right)^2 \frac{1}{\eta^2} < \frac{1}{\eta^4} \qquad & \text{for} \quad \mu\,\eta < \omega < \Gamma_{\rm W} \ , \\ \chi_{12} < \frac{m_{\rm W}^2}{E_{\rm W}^2} \qquad & \text{for} \quad \omega > \Gamma_{\rm W} \ . \end{aligned} \tag{32}$$

Therefore, in addition to the α_s^2 and $1/N_C^2$ suppression effects noted above, any reconnected quark system (including accidental colour singlets) proves to be practically inactive. The bulk of radiation (and thus of multihadron production) in the final state of process (1) is governed by the original $\mathrm{q}_1\overline{\mathrm{q}}_2$ and $\mathrm{q}_3\overline{\mathrm{q}}_4$ antennae, which radiate the primary gluons with $\omega \gg \Gamma_{\rm W}$ that initiate coherent showers. The corresponding hard scale for the non-reconnected parton showers is $m_{\rm W}$. Also accounting for cascade multiplication, the yield of the reconnection-sensitive particles can be quantified as the multiplicity at a hard scale of $\mathcal{O}(\Gamma_{\rm W})$.

All the argumentation based on the effects of a phase difference between the radiations accompanying two W decays remain valid also in the case when one of the W bosons is practically real and the other is far off the mass shell, i.e. $t_1 \sim 1/\Gamma_{\rm W}$ and $t_2 \sim 1/m_{\rm W}$. This case could be of interest for the intermediate mass Higgs decay [2]. The effects of the profile function χ_{12} are the same for $t_2 \ll t_1 \sim 1/\Gamma_{\rm W}$ as when $t_1, t_2 \sim 1/\Gamma_{\rm W}$.

3.6 Structure of inclusive particle flow in W-pair events

Let us discuss the general topology of events corresponding to process (1). The single-inclusive particle flow (antenna–dipole pattern) may be written as (see ref. [11] for details)

$$\frac{8\pi\,\mathrm{d}N}{\mathrm{d}\Omega_{\mathbf{n}}} = 2\,\left[(12)+(34)\right]\,N_{\rm q}'\left(\frac{m_{\rm W}}{2}\right) + R\,\left[(14)+(23)-(13)-(24)\right]\,N_{\rm q}'\left(k_{\rm max}^{\rm recon}\right) \ . \tag{33}$$

The distribution (ij) describes the angular radiation pattern of the $\widehat{ij}$ antenna,

$$(ij) \equiv \omega^2\,(\widehat{ij}) = \frac{a_{ij}}{a_i\,a_j} = \frac{1-\mathbf{n}_i\mathbf{n}_j}{(1-\mathbf{n}_i\mathbf{n})(1-\mathbf{n}_j\mathbf{n})} \ , \tag{34}$$

where the $\mathbf{n}_{i,j}$ denote the directions of the $\mathrm{q}/\overline{\mathrm{q}}$ momenta and $\mathbf{n}$ the direction of the registered flow. The factors

$$N_{\rm q}'(E_{\rm jet}) = \frac{\mathrm{d}}{\mathrm{d}\,\ln E_{\rm jet}} N_{\rm q}(E_{\rm jet}) \ , \tag{35}$$

with $N_{\rm q}(E_{\rm jet})$ the multiplicity inside a QCD jet of energy/hardness $E_{\rm jet}$, take into account the cascade particle multiplication. Approximately [11],

$$\frac{N'_{\rm q}}{N_{\rm q}} \simeq \sqrt{\frac{2N_C\alpha_s}{\pi}}\,(1+\mathcal{O}(\sqrt{\alpha_s}))\ . \tag{36}$$

The factor R describes the rearrangement strength. In principle, it could be computed within the perturbative scenario. However, for the purposes of this paper we shall here present only some order-of-magnitude estimates. Each squared diagram of Figs. 4, 6 and 7 (as well as the set of corresponding higher-order diagrams) contribute to the no-recoupling first term in eq. (33). Interferences between the diagrams of Fig. 6a and Fig. 6b and between the diagrams of Fig. 7 and Fig. 4 exemplify the lowest-order contribution to the reconnecting interference piece.

It follows from the discussion in the previous subsections that the rearrangement coefficient is expected to be

$$R \lesssim \mathcal{O}\left(\frac{\alpha_s}{N_C^2}\right)\ . \tag{37}$$

Moreover, the suppression of energetic radiation accompanying the reconnected systems makes the corresponding cascades practically sterile, so the rearrangement affects only a few particles,

$$\frac{N_{\rm q}(k_{\rm max}^{\rm recon})}{N_{\rm q}(m_{\rm W}/2)} \sim \mathcal{O}(10^{-1})\ . \tag{38}$$

Because of both these factors, the magnitude of the reconnection effects in the perturbative scenario is expected to be numerically small, $\mathcal{O}(10^{-2})$ or less. This gives the factor by which the maximal perturbative effects shown in Section 2 should be scaled down for a realistic estimate of perturbative reconnection effects.

One can derive the antenna pattern corresponding to colour transmutation (the second term in eq. 33), for instance by examining the interference between the diagrams of Fig. 7 with those of Fig. 4. The same structure appears for the interference contributions corresponding to the diagrams of Fig. 6a and Fig. 6b after integration over the momentum of one of the emitted gluons. The infrared divergences corresponding to the unobserved gluon are cancelled when both real and virtual emission contributions are taken into account.

From the antenna patterns given by eqs. (19) and (33) one immediately sees that, in addition to the two rearranged dipoles $\mathrm{q_1\overline{q}_4}$ and $\mathrm{q_3\overline{q}_2}$ present in the GPZ string picture, two other terms $\mathrm{q_1q_3}$ and $\mathrm{\overline{q}_2\overline{q}_4}$ appear. As was mentioned before, these terms are intimately connected with the conservation of colour currents. Moreover, the $\widehat{13}$ and $\widehat{24}$ antennae come in with a negative sign. In general, QCD radiophysics predicts both attractive and repulsive forces between quarks and antiquarks, see refs. [11, 17, 18]. Normally the repulsion effects are quite small, but in the case of colour-suppressed phenomena they may play an important rôle.

One can easily understand the physical origin of the attraction and repulsion effects with the help of the 'QED' model of ref. [18], where quarks are replaced by leptons. For illustration, the photonic interference pattern in

$$\gamma\gamma \to \mathrm{Z^0Z^0} \to \mathrm{e^+e^-}\mu^+\mu^- \tag{39}$$

could be examined. In addition to the attractive forces between opposite electrical charges ($\widehat{\mathrm{e^-}\mu^+}$ and $\widehat{\mathrm{e^+}\mu^-}$ QED-antennae) there is a negative-sign contribution ($\widehat{\mathrm{e^-}\mu^-}$ and $\widehat{\mathrm{e^+}\mu^+}$

QED-antennae) corresponding to the repulsive forces between two same-sign charges. In QED there is no equivalent to the colour suppression factor, so in the limit $\Gamma_Z \to \infty$ (i.e. $\chi_{12} \to 1$) the dipole radiation structure is simply given by the expression

$$\widehat{e^-e^+} + \widehat{\mu^-\mu^+} + \left(\widehat{e^-\mu^+} + \widehat{e^+\mu^-} - \widehat{e^-\mu^-} - \widehat{e^+\mu^+}\right) \ . \tag{40}$$

For instance, near the Z^0Z^0 threshold, the total interference is maximal and constructive (destructive) when e^- is collinear with μ^- (μ^+); for $\Gamma_Z \to \infty$ the radiation pattern is equivalent to that induced by a charge -2 (charge 0) particle.

By contrast to the perturbative QCD description, only the positive-sign dipoles appear in the Lund string model. This is because each string corresponds to a colour singlet, while the negative-sign $qq/\overline{qq}$ dipoles correspond to non-singlets (antitriplets/sextets). There need not be a physics conflict between the two pictures: one should remember that the perturbative approach describes short-distance phenomena, where partons may be considered free to first approximation, while the Lund string picture is a model for the long-distance behaviour of QCD, where confinement effects should lead to a subdivision of the full system into colour singlet subsystems (ultimately hadrons) with screened interactions between these subsystems.

Also the rôle of colour quantum numbers may differ, as follows. Reconnection is suppressed by a factor $1/(N_C^2 - 1)$ in the perturbative description. The same suppression would appear in the non-perturbative string model if only endpoint quark colours were considered. For instance, in the $W^+W^- \to q_1\overline{q}_2q_3\overline{q}_4$ process, with perturbative gluon emission neglected for the moment, the $q_1\overline{q}_4$ system would have to be in a colour singlet state for a reconnection to be possible. However, in a realistic picture, the string itself is made up of a multitude (an infinity) of coloured confinement gluons. Therefore all colours are well represented in the local neighbourhood of any potential string reconnection point. The local gluons can then always be rearranged in such a way that colour neutrality is maintained for the reconnected systems. Although some suppression of the reconnection probability might well remain, as a first guess we will assume that there is no such suppression in the non-perturbative phase.

Let us come now to the issue of observability of the reconnection effects in a real-life experiment. Analogously to the string [19] / drag [17] effect, colour rearrangement could generate azimuthal anisotropies in the distributions of the particle flow. That is, in the rest frame of one W the particle distribution relative to the daughter-quark direction could become azimuthally asymmetric (on top of the trivial kinematical effects caused by the overlap with the decay products of the other W). Such an asymmetry should be strongly dependent on the overall topology of the 4-jet $q_1\overline{q}_2q_3\overline{q}_4$ system. It is instructive to note that the negative-sign (13) and (24) dipoles of eq. (33) in fact act to increase the magnitude of the string-like anisotropy effects of the (14) and (23) dipoles.

It should be emphasized that, analogously to the other colour-suppressed interference phenomena (see refs. [11, 17, 20]), the rearrangement phenomenon can be viewed only on a completely inclusive basis, when all the antennae–dipoles are simultaneously active in the particle production. The very fact that the reconnection pieces are not positive-definite reflects their wave interference nature. Therefore the effects of recoupled sterile cascades should appear on top of a background generated by the ordinary-looking no-reconnection dipoles.

Again there is an important difference between the perturbative QCD radiophysics picture and the non-perturbative string model. The latter not only allows but even

requires a completely exclusive description: in the end the $q_1\overline{q}_2q_3\overline{q}_4$ system must be subdivided into and fragment as two separate colour singlets, either $q_1\overline{q}_2$ and $q_3\overline{q}_4$ or $q_1\overline{q}_4$ and $q_3\overline{q}_2$. (Neglecting the fact that the recoupling and fragmentation will involve additional partons emitted in the preceding perturbative phase, see below.) The string model therefore predicts effects that should be searched for on an event-by-event basis. Normally (such as in the $e^+e^- \to q\overline{q}g$ process) the two pictures work in quite peaceful coexistence; differences only become drastic when dealing with the small colour-suppressed effects.

Summing up the above discussion, it can be concluded that colour rearrangement affects only a few low energy particles. Not so far from the W^+W^- threshold the magnitude of the reconnection-induced anisotropy effects in the particle-flow distribution is expected to be

$$\frac{\Delta N^{\rm recon}}{N^{\rm no-recon}} \lesssim \frac{\alpha_s(\Gamma_{\rm W})}{N_C^2}\,\frac{N'_{\rm q}(k^{\rm recon}_{\rm max})}{N'_{\rm q}(m_{\rm W}/2)} \lesssim \mathcal{O}(10^{-2})\ . \tag{41}$$

In the integral inclusive cross section for $e^+e^- \to W^+W^- \to q_1\overline{q}_2q_3\overline{q}_4$, at and above the W^+W^- threshold, the reconnection effects are expected to be negligibly small,

$$\frac{\Delta\sigma^{\rm recon}}{\sigma} \lesssim \frac{(C_F\,\alpha_s)^2}{N_C^2}\,\frac{\Gamma_{\rm W}}{m_{\rm W}}\ , \tag{42}$$

where we would expect that the running coupling constant should be evaluated at a scale of $\mathcal{O}(\Gamma_{\rm W})$. Numerically, then, $\sigma^{\rm recon}/\sigma \ll 10^{-3}$.

Let us clarify the origin of the factor $\Gamma_{\rm W}/m_{\rm W}$ in eq. (42) (for details see ref. [15]). Because of the exact cancellation between the real and virtual soft ($|k^0| \ll m_{\rm W}$) gluon emissions, the interference rearrangement effects can manifest themselves only in terms of the order of $|k^0|/m_{\rm W}$. But the radiated energy in the reconnected systems is restricted to be in the $|k^0| \lesssim \Gamma_{\rm W}$ domain, and so the magnitude of the rearrangement phenomena should include the factor $\Gamma_{\rm W}/m_{\rm W}$. Note that the soft gluon cancellation argument is based on an integration over all gluon momenta; it does not apply for the registered particle flow, which is a more exclusive distribution.

Using the analogy with the QED radiation in reaction (39), the anisotropy of particle flow in QCD can be put in correspondence with that of photon emission in (39). The rearrangement effects in the integrated QCD process cross section would correspond to the interference radiative corrections to the cross section of process (39). The essential difference between the radiative phenomena in the two processes (1) and (39) is that in the QED case the interference terms contribute to the photon angular distribution (for $\omega \lesssim \Gamma_{\rm Z}$) with the same strength as the independent emission terms of each Z^0 decay. Only in the QCD case does the decay–decay recoupling interference acquire a small weighting factor, see eq. (37).

4 Non-perturbative models for topology dependence

Having demonstrated that perturbative colour rearrangement effects are negligibly small, in the rest of the paper we consider exclusively the possibility of reconnection occurring as a part of the non-perturbative fragmentation phase. Since fragmentation is not understood from first principles, this requires model building rather than exact calculations. We will use the standard Lund string fragmentation model [5] as a starting point, as summarized in Section 4.1. The colour reconnection phenomenon is therefore equated

with the possibility that the string drawing given by the preceding hard process and parton shower activity is subsequently modified. We expect the reconnection probability to depend on the detailed string topology, i.e. to vary as a function of c.m. energy, actual W masses, the amount of parton shower activity and the angles between outgoing partons.

Throughout this section, the discussion is entirely on the probabilistic level, i.e. any negative-sign interference effects are absent. This means that the original colour singlets $q_1\overline{q}_2$ and $q_3\overline{q}_4$ may transmute to new singlets $q_1\overline{q}_4$ and $q_3\overline{q}_2$, but that any effects e.g. of the q_1q_3 and $\overline{q}_2\overline{q}_4$ dipoles (cf. eq. (19)) are absent. In this respect, the non-perturbative discussion is more limited in outlook than the perturbative one above.

The imagined time sequence is the following (for details see Section 4.2). The W^+ and W^- fly apart from their common production vertex and decay at some distance. Around each of these decay vertices, a perturbative parton shower evolves from an original $q\overline{q}$ pair. The typical distance that a virtual parton (of mass $m \sim 10$ GeV) travels before branching is comparable with the typical W^+W^- separation, but shorter than the fragmentation time. Each W can therefore effectively be viewed as instantaneously decaying into a string spanned between the partons. These strings expand, both transversely and longitudinally, at a speed limited by that of light. They eventually fragment into hadrons and disappear. Before that time, however, the string from the W^+ and the one from the W^- may overlap. If so, there is some probability for a colour reconnection to occur in the overlap region. The fragmentation process is then modified.

The standard string model does not constrain the nature of the string fully. At one extreme, the string may be viewed as an elongated bag, i.e. as a flux tube without any pronounced internal structure. At the other extreme, the string contains a very thin core, a vortex line, which carries all the topological information, while the energy is distributed over a larger surrounding region. The latter alternative is the chromoelectric analogue to the magnetic flux lines in a type II superconductor, whereas the former one is more akin to the structure of a type I superconductor. We use them as starting points for two contrasting approaches, with nomenclature inspired by the superconductor analogy. In scenario I, the reconnection probability is proportional to the space–time volume over which the W^+ and W^- strings overlap, with strings assumed to have transverse dimensions of hadronic size. In scenario II, reconnections take place when the cores of two strings cross. These two alternatives are presented in Sections 4.4 and 4.5 respectively. As a warm-up exercise, Section 4.3 contains a discussion of a simplified variant of scenario I, here called scenario 0, where strings are replaced by simple spherical volumes.

4.1 Relevant features of string fragmentation

The string is the simplest Lorentz-invariant description of a linear confinement potential. The mathematical one-dimensional string can be thought of as parametrizing the position of the axis of a cylindrically symmetric flux tube or vortex line. The transverse extent of a physical string around this axis is unspecified. A string tension of $\kappa \approx 1$ GeV/fm combined with a bag constant of $(0.23 \text{ GeV})^4$ implies a radius of roughly 0.7 fm, i.e. comparable to the proton radius.

In the decay of a W, $W^\pm \to q\overline{q}$, a string is stretched from the q end to the $\overline{q}$ one. If a number of gluons are emitted during the perturbative phase, the string is stretched via these gluons, i.e. from the q to the first gluon, from there to the second one, ..., and from the last gluon to the $\overline{q}$ end, Fig. 9 [19]. The string can therefore be described in a dual way, either as a sequence of partons connected by string pieces, or as a sequence of

string pieces joined at gluon corners. The gluons play the rôle of energy and momentum carrying kinks on the string. Since a gluon is attached to two string pieces, the force acting on it is twice that acting on a quark, which always sits at the end of a string. This ratio may be compared with the standard QCD ratio of colour Casimir factors, $N_C/C_F = 2/(1 - 1/N_C^2) = 9/4$. In this, as in other respects, the string model can be viewed as a variant of QCD where the number of colours N_C is not 3 but infinite [17, 11]. Note that the factor of 2 above does not depend on the kinematical configuration: a smaller opening angle between two partons corresponds to a smaller string length drawn out per unit time, but also to an increased transverse velocity of the string piece, which gives an exactly compensating boost factor in the energy density per unit string length.

The ordering of the gluons along the string is ambiguous, but in practice the parton shower picture, used to generate the parton configurations, does keep track of the colour flow and should provide a reasonable first approximation. The string is preferentially stretched so as to minimize the total length, i.e. partons that are nearby in momentum space are also likely to be closely related in colour flow. In addition to the dominant branchings $\mathrm{q} \to \mathrm{q} + \mathrm{g}$ and $\mathrm{g} \to \mathrm{g} + \mathrm{g}$, the shower formalism also allows branchings $\mathrm{g} \to \mathrm{q} + \overline{\mathrm{q}}$. These latter split the string into two. They will not be much covered in this paper, but are included in the results we present.

Let us now turn to the fragmentation process, and start by considering a $\mathrm{q}\overline{\mathrm{q}}$ event without any energetic gluons. As the q and $\overline{\mathrm{q}}$ move apart, the potential energy stored in the string increases, and the string may break by the production of a new $\mathrm{q}'\overline{\mathrm{q}}'$ pair, so that the system splits into two colour-singlet systems $\mathrm{q}\overline{\mathrm{q}}'$ and $\mathrm{q}'\overline{\mathrm{q}}$. If the invariant mass of either of these string pieces is large enough, further breaks may occur. The string break-up process proceeds until only on-the-mass-shell hadrons remain, each hadron corresponding to a small piece of string with a quark at one end and an antiquark at the other.

If transverse momenta are neglected, each break-up vertex is characterized by two coordinates, e.g. (t, z) for a string aligned along the z axis. Adjacent string breaks are related by the requirement that the intermediate string piece should have the right mass to form a hadron. Each break-up therefore effectively corresponds to one degree of freedom. Break-ups are acausally separated, i.e. $(\Delta t)^2 - (\Delta z)^2 < 0$, which means that there is no unique ordering of them. They may thus be considered in any convenient order, e.g. from the quark end inwards. It is therefore useful to formulate an iterative scheme for the fragmentation, wherein hadrons are produced one after the other in sequence, starting at the q end. In each step the hadron carries away a fraction of the available light-cone momentum ($E + p_z$ for a quark travelling in the $+z$ direction), so that the remaining momentum of the string is gradually reduced. If $m_\perp$ denotes the transverse mass of the produced hadron and $\tilde{z}$ the fraction of remaining light-cone momentum taken by the hadron, then the $\tilde{z}$ probability distribution is given by the 'Lund symmetric fragmentation function',

$$f(\tilde{z}) \propto \frac{1}{\tilde{z}} \, (1 - \tilde{z})^a \, \exp(-b m_\perp^2 / \tilde{z}) \; . \tag{43}$$

The two parameters a and b are to be determined from experiment. When complemented by additional aspects, such as the generation of transverse momenta, the appearance of different flavours and hadron multiplets, and so on, a complete picture of the fragmentation process is obtained [5].

In this classical $(1 + 1)$-dimensional picture, the hadron formed by two string breaks at (t_1, z_1) and (t_2, z_2) (with $z_1 > z_2$ by convention) has $E = \kappa(z_1 - z_2)$ and $p_z = \kappa(t_1 - t_2)$. Starting from the endpoint of the string, the momenta of hadrons may then be used to

recursively define the space–time points of string breaks. The proper time τ of string breaks therefore has an inclusive distribution, which reflects the shape of $f(\tilde{z})$:

$$\mathcal{P}(\Gamma_{\rm frag}) \propto (\Gamma_{\rm frag})^a \, \exp(-b\Gamma_{\rm frag}) \; , \qquad \text{where } \Gamma_{\rm frag} = (\kappa\tau)^2 \; . \tag{44}$$

Subsequent formulae become especially simple for $a \equiv 0$. Since the best experimental values are not far away from that, we will henceforth use $a = 0$, $b \approx 0.4$ GeV^{-2}. (This ansatz is only needed for the inclusive proper time distribution; it is still possible to use a different set of a and b values in eq. (43), to obtain the momenta of hadrons.) This set gives a $\langle \Gamma_{\rm frag} \rangle = (1+a)/b$ in agreement with data, but somewhat larger fluctuations around this average than the best experimental estimate. Introducing $\tau_{\rm frag} = 1/\kappa b^{1/2} \approx 1.5\mu \approx 1.5$ fm (with $c = 1$) (cf. eq. (2)), eq. (44) then becomes

$$\mathcal{P}_{\rm frag}(\tau) \, {\rm d}\tau = \exp(-\tau^2/\tau_{\rm frag}^2) \, 2\tau {\rm d}\tau/\tau_{\rm frag}^2 \; , \tag{45}$$

where $\mathcal{P}_{\rm frag}(\tau)$ is the differential probability that the string will fragment at a time τ. The space–time area swept out by the string grows like τ^2; therefore an exponential decay in τ^2 (rather than in τ) is to be expected when the probability for the string to break is a constant per unit of time and length [21].

When the string contains several gluon kinks, the fragmentation process is much more complicated, but can still be described in a similar language [22]. The string is breaking along its full length, according to the same probability distribution in τ as above. Each string piece by itself fragments into hadrons, much like a simple $\rm q\overline{q}$ string, except at around the gluon kinks. There a hadron will straddle the kink, i.e. contain parts of two adjacent string pieces. Again an iterative scheme can be formulated to describe the fragmentation from the quark ends inwards. The simple picture becomes considerably more complicated when the invariant mass between two adjacent partons becomes small, i.e. for soft or collinear emission. For instance, a gluon loses its energy to the two string pieces it pulls out in a time $t_E = E_{\rm g}/2\kappa$; therefore a soft gluon with energy below roughly $E_{\rm g} \approx 2\kappa\tau_{\rm frag} \approx 3$ GeV will lose its energy on a time scale shorter than the fragmentation one. After the time t_E the string motion is considerably more complicated. We have a scheme for the momentum–energy fragmentation process also in this case [22], but have not tried to include the same subtleties in the space–time picture.

Clearly, the emphasis in the traditional description of string fragmentation is on the momentum–energy picture, as in eq. (43). A space–time equivalent may be derived, as a by-product, but is not to be trusted more than allowed by the uncertainty relations. For the current paper it would have been an advantage to turn this around, and start out from a 'micro description' of the space–time evolution. Specifically, one would have liked to trace the motion of the string pieces and the breaking of strings by $\rm q\overline{q}$ pair creation in time order, thereafter to translate this space–time picture into an momentum–energy one. Our continued discussion could then have been made more precise, in that the state of the system would be fully specified at any potential space–time point of colour reconnection.

The main problem with allowing string breaks in strict time order is that it is then more difficult to simultaneously fulfil the requirements of an overall Lorentz-invariant description and of correct masses for hadrons. One way out is to relax the mass constraint, by having the string break into variable-mass clusters rather than fixed-mass hadrons. This is the approach taken in the CALTECH-II model [23]. However, it was never possible to achieve a good agreement with data for CALTECH-II. In addition, there is no clear space–time picture for the subsequent decay of clusters into hadrons, as would be required in a complete description.

In this paper, we therefore rely on a slightly more primitive approach, which we still think will be enough to give a good first approximation to the more complicated full picture. The key simplification is to divide the full process into two steps, which are addressed in sequence rather than in parallel. In the first step, potential colour reconnections are considered. Here the inclusive decay distribution of eq. (45) is used to give the probability that the string did not yet fragment by the time of a potential recoupling, i.e.

$$\mathcal{P}_{\mathrm{no-frag}}(\tau) = \int_{\tau}^{\infty} \mathcal{P}_{\mathrm{frag}}(\tau')\,\mathrm{d}\tau' = \exp(-\tau^2/\tau^2_{\mathrm{frag}}) \; . \tag{46}$$

No other aspects of the fragmentation process are used here. Only in the second step, after the (possibly reconnected) string topology has been fixed, is the full machinery of the momentum–energy picture used to fragment the strings into an exclusive set of hadrons.

4.2 The general space–time picture

Consider the production of a $\mathrm{W}^+\mathrm{W}^-$ pair in the rest frame of the process. In general, the two masses $m^{\pm} = m(\mathrm{W}^{\pm})$ are unequal and differ from the nominal mass m_{W}. By momentum conservation, the absolute values of the three-momenta agree, $p^* = |\mathbf{p}^+| = |\mathbf{p}^-|$, but the energies $E^{\pm}$ are different, $E^{\pm} = (s \pm ((m^+)^2 - (m^-)^2))/2\sqrt{s}$, where $s = E^2_{\mathrm{cm}}$ is the squared c.m. energy. Also the boost factors, $\boldsymbol{\beta}^{\pm} = \mathbf{p}^{\pm}/E^{\pm}$ and $\gamma^{\pm} = E^{\pm}/m^{\pm}$, therefore differ.

In a complete description of the production process, there is a competition between the phase space and the $\mathrm{W}^{\pm}$ Breit–Wigners. (Also the form of the matrix element (including Coulomb final state interactions) plays a rôle, although we may neglect that for qualitative considerations.) For $E_{\mathrm{cm}} = 2m_{\mathrm{W}}$ this results in a $\langle p^* \rangle \approx 22$ GeV, rather than the naïve $p^* = 0$. The $\langle p^* \rangle$ does change with c.m. energy, but less rapidly than in the naïve picture, Fig. 10a. Above $2m_{\mathrm{W}}$ the competition gradually becomes less important; for $E_{\mathrm{cm}} = 200$ GeV the $\langle p^* \rangle$ is just what one would expect for W's on the mass shell. If instead the c.m. energy is decreased below $2m_{\mathrm{W}}$, at least one W can no longer benefit from the Breit–Wigner peak enhancement. Since the Breit–Wigner varies less rapidly in the tails, the phase space factor becomes more important, proportionally speaking. Therefore $\langle p^* \rangle$ is also increased at lower E_{cm}.

The average proper lifetime of a W depends on its mass m according to

$$\langle \tau \rangle = \tau_{\mathrm{dec}}(m) = \frac{\hbar m}{\sqrt{(m^2 - m^2_{\mathrm{W}})^2 + (\Gamma_{\mathrm{W}} m^2/m_{\mathrm{W}})^2}} \; , \tag{47}$$

where $1 = \hbar \approx 0.197$ GeV·fm. For a W on the mass shell this reduces to the standard experession $\tau_{\mathrm{dec}}(m_{\mathrm{W}}) = \hbar/\Gamma_{\mathrm{W}} \approx 0.1$ fm. However, with a standard Breit–Wigner distribution of masses, typically the W lifetime is only about two thirds as long as the naïve expectation, Fig. 10b. The W width $\Gamma_{\mathrm{W}} \approx 2.1$ GeV has been defined for $m = m_{\mathrm{W}}$; the variation of the width as a function of mass has been included as an explicit factor m/m_{W} in eq. (47).

The actual proper lifetime of a $\mathrm{W}^{\pm}$ is thus distributed according to

$$\mathcal{P}(\tau^{\pm})\,\mathrm{d}\tau^{\pm} = \exp(-\tau^{\pm}/\tau_{\mathrm{dec}}(m^{\pm}))\,\mathrm{d}\tau^{\pm}/\tau_{\mathrm{dec}}(m^{\pm}) \; . \tag{48}$$

If the $\mathrm{W}^+\mathrm{W}^-$ pair is created at the origin, $(\mathbf{x}^0_0, t^0_0) = (\mathbf{0}, 0)$, the $\mathrm{W}^{\pm}$ decay vertices are given by $(\mathbf{x}^{\pm}_0, t^{\pm}_0) = (\gamma^{\pm}\boldsymbol{\beta}^{\pm}\tau^{\pm}, \gamma^{\pm}\tau^{\pm})$. The average separations $|t^+_0 - t^-_0|$ and $|\mathbf{x}^+_0 - \mathbf{x}^-_0|$ as

a function of the c.m. energy are shown in Fig. 10b. At typical LEP 2 energies the time separation is about 0.08 fm and the spatial separation 0.05 fm.

Each W decays to a $\mathrm{q\overline{q}}$ pair. The quarks normally are off the mass shell and therefore branch further, $\mathrm{q} \to \mathrm{q} + \mathrm{g}$. The daughter partons may branch in their turn, and so on. A parton shower thus develops, to leading order made up out of the three branchings $\mathrm{q} \to \mathrm{q} + \mathrm{g}$, $\mathrm{g} \to \mathrm{g} + \mathrm{g}$ and $\mathrm{g} \to \mathrm{q} + \overline{\mathrm{q}}$. The branchings are ordered in mass, by trivial kinematical constraints, i.e. daughter partons have to be less virtual than the mother parton. In current parton shower algorithms, the evolution is stopped at some lower cut-off scale, typically $m_0 \approx 1$ GeV. Branchings may well occur at lower scales, but can no longer be described in perturbative terms; they are instead effectively included in the fragmentation description. The branching process is ambiguous, in the sense that one given partonic final state may be arrived at by a host of intermediate branching histories. However, coherence effects impose a further ordering in terms of decreasing emission angles [11], which limits this ambiguity. Several shower algorithms have been proposed, which differ in technical details, but agree in most of their predictions. (An exception is prompt photon production, which may offer an opportunity to learn more about shower evolution [24].) In the following, we use the one of ref. [4].

It is not unreasonable to neglect on-shell quark masses, since the heaviest quark produced with any significant rate is the c one ($\mathrm{W}^- \to \mathrm{b\overline{c}}$ decays are negligible). The average lifetime of a parton in a shower is then given by its off-shell mass m and energy E:

$$\langle t_{\mathrm{part}} \rangle = \gamma \, \langle \tau_{\mathrm{part}} \rangle = \frac{E}{m} \, \frac{\hbar}{m} = \frac{\hbar E}{m^2} \; . \tag{49}$$

A parton with a mass close to the lower cut-off, $m \approx m_0 \approx 1$ GeV, and a maximal energy, $E \approx m_{\mathrm{W}}/2 \approx 40$ GeV, would thus have time to travel about 8 fm before branching to the final partons. This is a distance much larger than the separation between the W^+ and W^- decays, and so it is to be feared that it is important to keep track of the space–time evolution of the shower. However, branchings at such low mass scales do not give rise to separate jets, but only to some additional transverse momentum smearing inside the hadron fragments of a jet. At LEP 1, the limit for meaningful jet resolution is typically $m \approx 10$ GeV ($y_{ij} = m_{ij}^2/E_{\mathrm{cm}}^2 > y_{cut} \approx 0.01$), which corresponds to $\langle t_{\mathrm{part}} \rangle \approx 0.1$ fm. The overall event structure is thus determined on a scale comparable to the separation between the W^+ and W^- decays, and at a time much shorter than typical fragmentation scales. For the subsequent discussion of string motion we will thus assume that all partons of a W decay have a common origin. The effects of the low-mass branchings will be studied by cutting off the shower at different m_0 scales.

As the partons move apart they pull out a string, made up of straight string pieces between adjacent partons. The most general case we need to consider is a string piece created at a point $(\mathbf{x}_0, t_0)$, with the two endpoints of the string moving out with velocities $\mathbf{v}_1 = \mathbf{p}_1/E_1$ and $\mathbf{v}_2 = \mathbf{p}_2/E_2$. Usually we will neglect the possibility that the endpoint partons are off the mass shell, i.e. assume that $|\mathbf{v}_1| = |\mathbf{v}_2| = 1$. The string position can then be described as

$$\mathbf{x}_{\mathrm{string}}(t) = \mathbf{x}_0 + (\mathbf{v}_1 + \alpha(\mathbf{v}_2 - \mathbf{v}_1)) \, (t - t_0) \; , \qquad 0 \leq \alpha \leq 1 \; , \tag{50}$$

with the centre of the string at $\alpha = 1/2$. Therefore the overall motion of the string is given by $\boldsymbol{\beta} = (\mathbf{v}_1 + \mathbf{v}_2)/2$ and a unit vector along the string direction by $\mathbf{u} = (\mathbf{v}_2 - \mathbf{v}_1)/|\mathbf{v}_2 - \mathbf{v}_1|$. One obtains $|\boldsymbol{\beta}| = \sqrt{(1 + \cos\theta_{12})/2} = \cos(\theta_{12}/2)$ and $\gamma = 1/\sin(\theta_{12}/2)$, where θ_{12} is the angle between the two partons. The γ factor gives the time dilatation for

the fragmentation process in the middle of the string, i.e. $\langle t_{\rm frag} \rangle = \gamma \tau_{\rm frag}$. The regions of the string closer to the endpoints of the string obviously fragment later, on the average.

We saw above that high-virtuality partons decay in times much shorter than typical fragmentation times. Low-mass partons, on the other hand, can travel distances larger than $\tau_{\rm frag}$, and so it is of some interest to study the importance of boost effects on the fragmentation process. Consider a quark or gluon with an energy E and mass m, where the two daughters take energy fractions z and $1-z$, respectively. The new string piece produced by the parton branching is spanned between these two daughters. The opening angle θ_{12} can be approximated by

$$\theta_{12} = \theta_1 + \theta_2 \approx \frac{p_\perp}{zE} + \frac{p_\perp}{(1-z)E} = \frac{p_\perp}{z(1-z)E} \approx \frac{m}{\sqrt{z(1-z)}E} \; , \tag{51}$$

where θ_i is the angle of either daughter and $p_\perp$ is their common transverse momentum with respect to the mother direction. Therefore

$$\langle t_{\rm frag} \rangle = \gamma \tau_{\rm frag} = \frac{\tau_{\rm frag}}{\sin(\theta_{12}/2)} \approx \frac{2\tau_{\rm frag}}{\theta_{12}} \approx 2\sqrt{z(1-z)}\,\frac{E}{m}\,\tau_{\rm frag} \; , \tag{52}$$

and

$$\frac{\langle t_{\rm frag} \rangle}{\langle t_{\rm part} \rangle} \approx \frac{2\sqrt{z(1-z)}E\tau_{\rm frag}/m}{\hbar E/m^2} = \frac{2}{\hbar}\sqrt{z(1-z)}\,m\,\tau_{\rm frag} \approx (15\ {\rm GeV}^{-1})\sqrt{z(1-z)}\,m \; . \tag{53}$$

It is easy to convince oneself that this ratio is comfortably bigger than unity in the whole physical region. In the extreme case of $m = m_0 \approx 1$ GeV and $z = E_1/E = (m_0/2)/(m_{\rm W}/2) \approx 1/100$, one obtains $\langle t_{\rm frag} \rangle / \langle t_{\rm part} \rangle \approx 1.5$.

The difference between the correct string drawing and the one obtained by setting $t_{\rm part} = 0$ is shown in Fig. 11 for a very simple example. The W decays to a $\rm q^* \overline{q}$ pair at point A. The $\rm q^*$ is virtual, and subsequently branches, $\rm q^* \to q + g$, at point B. The correct string topology at some later time is shown by Fig. 11a. Closest to the $\overline{\rm q}$ end is a string piece pulled out by the $\rm q^*$ and the $\overline{\rm q}$ before the $\rm q^*$ branched, and this piece is therefore aligned along the original $\rm q^* \overline{q}$ event axis. Next comes the string piece pulled out by the $\overline{\rm q}$ and the g after the latter was produced. The kink (C) that joins these two string pieces does not carry any energy, unlike an ordinary gluon kink. It was formed at the $\rm q^*$ decay vertex and is travelling in the $\overline{\rm q}$ direction with the speed of light. Finally, there is the string piece between the g and the q, expanding from point B. Figure 11b shows the same picture in the approximation that point B coincides with A, so that there is no string piece pulled out between $\rm q^*$ and $\overline{\rm q}$.

4.3 Scenario 0: spherical volumes

Strings are assumed to have a well-defined longitudinal direction. However, if the main jets of the $\rm W^+$ and the $\rm W^-$ are well separated, the strings only overlap in the middle. To first approximation, it is therefore useful to consider the case of a string being a completely spherical colour source. The probability for a reconnection to occur is taken to be proportional to the overlap of the $\rm W^+$ colour source with the $\rm W^-$ one, with details to be specified in the following.

The result is a very simple model for colour reconnection, which gives some feeling for the energy dependence of the reconnection probability, and where several results can

be obtained without recourse to a complete event generator. This toy model is thus not of comparable scope with the two other scenarios we will develop below. Clearly, any information on the angular distributions of the $\mathrm{W}^{\pm}$ decays is lost. In particular, if one jet from the W^+ and one from the W^- move out in the same general direction the strings will overlap for longer, and the spherical approximation is likely to break down.

The colour field strength Ω_0 of a spherically symmetric colour source at rest at the origin can be approximated by

$$\Omega_0(\mathbf{x}, t) = \exp(-\mathbf{x}^2/2r_{\mathrm{had}}^2)\ \theta(t - |\mathbf{x}|)\ \exp(-t^2/\tau_{\mathrm{frag}}^2)\ . \tag{54}$$

The first factor corresponds to a Gaussian fall-off of the field strength. Alternatives could certainly be considered, with a more or less sharp edge, but would not affect the qualitative picture. We have seen above that the typical transverse size of a string is $r_{\mathrm{cyl}} \approx 0.7$ fm when the string is described as a cylinder with a sharp edge. If this is replaced by a Gaussian fall-off in two transverse dimensions, an appropriate choice of width in each dimension is $r_{\mathrm{had}} \approx r_{\mathrm{cyl}}/\sqrt{2} \approx 0.5$ fm. The subsequent step function $\theta(t-|\mathbf{x}|)$ ensures that information on the decay of the W, assumed to take place at $t = 0$, spreads outwards at the speed of light ($c = 1$). The final factor is the probability that a string remains at time t, i.e. has not yet fragmented, eq. (46). The typical proper lifetime is $\tau_{\mathrm{frag}} \approx 1.5$ fm $\approx 3r_{\mathrm{had}}$. Some time-retardation could be included also here, but then it would be necessary to first specify the spatial point of fragmentation, which would mean taking the model more seriously than it warrants.

In a second step, we generalize to a moving colour source, again created at the origin but moving away with a speed $\boldsymbol{\beta}$. The evaluation of $\Omega(\mathbf{x}, t)$ is most conveniently done by performing a boost $-\boldsymbol{\beta}$ back to the rest frame of the source:

$$\Omega(\mathbf{x}, t; \boldsymbol{\beta}) = \Omega_0(\mathbf{x}', t')\ , \tag{55}$$

$$\mathbf{x}' = \mathbf{x} + \gamma \left(\frac{\gamma \boldsymbol{\beta}\mathbf{x}}{1+\gamma} - t \right) \boldsymbol{\beta}\ , \tag{56}$$

$$t' = \gamma(t - \boldsymbol{\beta}\mathbf{x}) \tag{57}$$

(remember that the volume element $\mathrm{d}^3\mathbf{x}\,\mathrm{d}t = \mathrm{d}^3\mathbf{x}'\,\mathrm{d}t'$ is boost-invariant). Finally, if the source is not created at the origin but at a point $(\mathbf{x}_0, t_0)$, the distribution is

$$\Omega(\mathbf{x}, t; \mathbf{x}_0, t_0; \boldsymbol{\beta}) = \Omega(\mathbf{x} - \mathbf{x}_0, t - t_0; \boldsymbol{\beta}) = \Omega_0((\mathbf{x} - \mathbf{x}_0)', (t - t_0)')\ . \tag{58}$$

Now consider the production of a $\mathrm{W}^+\mathrm{W}^-$ pair at the origin, moving out back-to-back. In this simple toy study we assume both W's to have the same nominal mass $m = m_{\mathrm{W}} = 80$ GeV. The common velocity is therefore $\beta = |\boldsymbol{\beta}| = \sqrt{1 - 4m_{\mathrm{W}}^2/s}$. The proper lifetime of each W is distributed according to eq. (48) with $\tau_{\mathrm{dec}} = \tau_{\mathrm{dec}}(m_{\mathrm{W}})$. The overlap of the two sources, averaged over the $\mathrm{W}^{\pm}$ lifetime spectra, is then given by

$$\mathcal{I}(\beta) = \int \mathcal{P}(\tau^+)\,\mathrm{d}\tau^+ \int \mathcal{P}(\tau^-)\,\mathrm{d}\tau^- \int \mathrm{d}^3\mathbf{x}\,\mathrm{d}t\ \Omega(\mathbf{x}, t; \gamma\tau^+\boldsymbol{\beta}, \gamma\tau^+)\ \Omega(\mathbf{x}, t; -\gamma\tau^-\boldsymbol{\beta}, \gamma\tau^-)\ . \tag{59}$$

Since the absolute normalization of $\mathcal{I}(\beta)$ is irrelevant, results are conveniently normalized to $\mathcal{I}(0)$, which is the maximum value. This ratio $\mathcal{I}(\beta)/\mathcal{I}(0)$ is shown in Fig. 12. There are a few comments to be made. Firstly, the variation of $\mathcal{I}(\beta)$ with c.m. energy is rather slow. In other words, the 'threshold region' of potentially large reconnection

probabilities covers the whole LEP 2 range, with a variation in $\mathcal{I}(\beta)$ of a factor 3–4. Secondly, the curves show that this variation is shared between three contributing factors: the motion of the sources, the time retardation factor, and the decay of $\mathrm{W}^{\pm}$ away from the origin. Of these, the last one is the least important, in spite of us having used the long lifetime of on-the-mass-shell W's. With a realistic W mass spectrum, the displacement of the W decay vertices is therefore even less significant.

We may assume the probability for string recoupling to be proportional to $\mathcal{I}(\beta)$, with some unknown constant of proportionality. However, should the probability become large, saturation must set in. In the current scenario only two configurations are possible, $\mathrm{q}_1\overline{\mathrm{q}}_2 + \mathrm{q}_3\overline{\mathrm{q}}_4$ and $\mathrm{q}_1\overline{\mathrm{q}}_4 + \mathrm{q}_3\overline{\mathrm{q}}_2$, so each recoupling corresponds to flipping between these two. The probability for the latter configuration should therefore exponentially approach a saturation value of 1/2 , i.e.

$$\mathcal{P}_{\mathrm{recon}} = \mathcal{P}(\mathrm{q}_1\overline{\mathrm{q}}_4 + \mathrm{q}_3\overline{\mathrm{q}}_2) = \frac{1}{2}\left(1 - \exp\left(-k_0\frac{\mathcal{I}(\beta)}{\mathcal{I}(0)}\right)\right) \quad . \tag{60}$$

Depending on the k_0 value chosen one may obtain widely different results for $\mathcal{P}_{\mathrm{recon}}$, see Fig. 13. Obviously, the energy variation of $\mathcal{P}_{\mathrm{recon}}$ is never faster than that of $\mathcal{I}(\beta)$.

To the list of uncertainties already mentioned, one should add the possibility of a modified velocity dependence in eq. (59). As it stands, this equation only gauges the geometrical overlap of two colour sources, but does not specify the mechanism whereby the colour reconnection occurs. Rapidly moving colour sources might interact differently than ones at rest, presumably more intensely, such that the net variation of reconnection probability with c.m. energy could be even slower than shown in Fig. 13.

In summary, the main lesson of this simple exercise is that the colour reconnection phenomenon is likely to have a very extended threshold region. An increase of LEP 2 energy could not be used to make an 'undesirable' phenomenon 'go away'. Let us recall that, also in the perturbative scenario, the magnitude of the reconnection effects (albeit small) is expected to be comparable at the threshold and reasonably far above it ($E_{\mathrm{W}} \sim \mathcal{O}(m_{\mathrm{W}})$).

4.4 Scenario I: elongated bags

In this scenario strings are assumed to be (time-retarded) cylindrical bags, and the recoupling probability to be proportional to the integrated overlap between such cylinders. The formalism has many similarities with the preceding one, but is intended to be more realistic, in a number of respects.

If a string, viewed in its rest frame, is expanding along the direction $\pm\mathbf{u}$, $|\mathbf{u}| = 1$, the colour field strength Ω_0 may be written as

$$\Omega_0(\mathbf{x}, t; \mathbf{u}) = \exp\left\{-(\mathbf{x}^2 - (\mathbf{ux})^2)/2r_{\mathrm{had}}^2\right\}\ \theta(t - |\mathbf{x}|)\ \exp\left\{-(t^2 - (\mathbf{ux})^2)/\tau_{\mathrm{frag}}^2\right\} \quad . \tag{61}$$

As for eq. (54), the first term gives a Gaussian fall-off, but now only in the transverse directions (if $\mathbf{u} = (0, 0, 1)$ then $\mathbf{x}^2 - (\mathbf{ux})^2 = r^2 - z^2 = x^2 + y^2$). The time retardation factor $\theta(t - |\mathbf{x}|)$ is unchanged. The last factor, the probability that the string has not yet fragmented, now depends on the proper time along the string axis ($\tau^2 = t^2 - (\mathbf{ux})^2 = t^2 - z^2$ for a string along the z axis).

Now consider a moving string piece, created at a point $(\mathbf{x}_0, t_0)$, with the string position described as in eq. (50). The transverse motion direction of the string piece is given by $\boldsymbol{\beta}$

and a unit vector along the string direction by $\mathbf{u}$. The colour field strength in an arbitrary point $(\mathbf{x}, t)$ is then

$$\Omega(\mathbf{x}, t; \mathbf{x}_0, t_0; \boldsymbol{\beta}; \mathbf{u}) = \Omega(\mathbf{x} - \mathbf{x}_0, t - t_0; \boldsymbol{\beta}; \mathbf{u}) = \Omega_0((\mathbf{x} - \mathbf{x}_0)', (t - t_0)'; \mathbf{u}) \; , \tag{62}$$

where boosted coordinates $\mathbf{x}'$ and t' are given by eqs. (56) and (57). Note that $\mathbf{u}$ is unchanged by the boost, $\mathbf{u}' = \mathbf{u}$, since $\boldsymbol{\beta}$ and $\mathbf{u}$ are orthogonal and $\mathbf{u}$ is a pure space-like vector ($v_i = (\mathbf{v}_i, 1) \Rightarrow u = (\mathbf{u}, 0)$).

Had perturbative QCD effects been neglected, each W would have decayed to a $\mathrm{q\overline{q}}$ pair, i.e. one single string piece, with the two endpoint vectors $\mathbf{v}_i$ given by the q and $\overline{\mathrm{q}}$. In the full description, however, the perturbative parton shower produces a number of gluons, and the string is therefore stretched from the q via these gluons to the $\overline{\mathrm{q}}$. A string with n partons, labelled $\mathrm{q}_1\,\mathrm{g}_2\,\mathrm{g}_3\,\cdots\,\mathrm{g}_{n-1}\,\overline{\mathrm{q}}_n$, has $n-1$ separate string pieces. Each of these gives a colour source $\Omega(\mathbf{x}, t; \mathbf{x}_0, t_0; \boldsymbol{\beta}_i; \mathbf{u}_i)$, where $(\mathbf{x}_0, t_0)$ is the common decay vertex of the W, while the $\boldsymbol{\beta}_i$ and $\mathbf{u}_i$ are defined by the direction vectors $\mathbf{v}_i$ and $\mathbf{v}_{i+1}$ of the two adjacent partons along the string.

Normally at most one of the many pieces of a string should contribute to the colour field in any specific space–time point. However, with the simple ansatz of eq. (61), there is no cut-off to stop the overlapping of several colour fields. Such overlaps are especially likely to happen close to a gluon corner, where two pieces meet, but also occur because our simple transverse Gaussians in principle extend all the way to infinity. Where overlaps do occur, normally one field is much more important than the rest. As a simple solution, the colour field strength of the decay products of a W is therefore defined as the maximum of all possible contributions,

$$\Omega_{\max}(\mathbf{x}, t; \mathbf{x}_0, t_0) = \max_{i=1,n-1} \Omega(\mathbf{x}, t; \mathbf{x}_0, t_0; \boldsymbol{\beta}_i; \mathbf{u}_i) \; . \tag{63}$$

In a $\mathrm{W^+W^-}$ event, the overlap between the colour fields of the $\mathrm{W^+}$ decay products, on the one hand, and the $\mathrm{W^-}$ ones, on the other, is thus given by

$$\begin{aligned} \mathcal{I}^{+-} &= \int \mathrm{d}^3\mathbf{x}\,\mathrm{d}t\; \Omega^+_{\max}(\mathbf{x}, t; \mathbf{x}_0^+, t_0^+)\; \Omega^-_{\max}(\mathbf{x}, t; \mathbf{x}_0^-, t_0^-) \\ &= \int \mathrm{d}^3\mathbf{x}\,\mathrm{d}t\; \Omega^+_{\max}(\mathbf{x}, t; \gamma^+\tau^+\boldsymbol{\beta}^+, \gamma^+\tau^+)\; \Omega^-_{\max}(\mathbf{x}, t; \gamma^-\tau^-\boldsymbol{\beta}^-, \gamma^-\tau^-) \; . \end{aligned} \tag{64}$$

The integral $\mathcal{I}^{+-}$ is too complicated to allow any analytical short-cuts, and has to be evaluated numerically for each individual event, since it explicitly depends on the specific parton configuration. This would be very time-consuming if good accuracy is strived for. Fortunately it is possible to take a numerical shortcut. If a Monte Carlo method is used to estimate the integral, then, to first approximation, the estimated $\mathcal{I}^{+-}$ value need not be the right one for each separate event, as long as the average is correct for an imagined infinite ensemble of identical events. It could be argued that, to second approximation, an error is made, since the reconnection probability $\mathcal{P}_{\mathrm{recon}}$ should saturate and therefore not be quite proportional to $\mathcal{I}^{+-}$, cf. eq. (60). However, in scenario 0 there was only one possible colour reconnection, while there is here a multitude of them, depending on which string pieces are involved. Saturation should therefore be related more to the local overlap of $\Omega^+_{\max}$ and $\Omega^-_{\max}$ than to the overlap integral over the full space–time. Further, the simple classical colour field configurations that we have introduced should be seen as smoothed-out averages of a more 'grainy' structure. Therefore we can make virtue

of necessity, and use the Monte Carlo approach as a way to introduce a more realistic interpretation of the colour field.

In this spirit, the integral is approximated by

$$\begin{aligned}
\mathcal{I}^{+-} &= \int \mathrm{d}^3\mathbf{x}\,\mathrm{d}t\;\Omega^+_{\max}(\mathbf{x},t;\mathbf{x}_0^+,t_0^+)\,\Omega^-_{\max}(\mathbf{x},t;\mathbf{x}_0^-,t_0^-) \\
&= \int \Omega_{\mathrm{trial}}(\mathbf{x},t)\,\mathrm{d}^3\mathbf{x}\,\mathrm{d}t\;\frac{\Omega^+_{\max}(\mathbf{x},t;\mathbf{x}_0^+,t_0^+)\,\Omega^-_{\max}(\mathbf{x},t;\mathbf{x}_0^-,t_0^-)}{\Omega_{\mathrm{trial}}(\mathbf{x},t)} \\
&\propto \left\langle \frac{\Omega^+_{\max}\Omega^-_{\max}}{\Omega_{\mathrm{trial}}}(\mathbf{x},t;\mathbf{x}_0^+,t_0^+;\mathbf{x}_0^-,t_0^-) \right\rangle \\
&\approx \frac{1}{100}\sum_{i=1}^{100}\frac{\Omega^+_{\max}\Omega^-_{\max}}{\Omega_{\mathrm{trial}}}(\mathbf{x}_i,t_i;\mathbf{x}_0^+,t_0^+;\mathbf{x}_0^-,t_0^-) \equiv \mathcal{I}^{+-}_{\Sigma}\ .
\end{aligned} \tag{65}$$

In the last two lines it is to be understood that the points $(\mathbf{x}_i, t_i)$ are to be selected at random according to the trial distribution Ω_{trial}, which has been taken as

$$\Omega_{\mathrm{trial}}(\mathbf{x},t) = \exp(-\mathbf{x}^2/f_r^2 r_{\mathrm{had}}^2)\ \exp(-2(t-t^{+-})^2/f_t^2\tau_{\mathrm{frag}}^2)\ \theta(t-t^{+-})\ , \tag{66}$$

with $t^{+-} = \max(\gamma^+\tau^+, \gamma^-\tau^-)$. The limit $f_r, f_t \to \infty$ corresponds to a 'correct' sampling of the full space–time, with vanishing probability to sample an interesting point. The values $f_r = 2.5$ and $f_t = 2$ give a compromise, which allows reasonable efficiency without introducing too much bias of saturation effects (see below). Results are not sensitive to this choice.

Out of the 100 space–time points selected for each event, only about 30 give a non-vanishing contribution; the others are outside the forward light-cone either of the W^+ string or of the W^- one. The sum of weights in eq. (65) is used to determine whether a recoupling should occur or not. In case of recoupling, one of the possible points is selected, with a probability proportional to the weight of this point. The selected point is associated with the overlap of a specific string piece from the W^+ with another from the W^-, any potential ambiguities having been resolved by the recipe of eq. (63). Thus it is possible also to select where on the two strings the reconnection occurs.

With reconnection possible in several different string pieces, it is not obvious at what value the reconnection probability should be forced to saturate, since two reconnections do not have to cancel each other. To see this, consider two strings $\mathrm{q}^+\mathrm{g}^+\overline{\mathrm{q}}^+$ and $\mathrm{q}^-\mathrm{g}^-\overline{\mathrm{q}}^-$ from the $\mathrm{W}^\pm$ decays. A first reconnection between the $\mathrm{q}^+\mathrm{g}^+$ and $\mathrm{g}^-\overline{\mathrm{q}}^-$ string pieces would give the two new strings $\mathrm{q}^+\overline{\mathrm{q}}^-$ and $\mathrm{q}^-\mathrm{g}^-\mathrm{g}^+\overline{\mathrm{q}}^+$. A second reconnection between the $\mathrm{q}^-\mathrm{g}^-$ and $\mathrm{g}^+\overline{\mathrm{q}}^+$ pieces would not give back the original configuration, but rather lead to a state consisting of three strings, $\mathrm{q}^+\overline{\mathrm{q}}^-$, $\mathrm{q}^-\overline{\mathrm{q}}^+$ and $\mathrm{g}^+\mathrm{g}^-$. (Multiple string reconnections could be an interesting source of pure gluonium states. Also a single string, e.g. in Z^0 decay, could fold back on itself in such a way that a gluon loop could be split off. This could be a production mechanism, e.g. for J/ψ and Υ states.)

For simplicity, we have chosen to allow at most one reconnection per event, but to set saturation at unit reconnection probability, i.e.

$$\mathcal{P}_{\mathrm{recon}} = 1 - \exp\left(-k_{\mathrm{I}}\, f_r^3 f_t\, \mathcal{I}^{+-}_{\Sigma}\right)\ . \tag{67}$$

Note that $\mathcal{I}^{+-}_{\Sigma}$ is somewhere in between a local and a global quantity, and therefore represents a pragmatic compromise between the conflicting demands. When all weights

in the sum are of moderate size, saturation is no problem, and the naïve behaviour is recovered, i.e. the reconnection probability in a point is given by the overlap $\Omega^+_{\rm max}\Omega^-_{\rm max}$ in that point. If one weight is very large, the averaging procedure with the other weights somewhat smoothens fluctuations in $\mathcal{P}_{\rm recon}$. Once the decision has been taken to allow a reconnection, however, the large weight does have its full impact on the choice of where this reconnection occurs. The above procedure contains one obvious error, namely that the saturation introduces an artificial dependence on the choice of $\Omega_{\rm trial}$. This tends to reduce the importance of recouplings at large distances and times, but not enough to provide a serious distortion of results.

A priori, the constant $k_{\rm I}$ in eq. (67) is unknown. Unlike the spherical case, there is no $\mathcal{I}(0)$ to normalize to, so we only explicitly separate out the dependence on the choice of $\Omega_{\rm trial}$. Instead $k_{\rm I}$ will later be determined by comparison with scenario II below.

4.5 Scenario II: vortex lines

In scenario II it is assumed that strings are like vortex lines in type II superconductors. Then all the topological information is given by the small core region, even if most of the energy is stored in the region surrounding the core. Reconnections can only take place when the core regions of two string pieces cross each other. This means that the transverse extent of strings can be neglected, which leads to considerable simplifications compared with the previous scenario. It is every bit as well founded physically as scenario I.

Consider string piece i spanned between partons i and $i+1$ of the $\rm W^+$ string, and string piece j spanned between partons j and $j+1$ of the $\rm W^-$ string. By analogy with eq. (50), the position of the two string pieces may be described as

$$\begin{aligned} \mathbf{x}_i^+(t,\alpha^+) &= \mathbf{x}_0^+ + (\mathbf{v}_i + \alpha^+(\mathbf{v}_{i+1}-\mathbf{v}_i))\,(t-t_0^+)\;, \qquad 0 \le \alpha^+ \le 1\;, \\ \mathbf{x}_j^-(t,\alpha^-) &= \mathbf{x}_0^- + (\mathbf{v}_j + \alpha^-(\mathbf{v}_{j+1}-\mathbf{v}_j))\,(t-t_0^-)\;, \qquad 0 \le \alpha^- \le 1\;. \end{aligned} \tag{68}$$

To find whether the two string pieces cross, one could step through the string evolution as a function of time. However, it is more convenient to solve

$$\mathbf{x}_i^+(t,\alpha^+) = \mathbf{x}_j^-(t,\alpha^-)\;. \tag{69}$$

This is a system of three equations — x, y and z — with three unknowns — t, α^+ and α^-. If the values of the unknowns are not constrained, the system always has exactly one solution, except for trivial pathologies such as two strings completely at rest or exactly parallel to each other. The uniqueness of the solution is easy to understand, by simple geometrical considerations for two moving, infinitely long strings. To find out if two string pieces actually do cross each other, it is therefore only necessary to check whether the solution is in the physical domain $t > \max(t_0^+, t_0^-)$, $0 \le \alpha^+ \le 1$, and $0 \le \alpha^- \le 1$.

To the above requirements comes the additional constraint that neither string piece must have had time to fragment before the time of crossing. In agreement with our earlier assumption, this is taken to be given by a Gaussian fall-off in the proper time of each string piece at the point of crossing,

$$\mathcal{P}_{\rm no-frag} = \exp\left(-\frac{(t-t_0^+)^2 - (\mathbf{x}_i^+(t,\alpha^+)-\mathbf{x}_0^+)^2}{\tau_{\rm frag}^2}\right)\,\exp\left(-\frac{(t-t_0^-)^2 - (\mathbf{x}_j^-(t,\alpha^-)-\mathbf{x}_0^-)^2}{\tau_{\rm frag}^2}\right)\;. \tag{70}$$

If a string crossing occurs, according to the above criteria, then a reconnection is assumed to take place with unit probability.

This scenario does not have any free parameters at all, except for $\tau_{\rm frag}$, of course, which may be considered as a known constant. It is therefore much more constrained and predictive than the ones encountered above. However, it would be wrong to leave the impression that everything is understood. Below we give a list of some uncertainties that one should be aware of, and also of some potential variations from the basic model.

- Occasionally an event may allow several string crossings, which could then, for instance, give rise to closed gluon loops, as discussed before. In the current study, at most one reconnection has been allowed, namely the one (among the potential ones) that occurs first in time. We do not expect the inclusion of some additional reconnections to have any influence on the studies presented in this paper.
- The gain in string length by a reconnection depends on the topology of the event, as illustrated in Fig. 14. (For string pieces spanned between gluons, a g is represented by a q or a $\overline{\rm q}$, depending on the direction of the colour flow along the string.) In a configuration like the one in Fig. 14a, the change in string topology is drastic, so a reconnection would almost certainly occur. If the configuration is more like Fig. 14b, where the two q (and/or $\overline{\rm q}$) ends are close together, a reconnection does not imply a major change. If quantum mechanical fluctuations are introduced around the classical limit, one might then expect the reconnection probability to be close to 1/2. It is also possible to have crossings where the string length would be increased by a reconnection, such as Fig. 14c, and the reconnection probability consequently could be smaller than 1/2. Crossings which give a large increase in string length are not favoured geometrically, but some 20% of all crossings correspond to an increase rather than a decrease (at 170 GeV). Additional parameters would be needed to model a smooth change in the reconnection probability with topology, without necessarily adding new insights. Therefore we have not pursued it, except to study an option where recouplings are allowed only if they reduce the string length. For two $\rm q_1\overline{q}_2$ and $\rm q_3\overline{q}_4$ (or equivalents with gluons) string pieces, this translates into the requirement that $m_{14}m_{23} < m_{12}m_{34}$, where m_{ij} is the invariant mass of partons i and j. We call this scenario II$'$.
- It could be argued that strings with different endpoint colours could pass through each other without interacting, so that the interaction probability would be further reduced. Based on the discussion in section 3.6 we choose to neglect this possibility. (The same argument could be raised for scenarios 0 and I, although colour is more smeared-out in those two, so that the reduction is more likely to be in the parameters k_0, $k_{\rm I}$ than in $\mathcal{P}_{\rm recon}$ itself. Thus nothing new is introduced, given that k_0, $k_{\rm I}$ are unknown anyway.)
- The more gluon emission is occurring in the parton shower evolution, the more a string will twist around in space, and the more likely it is that the strings from the two W's intersect. Results are therefore sensitive to the amount of soft-gluon emission, i.e. to the m_0 cut-off in the parton shower. This sensitivity will be studied later on. Also scenario I has a dependence on the partonic state, but not to the same extent: a tube around a string core is a smoother object than the core itself.
- The approach of letting all string regions expand away from the W vertex, as we do, is not correct. Low-virtuality partons travel out a long distance before they branch. This means that some string regions will not be formed until after the system has

spread outwards enough for string crossings to be rare. However, such string pieces generally subtend small angles, and are therefore not likely to be the ones that cross in the first place. Further, before the parton branched, it is not that a given angular region was empty of strings; that region was still filled, only by a string with one less kink. This uncertainty is therefore intimately related to the soft-gluon issue above.

5 Non-perturbative model predictions

In this section we present results based on a complete simulation of the non-perturbative scenarios I and II described in Section 4.

5.1 Reconnection probability

The reconnection probability $\mathcal{P}_{\rm recon}$ is predicted in scenario II without any adjustable parameters, although with uncertainties as already noted. Scenario I contains a completely free strength parameter $k_{\rm I}$, which could be adjusted to give any desired $\mathcal{P}_{\rm recon}$. To ease comparisons between the two alternatives, we have chosen $k_{\rm I} = 0.6$, such that the rates of reconnected events agree at $E_{\rm cm} \approx 170$ GeV.

The resulting energy dependence of $\mathcal{P}_{\rm recon}$ is shown in Fig. 15a. The main message is that the variation is very slow: the reconnection probability varies by at most a factor of 2 over the c.m. energy range 150–200 GeV. This is much slower than in scenario 0, see Fig. 13. The key difference is that scenario 0 did not include any Breit–Wigners for the W masses, so that the two W's were produced at rest for $E_{\rm cm} = 2m_{\rm W}$. In scenarios I and II, on the other hand, the effects of Breit–Wigners are included. As shown in Fig. 10a, this leads to a less rapid variation of $\langle p^* \rangle$. A larger $\langle p^* \rangle$ gives $\rm W^+$ and $\rm W^-$ decay points that are more separated, Fig. 10b, and W decay products that are faster moving away from each other. The variation of the reconnection probability is thus directly related to that of the $\langle p^* \rangle$. Below $2m_{\rm W}$ the picture is of one low-mass W, which decays very rapidly, but with decay products swiftly moving away from the central region, while the heavier W is essentially on the mass shell and therefore decays later. The decrease in $\mathcal{P}_{\rm recon}$ below 160 GeV thus reflects that the lighter W has fewer decay products, and that those products are faster boosted away from the origin.

The variation of $\mathcal{P}_{\rm recon}$ with c.m. energy is a bit more pronounced in scenario II than in scenario I. This is fully understandable, in the sense that a faster motion of the W's away from each other implies that the $\rm W^+$ and $\rm W^-$ decay products are better separated. The probability for a head-on crossing of two string cores, as required in scenario II, therefore dies away faster with increasing p^* and β than the probability for the Gaussian tails of the strings to overlap, as is sufficient in scenario I.

The difference between the two scenarios is even more marked in Fig. 15b, where the dependence of $\mathcal{P}_{\rm recon}$ on the parton shower cut-off scale is shown for a fixed energy $E_{\rm cm} = 170$ GeV. The $k_{\rm I} = 0.6$ choice is made such that the two curves agree for the nominal cut-off $m_0 = 1$ GeV. In the other limit, when $m_0 \geq m_{\rm W}/2$, there is no parton shower evolution, i.e. each W gives a simple $\rm q\overline{q}$ system.

When each W only decays to one string piece, the solution to eq. (69) in scenario II is $t = 0$, $\alpha^+ = \alpha^- = 0.5$, i.e. in the unphysical region before the W's have decayed. In other words, if there is no parton shower evolution, the two string pieces are moving away from

each other and cannot cross. The reconnection probability thus has to vanish in the large m_0 limit. Conversely, the more string pieces there are, the larger is the probability that two of these pieces will cross. However, the overall string drawing is mainly determined by the energetic gluons emitted at large virtualities, while low-virtuality branchings only add smaller wrinkles to this. $\mathcal{P}_{\rm recon}$ therefore does not increase as fast as the product of the numbers of W^+ and W^- string pieces.

By contrast, scenario I only shows a small dependence on the parton shower cut-off scale: the ~ 0.5 fm thick strings produced ~ 0.1 fm apart can overlap even if no gluons at all are emitted, and introducing further structure to these strings can go both ways, with only a small net increase in overlap. To understand this, compare a $\mathrm{q\overline{q}}$ and a $\mathrm{q\overline{q}g}$ decay of a W at rest. In the former, the string is expanding out on two sides but always passes through the origin. In the latter, both string pieces (qg and $\mathrm{g\overline{q}}$) are boosted away from the origin. Two W's that decay to multijets will therefore usually have a smaller overlap close to the middle of the event than would two W's decaying to $\mathrm{q\overline{q}}$, which partly compensates for the gain in overlap away from the middle.

In Section 4.2 we argued that shower evolution at scales above 10 GeV occur at distances smaller than the separation between W^+ and W^- decays. However, also a parton with a virtuality below 10 GeV would often have time to branch and produce a new string piece which could interact — the W^+–W^- separation only sets a lower limit for how soon strings meeting head-on can collide. Further, because of the way the shower algorithm is constructed, the usage of an $m_0 = 10$ GeV cut-off in fact also removes some branching configurations that would be allowed for an $m = 10$ GeV parton in a shower with $m_0 = 1$ GeV. While it may be that a shower with $m_0 = 1$ GeV gives a string with more wrinkles than is realistically resolved at the time of overlap, the above arguments indicate that an $m_0 = 10$ GeV scenario is too far in the other extreme. A realistic range of uncertainty for $\mathcal{P}_{\rm recon}$ would probably correspond to the variation between $m_0 = 1$ GeV and $m_0 = 2$–3 GeV, i.e. at most a factor of 2 for scenario II and negligibly little for scenario I.

Even for c.m. energy, m_0 cut-off and other parameters fixed, the reconnection probability varies from one event to the next as a function of the partonic configuration generated on the perturbative level. Generally speaking, events with large partonic activity also have a large $\mathcal{P}_{\rm recon}$. Fig. 16a shows the dependence of $\mathcal{P}_{\rm recon}$ on the number of reconstructed jets (using `LUCLUS` with the default $d_{join} = 2.5$ GeV [6]). The reconnection probability varies by about a factor of 2 between small and large jet multiplicities. As explained in the previous paragraphs, results in scenario II are more sensitive to the number of partons, and therefore show a larger variation of $\mathcal{P}_{\rm recon}$ with $n_{\rm jet}$. Since a larger number of jets also translates into a larger charged multiplicity, $\mathcal{P}_{\rm recon}$ varies almost as much with $n_{\rm ch}$ as with $n_{\rm jet}$, Fig. 16b. Again differences between scenarios I and II are obvious. Among simpler measures, the charged multiplicity seems to be the one that gives the largest variation in $\mathcal{P}_{\rm recon}$. By contrast, global event measures such as thrust mainly reflect the topology of the $\mathrm{q_1\overline{q}_2q_3\overline{q}_4}$ configuration (before parton showers) and $\mathcal{P}_{\rm recon}$ is therefore rather insensitive to them. The T_4, i.e. the thrust minimized with respect to four different jet directions, is of about comparable quality with $n_{\rm ch}$.

5.2 Event properties

In Fig. 2 we showed how large the effects of reconnections can be in the case of a particularly favourable event topology and instantaneous reconnections. It is now time to

see how much of that survives. We have already demonstrated that the instantaneous reconnection scenario is incompatible with perturbative QCD calculations. Furthermore, phase space is vanishing for the topology of Fig. 2, i.e. with the W^+ and W^- at rest. While some selection might still be made based on event topology, to first approximation it is more realistic to integrate over all configurations at a fixed c.m. energy. The intermediate reconnection scenario shown in Fig. 3 is therefore a more reliable guide to how large are the effects to be expected. With the exception of the W mass plot, differences to the no-reconnection baseline scenario are small. The results of Fig. 3 were still for 100% reconnected events. A realistic scenario with ∼30% reconnection, as obtained above, would therefore be expected to show even smaller differences to the no-reconnection scenario. The reduction would not have to be exactly by a factor of 0.3, since our scenarios I and II allow reconnections to take place between any two string pieces, while the intermediate scenario assumes all reconnections to occur in the middle of the event.

As expected, the charged multiplicity distribution comes out very similar with and without reconnection, Fig. 17a. The averages are $\langle n_{\rm ch} \rangle = 36.63$, 36.31 and 36.45 for no reconnection, scenario I and scenario II, respectively. These numbers are based on a Monte Carlo sample of 40,000 events, so with a width of the multiplicity distributions of about 7.9 this gives a statistical error of 0.04. The differences between the models thus are statistically significant, but are at a level well below experimental observability: LEP 2 will have to face lower statistics, a large background from other processes, QED radiation from the initial and final state, and a need to construct the expected no-reconnection multiplicity by extrapolation from Z^0 data at LEP 1. On top of that, essentially all the multiplicity difference is appearing in the low-momentum region, $|\mathbf{p}| < 1$ GeV, where detector efficiency may be limited.

Unfortunately, effects seem to be very small also for the other simple event properties we have studied, such as the rapidity distribution $\mathrm{d}n_{\rm ch}/\mathrm{d}y$, the number of charged particles in $|y| < 1$, the thrust and T_4 distributions, and the number of jets. Also trivial correlations, such as the average charged multiplicity as a function of the number of jets, show no significant effects.

It will therefore be necessary to devise more specific measures, which are intended to probe in detail the regions of phase space where differences are expected. This will be a delicate task, and we have no good proposal at the moment. As an example, which again does not show sufficiently large effects to be interesting in itself, consider Fig. 17b. Exactly four jets are found in each event with `LUCLUS`, and all particles are assigned to one of these jets. The azimuthal distribution of particles around the jet axis is plotted for particles belonging to the jet, with $\varphi = 0$ defined by the nearest other jet. No attempt is made to specify an orientation around the jet axis to distinguish $-\varphi$ from $+\varphi$, so the range is $0 \leq \varphi \leq \pi$. For the plot in Fig. 17b we have additionally required that the opening angle to the nearest jet should be at least 1 radian, and only considered particles with a transverse momentum relative to the jet axis in the range $0.3 \text{ GeV} < p_\perp < 0.8 \text{ GeV}$. These cuts slightly enhance the dynamical effects discussed below, but are not essential.

To zeroth approximation one would expect a flat distribution $\mathrm{d}n/\mathrm{d}\varphi$. To first approximation, the particle density should be suppressed close to $\varphi = 0$, since particles which emerge in that direction can easily be assigned to the nearest other jet instead. There should also be a somewhat smaller suppression close to $\varphi = \pi$, around the next-to-nearest other jet — remember that the event topology is essentially that of two back-to-back jet pairs, one pair from each W, so the nearest and next-to-nearest jets should be close to opposite in azimuth. On top of this now comes potential dynamical string effects. The

original string stretchings are between almost back-to-back jets, and therefore are not expected to give large azimuthal anisotropies. In addition, with our choice of $\varphi = 0$, the azimuthal angle of the almost back-to-back jet is fairly isotropically distributed. If a reconnection occurs, it will therefore show up as a string stretched either to the nearest or to the next-to-nearest other jet, i.e. lead to more particle production close to $\varphi = 0$ or $\varphi = \pi$ and less at around $\varphi = \pi/2$. Unfortunately, it seems that effects in scenarios I and II are too small to be detectable, although the results for the (unphysical) instantaneous scenario confirm that the distribution is in principle sensitive to effects.

A more ambitious goal would be to search for phenomena that would be impossible without reconnections. However, the ones we have been able to think of are all flawed. Consider e.g. the production of particles at large $x = 2E/E_{\rm cm}$. The kinematical limit is $x \leq 1$ in an $\mathrm{e^+e^-} \to \gamma^*/\mathrm{Z}^0 \to \mathrm{q\overline{q}}$ event, but less in an $\mathrm{e^+e^-} \to \mathrm{W^+W^-} \to \mathrm{q_1\overline{q}_2q_3\overline{q}_4}$ one, because the energy is shared between more primary partons. For instance, for the two W's at rest and with equal masses the limit is $x \leq 1/2$. So an excess at large x would be a signal that particles are allowed to pick up energy from both the $\mathrm{W^+}$ and $\mathrm{W^-}$ during the fragmentation stage, i.e. evidence for reconnections. However, the string topology has to be very special for large-x production to be possible at all, with e.g. the $\mathrm{q_1}$ and $\overline{\mathrm{q}}_4$ closely parallel. Therefore we do not observe a large-x excess in the reconnection scenarios. Even if we had done so, the excess would have had to be very large to be able to compete against the background of $\mathrm{e^+e^-} \to \gamma^*/\mathrm{Z}^0 \to \mathrm{q\overline{q}g}$ events with the same topology, where large-x production is not suppressed.

String reconnection would also allow a new way of producing J/ψ mesons: in a $\mathrm{W^+W^-} \to \mathrm{c\overline{s}\,s\overline{c}}$ event the c and $\overline{\mathrm{c}}$ may be reconnected into a colour singlet, which 'collapses' into one single J/ψ particle. (If the $\mathrm{c\overline{c}}$ invariant mass is too large, the system will fragment into a pair of D mesons plus further hadrons, a final state which is indistinguishable from no-reconnection D meson production.) In a sample of 50,000 scenario II hadronic $\mathrm{W^+W^-}$ events we found one such occurrence. This is overwhelmed by a ten times larger background from $\mathrm{c} \to \mathrm{c\,g} \to \mathrm{c\,\overline{c}c} \to \mathrm{J}/\psi\,\mathrm{c}$, i.e. parton shower branchings followed by a 'collapse' of a low-mass colour singlet $\mathrm{c\overline{c}}$ system, and $\mathrm{W^+} \to \mathrm{c\overline{b}}$ decays and $\mathrm{g} \to \mathrm{b\overline{b}}$ shower branchings with a B hadron decaying to J/ψ. In an experiment with several hundred times the expected LEP 2 statistics, one could presumably also require a large x to enhance the signal, but the background from processes such as $\gamma^*/\mathrm{Z}^0 \to \mathrm{b\overline{b}g}$ would almost certainly be overwhelming.

We close this subsection with an indirect investigation of string reconnection effects, viewed as a function of the position of the string piece where the reconnection is occurring. In our approach it is not meaningful to try to define position better than this, i.e. to a specific point along the string piece, since the whole piece is affected by a reconnection. If partons are ordered along the (original) string from one end to the other, and partons on the two sides of the affected string piece have total energies E_1 and E_2 in the rest frame of the W, then the reconnection position can be defined by

$$d_{\rm rec} = \frac{|E_1 - E_2|}{E_1 + E_2} \; , \tag{71}$$

where the denominator is nothing but the mass of the W. A $d_{\rm rec} \approx 0$ corresponds to a reconnection close to the middle of the string, while a $d_{\rm rec} \approx 1$ is a reconnection close to the string endpoint. Each reconnection is characterized by one $d_{\rm rec}$ for the $\mathrm{W^+}$ and one for the $\mathrm{W^-}$; below we only consider the average $\overline{d}_{\rm rec} = (d^-_{\rm rec} + d^+_{\rm rec})/2$. The distribution of $\overline{d}_{\rm rec}$ values is shown in Fig. 18a. The mean is $\langle \overline{d}_{\rm rec} \rangle \approx 0.18$. However, this number

comes from the convolution of two effects, the one quoted above and the parton shower evolution. The latter allows the two jets to have different masses and thus $E_1 \neq E_2$. In the intermediate scenario, where naïvely reconnections occur at $\overline{d}_{\rm rec} \equiv 0$, parton showers actually give a $\langle \overline{d}_{\rm rec} \rangle \approx 0.06$.

One would like to study how a reconnection changes e.g. the multiplicity of an event, as a function of $\overline{d}_{\rm rec}$. However, effects are too small to be studied well that way, given that fluctuations in the fragmentation process are non-negligible. Instead we use the λ-measure of string length [25], which is roughly proportional to the expected hadronic multiplicity but does not contain the fragmentation fluctuations. The complete formulae for λ are quite complicated, but it is here enough to use the simpler form

$$\lambda = \sum_i \ln\left(1 + \frac{m_i^2}{m_\rho^2}\right) \quad . \tag{72}$$

The sum runs over all string pieces i in the event, with m_i the string piece invariant mass (calculated from the momenta of the partons that span the string, with gluon momenta split equally between the two adjacent pieces), while m_ρ sets a suitable hadronic mass scale. A reconnection means that two terms in the sum have to be replaced by two new terms. The change induced by a reconnection is defined as $\Delta\lambda = \lambda_{\rm new} - \lambda_{\rm old}$.

Fig. 18b shows how $\langle \Delta\lambda \rangle$ varies as a function of $\overline{d}_{\rm rec}$. To set the scale, $\langle \lambda \rangle \approx 20$. In fact, not much variation is observed in scenario I. In scenario II there is a clear trend that reconnections at larger $\overline{d}_{\rm rec}$ give a smaller change $\Delta\lambda$. In part, this is related to a larger admixture of reconnections with a topology like the one shown in Fig. 14c. In scenario II$'$, where events with an increased string length are removed, almost the same behaviour is recovered as in scenario I. (The cut in scenario II$'$ is in terms of the criterion $m_{14}m_{23} > m_{12}m_{34}$, which is essentially equivalent to $\Delta\lambda > 0$.) This does not fully explain why the curves are so flat for scenario I, since also this scenario contains reconnections with $\Delta\lambda < 0$, although fewer, and these were not removed.

In principle, the $\overline{d}_{\rm rec}$ and $\Delta\lambda$ quantities could be related to experimental observables, such as the event topology and multiplicities in different regions of the event. Unfortunately, the results above then indicate that it may be difficult to distinguish between scenarios I and II experimentally, given that minor variations of scenario II may give a spread in observables as big as the one between scenarios I and II in the first place. Further studies are therefore needed to understand the implications of reconnections as a function of event topology and reconnection scenario, and to invent more sensitive experimental observables.

5.3 W mass determinations

The most critical single observable for LEP 2 physics is the W mass. Experimentally, $m_{\rm W}$ depends on all particle momenta of an event in a non-trivial fashion.

If there are no interference effects between the $\rm W^+$ and $\rm W^-$ decays, each final state particle uniquely comes from one of the decays. Given a correct separation of particles into these two classes, the $\rm W^\pm$ four-momenta can be reconstructed and squared to give the $\rm W^\pm$ masses. In practice, several complications have to be faced:

1. the purely statistical error is $\sim \Gamma_{\rm W}/\sqrt{n}$ for n observed W's, from the fluctuations in the mass of produced W's;

2. the average W mass at LEP 2 is not the fundamental W mass parameter of the theory, since it is offset because of phase-space and (Born-level) matrix-element distortions, and of higher-order QED and weak corrections;
3. background events may be mistaken for signal ones;
4. particle four-momentum determinations have experimental errors;
5. some particles are not observed at all, e.g. neutrinos from charm decays and particles at low angles to the beam direction;
6. initial state photons may go unobserved or may (mistakenly) be assigned to either W;
7. a particle coming from the W^+ decay may be assigned to the W^-, and vice versa; and, finally,
8. QCD interference effects, perturbative or non-perturbative, may efface the separate identities of the W^+ and W^- systems.

It is not our intention to cover points 1–6 here; for a study of those aspects see ref. [3]. The first two points are sidestepped by comparing, event by event, the actually generated W masses with the reconstructed ones. (For an 80 GeV input mass the actually generated average mass is 79.2 GeV at our standard energy of 170 GeV. The 0.8 GeV difference, or whatever a more detailed formalism gives, can always be compensated analytically at the end of the day.) Background processes are not at all studied; presumably they can be controlled by fairly standard cuts. Points 4–6 would experimentally be addressed by a variety of techniques, including making use of energy–momentum constraints, based on the known beam energy. We, however, will assume that all particles are perfectly well measured.

If a particle or a collection of particles (of reasonably small total energy) are misassigned between the W^+ and W^-, it is easy to see that the W^+ and W^- mass estimates will be shifted in opposite directions. The shifts do not have to have the same size, but a significant cancellation of errors is obtained if the average $\overline{m}_\mathrm{W} = (m^+_\mathrm{W} + m^-_\mathrm{W})/2$ is used rather than the individual W masses. The cancellation more than compensates for the statistics loss of having only one W mass number from each event rather than two. Experimentally, the assumption that the two W masses of the events are the same is even more useful: if the beam energy is known and initial state QED radiation is neglected then only one number need be determined, namely $p^* = |\mathbf{p}^+| = |\mathbf{p}^-|$. This number mainly depends on the (acollinearity) angles between jets, which presumably can be measured well, while less well measured jet energies can be constrained by kinematics.

To study the effects of point 8, and those of point 7 that survive the W mass averaging, the following procedure is adopted. The `LUCLUS` algorithm [6] is used to reconstruct four or more jets, with the jet distance parameter $d_{join} = 8$ GeV. This gives almost 25% of events with five or more jets. These events are eliminated from the subsequent analysis, since events which contain hard gluon radiation give much worse W mass resolution — a whole jet may be misassigned. Further, it is required that each jet has an energy of at least 20 GeV and that the distance between any two jets is larger than 0.5 radians — misassignment of particles is much more likely if two jets are nearby. In total about 60% of the events survive all the cuts (the number goes up to about 64% for the instantaneous scenario, owing to a reduced amount of QCD radiation). The cuts have not been optimized, but should constitute a sensible first approximation. For the surviving events, the jet–jet invariant masses are calculated.

The four jets may be paired in three different ways, so that each event yields three

possible $\overline{m}_{\mathrm{W}}$ values. Very often one combination stands out as the most likely one, but ambiguities are not so infrequent. It is quite feasible to histogram all three combinations and treat the wrong ones as a background to the peak. We have instead tried a few different criteria to pick one of the three combinations.

1. In a Monte Carlo one has the advantage of knowing the original $\mathrm{q}_1\overline{\mathrm{q}}_2\mathrm{q}_3\overline{\mathrm{q}}_4$ configuration, before parton showers and fragmentation. The reconstructed jets are thus matched one-to-one to the original partons; this is done by picking the matching that minimizes the product of the invariant masses between each jet and its associated parton. The subdivision into W^+ and W^- jets is thereafter automatic.
2. Since we already know that the W mass is close to 80 GeV, one may pick the combination that minimizes $|\overline{m}_{\mathrm{W}} - 80|$.
3. It could be argued that the above recipe would accept false combinations, where one mass is too small and the other too large, so alternatively one could instead minimize $|m_{\mathrm{W}}^{(1)} - 80| + |m_{\mathrm{W}}^{(2)} - 80|$, where $m_{\mathrm{W}}^{(1,2)}$ are the two reconstructed jet–jet masses.
4. Close to threshold the jets from the same W should be almost back-to-back. One can therefore maximize the sum of opening angles between jets from the same pair.

By and large, these procedures give comparable results. In particular, the use of parton-level information in the first procedure does not offer significant gains — ambiguities in events mainly arise because of hard QCD radiation, and then the original $\mathrm{q}_1\overline{\mathrm{q}}_2\mathrm{q}_3\overline{\mathrm{q}}_4$ configuration is not too reliable a guide.

The results presented in Section 2 and Fig. 3d are based on the first method. Corresponding results for scenarios I and II are shown in Fig. 19a, while Figs. 19b–19d show results for methods 2, 3 and 4. Considering the no-reconnection events, method number 2 is the one that gives the smallest systematic offset, $\langle \Delta\overline{m}_{\mathrm{W}} \rangle = \langle (\overline{m}_{\mathrm{W}})_{\mathrm{reconstructed}} - (\overline{m}_{\mathrm{W}})_{\mathrm{generated}} \rangle$, see Table 1. Method number 1 gives the narrowest distribution, defined in terms of the width of the $\Delta\overline{m}_{\mathrm{W}}$ distribution in the range ± 10 GeV. Since this method makes use of knowledge hidden in real life, unlike the others, it is surprising that the advantage is not bigger than it is. Method number 4, which makes no assumption about the W mass value, is the least successful one. The tails of the $\Delta\overline{m}_{\mathrm{W}}$ distributions are very broad and act to push up the width. To the spreads $\sigma(\overline{m}_{\mathrm{W}})$ of Table 1 should be added the effect of the far wings, when $|\Delta\overline{m}_{\mathrm{W}}|$ is larger than 10 GeV. Typically 2%–4% are found in these regions; predominantly $\Delta\overline{m}_{\mathrm{W}} < 10$ GeV for methods 1 and 3 and $\Delta\overline{m}_{\mathrm{W}} > 10$ GeV for methods 2 and 4. The importance of the wings should not be overstated; any actual fitting program for the W mass would be mostly sensitive to events in the region close to the peak.

The systematic mass shifts obtained for the no-reconnection scenario are not so critical: they can be calculated by standard Monte Carlo methods and corrected for. Any method that performs well in other respects can therefore be adopted, even when it is known to induce a non-negligible systematic shift. Worse is any additional shift appearing when reconnection effects are considered. Such shifts may have to be included among the systematic errors of an experimental W mass determination. Also other aspects of the distributions could be of some importance, such as the differences in peak height visible in Fig. 19.

The systematic mass shifts of scenarios I and II are shown in Table 1. Numbers are also given for the intermediate and instantaneous scenarios: although we know these latter two to be unphysical, they are somewhat easier to study because of the larger size of the shifts.

If shifts are suitably scaled down, the instantaneous scenario may also give some feel for the size of potential perturbative effects. Rather surprisingly, the sign of the mass shifts need not be the same. Specifically, while the reconstructed $\overline{m}_{\mathrm{W}}$ always is shifted upwards in the intermediate and instantaneous scenarios, compared to the no-reconnection one, the shifts are very small and of uncertain sign for scenario I and large and negative for scenario II.

We have no detailed understanding of these mass shifts, but a few general comments can be made. One way of viewing the W mass determination is to consider the angles between the four jets. If those jets appear as two back-to-back pairs then the event is reconstructed as two W's at rest, with a mass sum equal to the c.m. energy. The further away from 180° the angle between the two jets of a W gets to be, the lower is its mass, other things being the same. Now consider the two original massless partons from one of the W decays, where the W is not at rest. The W mass is then given by

$$m^2 = (p_1 + p_2)^2 = 2E_1E_2(1 - \cos\theta_{12}) \; . \tag{73}$$

The fragmentation products are boosted in the W direction of motion, and thus soft particles are shifted into the angular range between partons 1 and 2 (the familiar string/dipole result). This leads to a systematic shift inwards of reconstructed jet directions [26], i.e. a reduction of θ_{12}. Were eq. (73) to be used, this would lead to an underestimate of m. However, the fragmentation also implies that the two reconstructed jets acquire masses $m_{1,2}$, so that the correct formula to use is

$$m^2 = m_1^2 + m_2^2 + 2E_1E_2 - 2\sqrt{E_1^2 - m_1^2}\sqrt{E_2^2 - m_2^2}\cos\theta_{12} \; . \tag{74}$$

The introduction of jet masses exactly compensates the reduction in θ_{12}.

Let us now assume that a reconnection occurs before the fragmentation. Depending on how the new strings are stretched, i.e. how soft particles are distributed between jets, the reconstructed θ_{12} may be shifted in different directions. As a first approximation, imagine that this shift is completely at random, i.e. that the new colour partner is isotropically distributed in azimuth with respect to the old partner. On the average, θ_{12} then remains unchanged in the fragmentation stage, rather than being reduced. If eq. (74) is still used, the mass terms will then lead to m being overestimated. This is likely to be what is going on in the intermediate and instantaneous reconnection scenarios.

In scenarios I and II, reconnections do not necessarily occur close to the middle of events, i.e. close to the original $\mathrm{W}^+\mathrm{W}^-$ production and decay volume. Many low-momentum particles will therefore be distributed along the naïve string direction, as if no reconnection had occurred. The mass shift then also comes from other regions of the event, which are less transparent to analyse. Branchings at the end of the parton showers (which occur late and therefore should maybe not be included in the reconnection description) do not seem to play any particular rôle: results with $m_0 = 2$ GeV are consistent with the default $m_0 = 1$ GeV ones. Also note that the results for scenario II′ are very close to those of scenario II, i.e. here reconnections that increase the string length do not seem to have any special significance, unlike the results of Fig. 18b. It is tempting to speculate that the observed difference could be related to the fact that string crossings have to be 'head-on' in scenarios II and II′ while they need only be grazing in scenario I, and that this translates into different sets of events for which reconnections occur away from the middle.

The numbers in Table 1 are based on a total statistics of 160,000 events for each of the scenarios considered, whereof $n \approx 100,000$ survive the cuts. (The statistical error on the W mass will be limited by the number of LEP 2 events. Here we are considering the statistical error on an evaluation of a systematic error, and for this purpose Monte Carlo statistics well in excess of the experimental sample is not inappropriate.) This gives a typical error of $\sigma(\overline{m}_{\mathrm{W}})/\sqrt{n} \approx 2$ GeV$/10^{2.5} \approx 6$ MeV for each $\langle \Delta \overline{m}_{\mathrm{W}} \rangle$ determination in a specific scenario and a factor of $\sqrt{2}$ larger than that for the systematic mass shift between scenarios. While systematic effects in the intermediate and instantaneous scenarios are thus established beyond doubt, the size of effects in scenarios I, II and II′ remains ill defined. From Table 1, one could assume that non-perturbative effects are bounded by 30 MeV, say. Admittedly, some numbers for scenarios II and II′ are slightly larger than this, but optimized methods are likely to do somewhat better. Although we primarily base ourselves on scenarios I and II, the 30 MeV number is also consistent with the intermediate scenario scaled down by $\mathcal{P}_{\mathrm{recon}} \approx 1/3$. We have argued that perturbative effects are strongly suppressed, by at least a factor of 10^{-2} compared with the instantaneous scenario, so any perturbative systematic effects should at most be at the 5 MeV level. There could also be an interplay between the perturbative and non-perturbative phases (see below in the summary). We have no way of estimating the size of such effects, but would not expect them to be larger than the ones we already studied. So assume it to be another 5 MeV, with numbers to be added linearly since they are not unrelated.

In total, our best estimate of the systematic uncertainty on the W mass would thus be a number roughly like 40 MeV from the reconnection phenomenon alone. In view of the limit set by LEP 2 statistics, this number is manageable, but not negligible. It may well be the largest individual source of systematic error for W mass determinations in doubly hadronic $\mathrm{W^+W^-}$ decays [3]. However, note that our W mass reconstruction methods are not the experimental ones. Other methods may be more or less sensitive to the differences between the scenarios: today we do not know. It is therefore important that each experimental m_{W} reconstruction method is checked against the scenarios in this paper. For instance, the importance given to the wings of the mass peak could quite likely be tuned to reduce the uncertainty by some amount. It is also important that the data are checked for any trace of reconnection effects. So far we did not find the good variable(s), but if the W mass is shifted by reconnection effects, this must mean that some particles somewhere in the event are affected. Detailed experimental studies, based on a deepened understanding of the reconnection phenomenon, should therefore allow a self-screening of the data to be carried out, with the possibility to apply systematic mass corrections as a function of the observed deviations from the no-reconnection scenario.

6 Summary and Outlook

It should by now be clear that the phenomenon of colour reconnection — which has to be there, at some level (remember $\mathrm{B} \to \mathrm{J}/\psi$) — is not totally understood. In this paper we have shown why perturbative colour rearrangements are strongly suppressed, while non-perturbative recouplings may be quite frequent. However, we are aware that the paper may raise more new questions than it answers old ones.

The main points of the pertubative description of the $\mathrm{W^+W^-} \to \mathrm{q_1\overline{q}_2q_3\overline{q}_4}$ production not far from threshold are the following:

- Any reconnection effects come with a factor $\alpha_s^2/(N_C^2 - 1)$, i.e. they cannot appear

in first but only in second order, and are colour-suppressed.

- The difference between the W^+ and W^- decay times implies a relative phase between the radiation accompanying the $W^\pm$ decays. This leads to a suppression of the interference terms for gluon energies $\omega \gtrsim \Gamma_W$. Interference effects are thus limited to a few low-momentum hadrons.
- In a $W^+W^- \to q_1\overline{q}_2q_3\overline{q}_4$ decay the original dipole structure is $\widehat{12} + \widehat{34}$, while colour transmutation corresponds to an admixture of the further dipole combination $\widehat{14} + \widehat{23} - \widehat{13} - \widehat{24}$. The appearance of negative-sign dipoles can only be understood in an inclusive sense, i.e. the complete dipole combination is active in the production of particles in each hadronic event.
- In the total cross section, the cancellation between real and virtual soft gluon emission leads to the interference terms being suppressed by at least a factor of Γ_W/m_W, in addition to the overall factor $\alpha_s^2/(N_C^2 - 1)$ noted above.

Of course, the degree of suppression of interference terms needs to be analysed for each specific observable. The suppression need not always be large. Generically, the higher the degree of inclusiveness, the stronger the suppression.

In order to address non-perturbative colour reconnection effects, we have developed several alternative models for the space–time structure of the string fragmentation process. To the best of our knowledge, nothing similar has ever been attempted before. Our two main scenarios are called I and II, by analogy with type I and type II superconductors, respectively. The type II superconductor is often used as a toy model for confinement in QCD, while scenario I is closely related to the bag model approach to QCD wave functions, so both have some credibility. Nature could well correspond to something in between these extremes, however, or even to something altogether different. Unlike the (amplitude-level-based) perturbative description, the (probabilistic) non-perturbative string always corresponds to a well-defined colour topology of the event: you either have strings $q_1\overline{q}_2$ and $q_3\overline{q}_4$ or strings $q_1\overline{q}_4$ and $q_3\overline{q}_2$, not both at the same time. And you do not have the negative-sign dipoles q_1q_3 and $\overline{q}_2\overline{q}_4$.

To make any progress at all, we have had to rely on models that are far from perfect. The uncertainty comes in many forms:

1. As a positive asset: the fact that different models for the colour string give different predictions means that it may be possible to learn about the structure of the QCD vacuum. It is here essential that the colour rearrangement is almost exclusively a non-perturbative phenomenon. Had perturbative aspects dominated, the whole topic would just have been one of testing our calculational skills, without any chance to learn something fundamentally new.
2. Because of 'laziness': we have introduced various approximations in the description of the string motion and the fragmentation process. With a lot of hard work, but without the need for any truly new ideas, it would be possible to improve on these aspects. The amount of work would be out of proportion with the potential gains in precision, however, so long as there is no possibility to receive any experimental feedback.
3. As a true limit in our current physics understanding: one example is the question of an interplay between the perturbative and non-perturbative phases, see discussion below.

To begin with, consider the production of two W's at rest. One of the two will decay first. The partons of this decay, both the original $q\overline{q}$ ones and additional bremsstrahlung

gluons (and $q'\overline{q}'$ pairs), will spread outwards from the origin with the speed of light. The partonic activity is therefore concentrated in an outward-moving shell of roughly $1/m_{\mathrm{W}}$ thickness, if one just considers the W decay process. The production of massive partons in the shower evolution increases the width of the shell by some amount, but does not change the overall picture. This shell is not equally populated, but contains 'hot spots' around the directions of the outgoing q and $\overline{q}$, while most of the shell is empty. Inside the expanding shell there are no perturbative partons, but only the softer confinement gluons.

When the second W decays, there is no possibility for its perturbative partons to interact directly with the pertubative partons of the first W: the first shell is always spreading ahead of the second one. However, the perturbative partons of the second W may directly interact with the left-behind confinement partons (i.e. the strings or colour flux tubes) of the first. This phenomenon is what we mean by an interplay between the perturbative and non-perturbative phases. Maybe it could one day be addressed as 'W decay and parton shower evolution in a heat bath', with techniques similar to those being developed in heavy-ion physics. For now, it is completely neglected. All colour rearrangements are therefore attributed to the interactions between the confinement gluons of the two W decays.

One can obtain very large reconnection effects with optimistic physics assumptions applied to idealized experimental conditions, cf. the GPZ study. However, if we consider a realistic physics model in a real-life situation, like $\mathrm{W}^+\mathrm{W}^-$ decay at LEP 2, all studied effects turn out to be very small. The most spectacular one is the implied 40 MeV systematic uncertainty on the W mass. The reader may well wonder: how come it is so difficult to find other variables that show large effects, when we already have one? Well, in fact, the W mass shifts we discuss here are not large, it is only that we are set to measure m_{W} with the highest possible accuracy. A 40 MeV uncertainty corresponds to a relative error on m_{W} of half a per mille. We already noted that the total charged multiplicity shows effects a factor of 10 bigger than this — but also concluded that various uncertainties will make $\langle n_{\mathrm{ch}} \rangle$ useless as a probe of reconnection effects. Maybe the best we can hope for is a probe that gives differences, if only at the per cent level, but where the no-reconnection prediction is very well understood. In the long run, we believe such measures will be constructed.

One interesting cross-check on models could potentially be provided by Bose–Einstein effects. The typical separation of W^+ and W^- decay vertices is smaller than the observed Bose–Einstein radius, so naïvely all hadrons could be viewed as produced from a single source. However, if the strings from the W^+ and W^- decays keep their separate identities, i.e. act as independent sources, the observable magnitude of Bose–Einstein effects will be smaller in $\mathrm{W}^+\mathrm{W}^-$ events than in Z^0 ones. A behaviour of this kind may already have been seen in the UA1 data [27]. It would be particularly exciting if the size of Bose–Einstein effects at LEP 2 varied as a function of event topology in a way related to the reconnection probability.

Our current 40 MeV estimate for systematic uncertainties on the W mass is the sum of 30 MeV from non-perturbative reconnections, 5 MeV from perturbative ones and (out of thin air) 5 MeV from the interplay of the perturbative and non-perturbative phases. The 30 MeV number depends sensitively on the assumed reconnection probability, which is a completely free parameter in scenario I and has a non-negligible uncertainty in scenario II. (Most notably, maybe strings can only reconnect the third of the time when the endpoint colours match.) However, the reconnection probability cannot be too low, or one would

not observe J/ψ in B decay. Even if, arbitrarily, one were to reduce the non-pertubative contribution by a factor of 2, the net uncertainty would still be 25 MeV, which is not quite negligible. The issue therefore has to be studied further, e.g. for the choice of the best experimental algorithm to use.

Despite its evident shortcomings (large missing momentum) the mixed leptonic–hadronic channel is free from the potential reconnection-induced ambiguities. Also QED-induced interference effects would be under control [13, 14, 15]. The relative importance to be assigned to results from different $\mathrm{W^+W^-}$ decay channels therefore has to be assessed carefully.

A high-statistics run above the $\mathrm{Z^0Z^0}$ threshold would allow an unambiguous determination of any systematic mass shift, given that the $\mathrm{Z^0}$ mass is already known from LEP 1 [28]. Such a shift could then be used to correct the W mass. If the various potential sources of systematic error could be disentangled, it could also imply a direct observation of reconnection effects. More generally, $\mathrm{Z^0}$ events from LEP 1 can be used to predict a number of properties for $\mathrm{Z^0Z^0}$ events, such as the charged multiplicity distribution. Any sign of deviations would provide important information on the reconnection issue.

Perturbative and non-perturbative calculations alike show only a very slow variation of effects with c.m. energy: there is no essential variation over the range of $\mathrm{W^+W^-}$ energies that can be probed by LEP 2. If we want to call colour reconnection a threshold effect, we have to acknowledge that the threshold region is very extended.

In some sense, the effects studied here could be considered as only the tip of an iceberg. Colour reconnection can occur in any process which involves the simultaneous presence of more than one colour singlet, such as $\mathrm{t\overline{t}}$ events, decays of colour singlet resonances produced in hadron colliders, and so on. Many of the techniques developed for $\mathrm{W^+W^-}$ could be directly applied to these problems. Additional aspects may have to be addresses, such as the presence of colour in the initial state for hadron colliders.

A related set of phenomena can occur in reactions with only one colour singlet, and hence without the possibility of a colour rearrangement in the sense of this paper. Specifically, we have in mind a simple process such as $\mathrm{e^+e^- \to t\overline{t} \to bW^+\,\overline{b}W^- \to b\ell^+\nu_\ell\,\overline{b}\ell^-\overline{\nu}_\ell}$. If the top mass is sufficiently large ($m_\mathrm{t} \gtrsim 120$ GeV) and one is not too far from threshold, the t and $\overline{\mathrm{t}}$ quarks do not have time to hadronize before they decay [29]. The b and $\overline{\mathrm{b}}$ therefore form part of one colour singlet. However, because of the time difference between the t and $\overline{\mathrm{t}}$ decays, emission of energetic gluons occurs independently from the b quark (the $\widehat{\mathrm{tb}}$ dipole) and from the $\overline{\mathrm{b}}$ one (the $\widehat{\overline{\mathrm{t}}\overline{\mathrm{b}}}$ dipole). The $\widehat{\mathrm{b}\overline{\mathrm{b}}}$ dipole is sterile in the same sense as discussed in section 3.5, i.e. it can only radiate gluons with $\omega \lesssim \Gamma_\mathrm{t}$. Therefore the connection between the b and the $\overline{\mathrm{b}}$ (each with accompanying hard gluons) is mainly provided by the long-distance fragmentation mechanism.

In addition to the observables we have considered, such as the W mass, quite a few other interesting phenomena could be affected as well. Among them are (see also [15]):

1. The possibility to discriminate between the co-called 1-string and 3-string scenarios [30] in the process $\mathrm{e^+e^- \to t\overline{t} \to bW^+\overline{b}W^-}$.
2. The 'b-quark attraction effect', namely the possible enhancement of the amplitude of the b-quarks near the origin in the field of t-quarks produced in the threshold region of the same process as above [31].
3. Effects of the $\overline{\mathrm{t}}\mathrm{b}$, $\mathrm{t}\overline{\mathrm{b}}$ and $\mathrm{b}\overline{\mathrm{b}}$ interactions on the forward–backward asymmetry in $\mathrm{e^+e^- \to t\overline{t}}$ [32].
4. The azimuthal asymmetry of b-jets in $\mathrm{t\overline{t}}$ events.

We therefore expect colour transmutation phenomena to be of topical interest over the years to come.

Acknowledgements

This work was supported in part by the UK Science and Engineering Research Council. The authors are grateful to Yu.L. Dokshitzer and V.S. Fadin for useful discussions.

References

[1] G. Gustafson, U. Pettersson and P. Zerwas, Phys. Lett. **B209** (1988) 90

[2] T. Sjöstrand, in 'e^+e^- Collisions at 500 GeV: The Physics Potential', ed. P.M. Zerwas, DESY 92-123A, p. 453

[3] LEP 2 workshop presentation by L. Camilleri at the LEPC open meeting, CERN, November 1992

[4] M. Bengtsson and T. Sjöstrand, Nucl. Phys. **B289** (1987) 810

[5] B. Andersson, G. Gustafson, G. Ingelman and T. Sjöstrand, Phys. Rep. **97** (1983) 31

[6] T. Sjöstrand, Comput. Phys. Commun. **39** (1986) 347;
T. Sjöstrand and M. Bengtsson, Comput. Phys. Commun. **43** (1987) 367

[7] H.-U. Bengtsson and T. Sjöstrand, Comput. Phys. Commun. **46** (1987) 43;
T. Sjöstrand, CERN-TH.6488/92

[8] R.W. Brown and K.O. Mikaelian, Phys. Rev. **D19** (1979) 922;
T. Muta, R. Najima and S. Wakaizumi, Mod. Phys. Lett. **A1** (1986) 203

[9] J.F. Gunion and Z. Kunszt, Phys. Rev. **D33** (1986) 665

[10] T. Hebbeker, Phys. Rep. **217** (1992) 69;
S. Bethke, in Proceedings of the XXVI International Conference on High Energy Physics, Dallas, Texas, 1992, ed. J.R. Sanford, AIP conference proceedings, vol. 1, p. 81

[11] Yu.L. Dokshitzer, V.A. Khoze, A.H. Mueller and S.I. Troyan, 'Basics of Perturbative QCD', ed. J. Tran Thanh Van (Editions Frontières, Gif-sur-Yvette, 1991)

[12] Yu.L. Dokshitzer, V.A. Khoze and S.I. Troyan, Z. Phys. **C55** (1992) 107

[13] Yu.L. Dokshitzer, V.A. Khoze, L.H. Orr and W.J. Stirling, Nucl. Phys. **B403** (1993) 65

[14] V.A. Khoze, L.H. Orr and W.J. Stirling, Nucl. Phys. **B378** (1992) 413

[15] V.S. Fadin, V.A. Khoze and A.D. Martin, Durham preprints DTP/93/18 and DTP/93/64

[16] V.S. Fadin, V.A. Khoze and A.D. Martin, Phys. Lett **B311** (1993) 311

[17] Ya.I. Azimov, Yu.L. Dokshitzer, V.A. Khoze and S.I. Troyan, Phys. Lett. **165B** (1985) 147

[18] Yu.L. Dokshitzer, V.A. Khoze, A.H. Mueller and S.I. Troyan, Rev. Mod. Phys. **60** (1988) 373

[19] B. Andersson, G. Gustafson and T. Sjöstrand, Phys. Lett. **94B** (1980) 211

[20] Yu.L. Dokshitzer, V.A. Khoze and S.I. Troyan, Sov. J. Nucl. Phys. **50** (1990) 505

[21] X. Artru and G. Mennessier, Nucl. Phys. **B70** (1974) 93

[22] T. Sjöstrand, Nucl. Phys. **B248** (1984) 469

[23] T.D. Gottschalk and D.A. Morris, Nucl. Phys. **B288** (1987) 729

[24] See Proc. Workshop on photon radiation from quarks, ed. S. Cartwright, CERN 92-04 (Geneva, 1992)

[25] B. Andersson, P. Dahlqvist and G. Gustafson, Z. Phys. **C44** (1989) 455

[26] JADE Collaboration, W. Bartel et al., Phys. Lett. **157B** (1985) 340

[27] UA1 Collaboration, C. Albajar et al., Phys. Lett. **B226** (1989) 410

[28] We thank V. Innocente for reminding us of this possibility

[29] J.H. Kühn, Acta Phys. Aust. Suppl. **24** (1982) 203;
I.I. Bigi, Yu.L. Dokshitzer, V.A. Khoze, J.H. Kühn and P.M. Zerwas, Phys. Lett. **B181** (1986) 157

[30] T. Sjöstrand and P. Zerwas, in 'e^+e^- Collisions at 500 GeV: The Physics Potential', ed. P.M. Zerwas, DESY 92-123A, p. 463

[31] M. Jezabek, J.H. Kühn and T. Teubner, Z. Phys. **C56** (1992) 653

[32] H. Murayama and Y. Sumino, Phys. Rev. **D47** (1992) 82

Table

Table 1: Systematic mass shifts for W mass determinations at 170 GeV. Results are for the four methods described in the text. The $\langle \Delta \overline{m}_{\mathrm{W}} \rangle$ and $\sigma(\Delta \overline{m}_{\mathrm{W}})$ numbers are the average and spread of the difference between the reconstructed and the generated $\overline{m}_{\mathrm{W}} = (m^{+}_{\mathrm{W}} + m^{-}_{\mathrm{W}})/2$ mass of an event, defined for the no-reconnection scenario. The further columns give the additional systematic mass shift obtained when reconnections are allowed, $\langle \delta \overline{m}_{\mathrm{W}} \rangle = \langle \Delta \overline{m}_{\mathrm{W}} \rangle^{\mathrm{recon}} - \langle \Delta \overline{m}_{\mathrm{W}} \rangle^{\mathrm{no-recon}} = \langle \overline{m}_{\mathrm{W}} \rangle^{\mathrm{recon}} - \langle \overline{m}_{\mathrm{W}} \rangle^{\mathrm{no-recon}}$. (The results for scenario II with $m_0 = 2$ GeV are relative to no-reconnection numbers with the same cut-off, not shown. This makes about 5 MeV difference, which would likely vanish if fragmentation parameters are properly retuned for the higher m_0 scale.) All numbers are in MeV. The statistical error on $\langle \Delta \overline{m}_{\mathrm{W}} \rangle$ is about 6 MeV and on each $\langle \delta \overline{m}_{\mathrm{W}} \rangle$ about 10 MeV.

Method	$\langle \Delta \overline{m}_{\mathrm{W}} \rangle$ (MeV)	$\sigma(\Delta \overline{m}_{\mathrm{W}})$ (MeV)	$\langle \delta \overline{m}_{\mathrm{W}} \rangle$ (MeV)					
			I	II	II ($m_0 = 2$)	II′	Inter-mediate	Instan-taneous
1	−276	1570	+14	−21	−23	−17	+136	+576
2	+158	2060	−10	−34	−33	−28	+62	+286
3	−355	2050	+14	−34	−31	−27	+88	+496
4	+471	2210	+1	−27	−28	−31	+74	+275

Figure Captions

Fig. 1 Schematic pictures of the toy alternatives of Section 2 (see text). In (b) to (d) the '+' sign separates (colour singlet) parton systems that fragment independently of each other.
a) Original parton configuration.
b) No reconnection.
c) Instantaneous reconnection, with reduced showering activity.
d) Intermediate reconnection, with same showering as in the no-reconnection case, but different fragmentation.

Fig. 2 Event properties when the two W's are at rest with a relative decay angle of 30°, see text.
a) Charged multiplicity.
b) Rapidity distribution of charged particles.
c) Charged multiplicity in the rapidity range $|y| < 1$.
d) Charged multiplicity flow in the first quadrant of the event planes (the other quadrants may be obtained by symmetry).
Full histograms for no reconnection, dashed for intermediate, and dash-dotted for instantaneous reconnection.

Fig. 3 Event properties at 170 GeV, for a mixture of W^+W^- events.
a) Charged multiplicity.
b) Rapidity distribution of charged particles.
c) Charged multiplicity in the rapidity range $|y| < 1$.
d) Difference between reconstructed and generated average W mass of an event.
Full histograms for no reconnection, dashed for intermediate, and dash-dotted for instantaneous reconnection.

Fig. 4 Diagrams for single primary gluon emission in $e^+e^- \to W^+W^- \to q_1\overline{q}_2q_3\overline{q}_4$. Here and in what follows the 'radiative blobs' are intended to reflect that the emission is caused by the conserved-colour quark currents.

Fig. 5 An example of a single-gluon decay–decay interference contribution to the cross section for $e^+e^- \to W^+W^- \to q_1\overline{q}_2q_3\overline{q}_4$. The gluons are real or virtual depending on the position of the vertical dashed line.

Fig. 6 Diagrams for double primary gluon emission in $e^+e^- \to W^+W^- \to q_1\overline{q}_2q_3\overline{q}_4$.

Fig. 7 Diagrams for radiatively corrected single gluon emission in $e^+e^- \to W^+W^- \to q_1\overline{q}_2q_3\overline{q}_4$. Colour rearrangement could arise as a result of interference between the diagrams of Fig. 4 and Fig. 7.

Fig. 8 An example of the double-gluon decay–decay interference contribution to the cross section for $e^+e^- \to W^+W^- \to q_1\overline{q}_2q_3\overline{q}_4$. Each gluon could be real or virtual depending on the position of the vertical dashed line.

Fig. 9 A W decaying to $qg_1g_2g_3\overline{q}$, with a schematic representation of the motion of the partons (arrows) and the strings (thick lines) drawn out between the partons.

Fig. 10 a) Average kinematical variables in W^+W^- events as a function of c.m. energy. Full the common momentum p^*, dashed (dash-dotted) the minimum (maximum) of the W^+ and W^- masses. For comparison, the dotted curve gives the naïve behaviour $p^* = \sqrt{(E_{cm}/2)^2 - m_W^2}$.
b) Average proper time of $W^\pm$ decays (full curve), and time (dashed) and space (dash-dotted) separation (in fm) between the W^+ and W^- decays, as a function of c.m. energy.

Fig. 11 Comparison of string topology with the lifetime of the parton taken into account (a) and not (b). See text for details. Dashed lines show past motion of partons, arrows indicate direction vectors of motion, and thick full lines represent the string.

Fig. 12 $\mathcal{I}(\beta)/\mathcal{I}(0)$, i.e. the overlap of two spherical colour sources normalized to the value at threshold. Full curve is for the full expression of eq. (59), dashed when $W^\pm$ are assumed to decay instantaneously, $\mathcal{P}(\tau^\pm) = \delta(\tau^\pm)$, and dash-dotted when $W^\pm$ are assumed to decay instantaneously and additionally the time retardation factor $\theta(t - |\mathbf{x}|)$ in eq. (54) is neglected.

Fig. 13 Probability for colour reconnection, $\mathcal{P}_{\text{recon}}$ according to eq. (60); full curve for $k_0 = 1$, dashed for $k_0 = 5$, and dash-dotted for $k_0 = 0.2$.

Fig. 14 Schematic illustration of string topologies, where any gluon has been represented by either a q or a $\overline{\text{q}}$ in such a way as to maintain the correct colour topology. Blobs represent positions of W decays, thin dashed lines and arrows indicate motion of string endpoints, thick dashed and full lines show strings before and after the reconnection. Figures (a), (b) and (c) are for different topologies, see text.

Fig. 15 Probability that a reconnection will occur as a function of (a) c.m. energy E_{cm} and (b) parton shower cut-off m_0. Full lines for scenario II and dashed ones for scenario I.

Fig. 16 Probability that a reconnection will occur as a function of (a) the number of jets in the event and (b) the charged multiplicity. Full lines for scenario II and dashed ones for scenario I. Kindly note that statistical fluctuations are not quite negligible in the few first and last bins.

Fig. 17 Event properties at 170 GeV, for a mixture of W^+W^- events.
a) Charged multiplicity.
b) Particle-multiplicity distribution around jet axis; see text for details.
Full lines for scenario II, dashed ones for scenario I, dash-dotted ones for no-reconnection and (in (b)) dotted ones for the instantaneous scenario.

Fig. 18 a) Distribution in $\overline{d}_{\text{rec}}$, the position of string reconnection, for 170 GeV W^+W^- events.
b) Average change in string length, $\langle \Delta\lambda \rangle$, as a function of $\overline{d}_{\text{rec}}$.
Full lines for scenario II, dashed ones for scenario I, and dotted ones for scenario II′.

Fig. 19 Difference between the reconstructed and generated average W mass of an event. Figures (a)–(d) correspond to methods 1–4 of Section 5.3 for picking the right pairing of jets. Full histogram for scenario II, dashed one for scenario I, dash-dotted for no-reconnection and dotted for the instantaneous scenario.

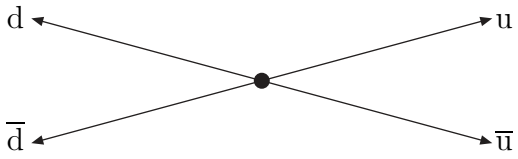
d
u
$\overline{\mathrm{d}}$
$\overline{\mathrm{u}}$

(a)

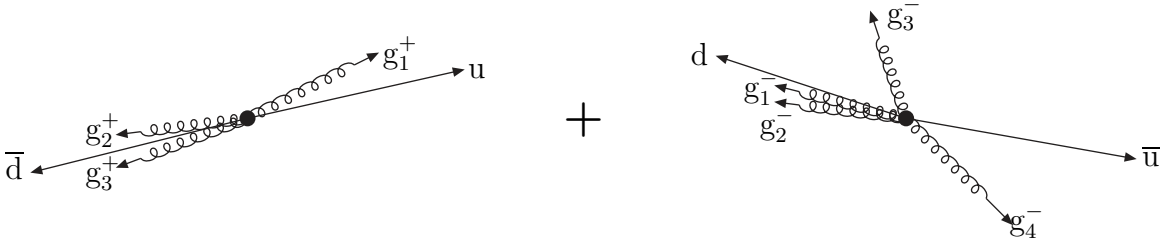
g_1^+
u
g_2^+
$\overline{\mathrm{d}}$
g_3^+
+
g_3^-
d
g_1^-
g_2^-
$\overline{\mathrm{u}}$
g_4^-

(b)


d
g
$\overline{\mathrm{d}}$
+
u
g
$\overline{\mathrm{u}}$

(c)

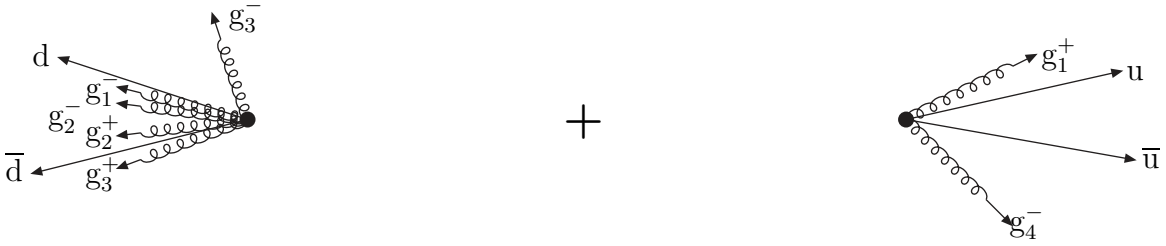
g_3^-
d
g_1^-
g_2^-
g_2^+
$\overline{\mathrm{d}}$
g_3^+
+
g_1^+
u
$\overline{\mathrm{u}}$
g_4^-

(d)

Fig. 1

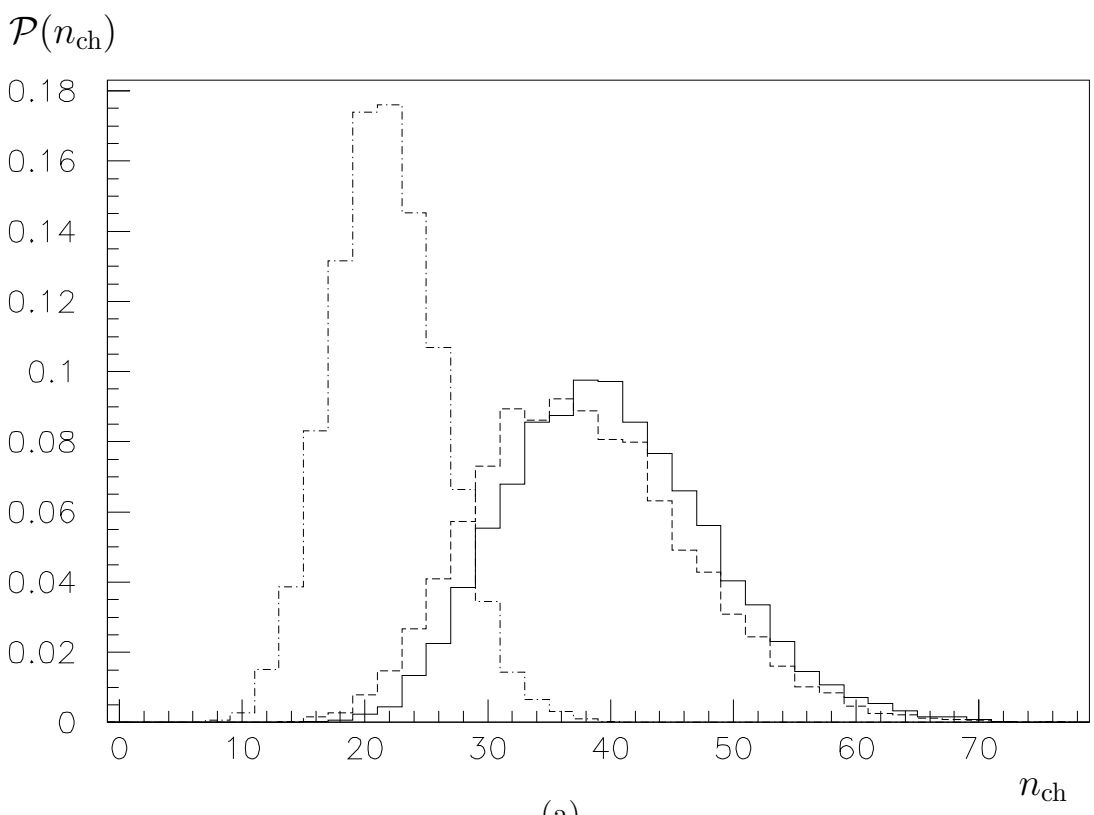
$\mathcal{P}(n_{\rm ch})$
0.18
0.16
0.14
0.12
0.1
0.08
0.06
0.04
0.02
0
0
10
20
30
40
50
60
70
$n_{\rm ch}$

(a)

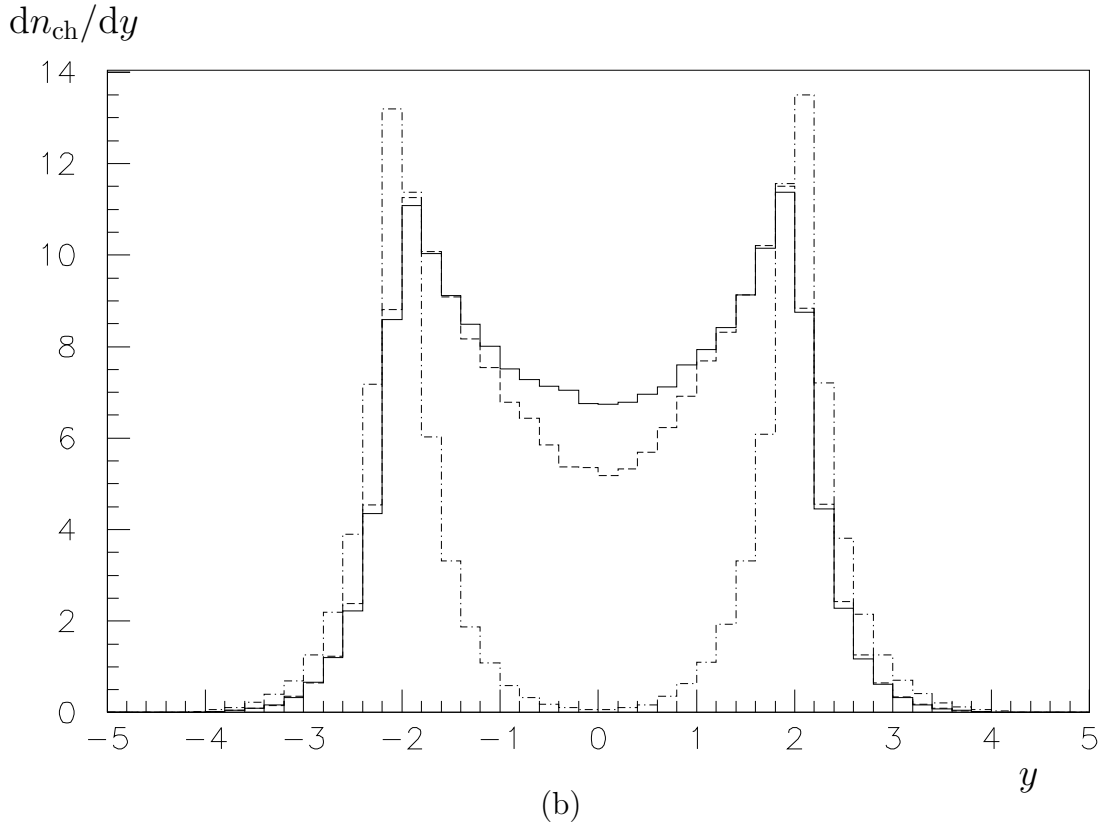
$\mathrm{d}n_{\rm ch}/\mathrm{d}y$
14
12
10
8
6
4
2
0
−5
−4
−3
−2
−1
0
1
2
3
4
5
y

(b)

Fig. 2

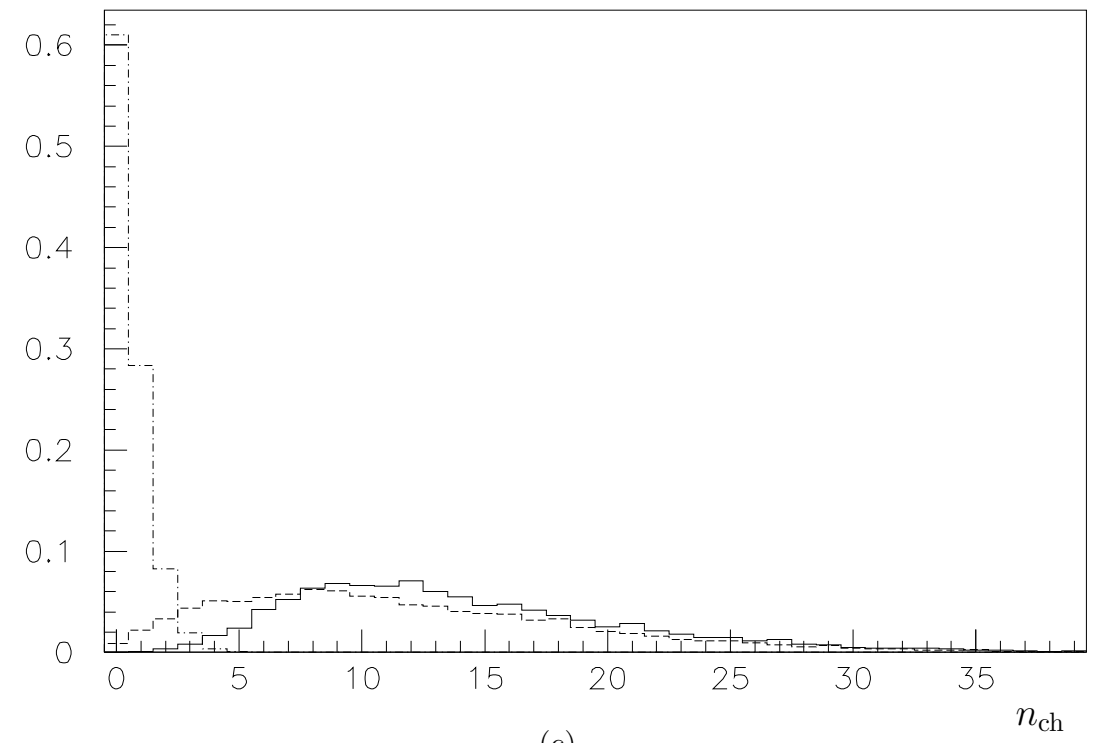
$\mathcal{P}(n_{\rm ch}$ in $|y| < 1)$
0.6
0.5
0.4
0.3
0.2
0.1
0
0
5
10
15
20
25
30
35
$n_{\rm ch}$

(c)

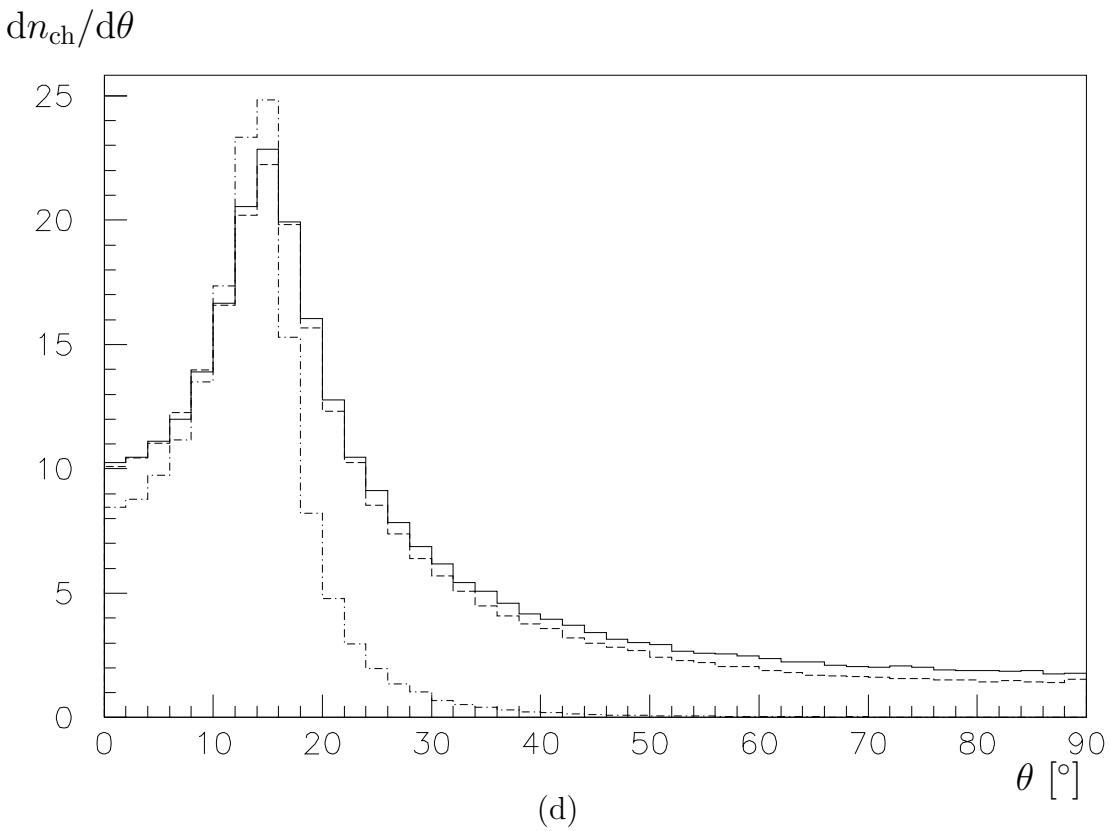
$\mathrm{d}n_{\rm ch}/\mathrm{d}\theta$
25
20
15
10
5
0
0
10
20
30
40
50
60
70
80
90
θ [°]

(d)

Fig. 2

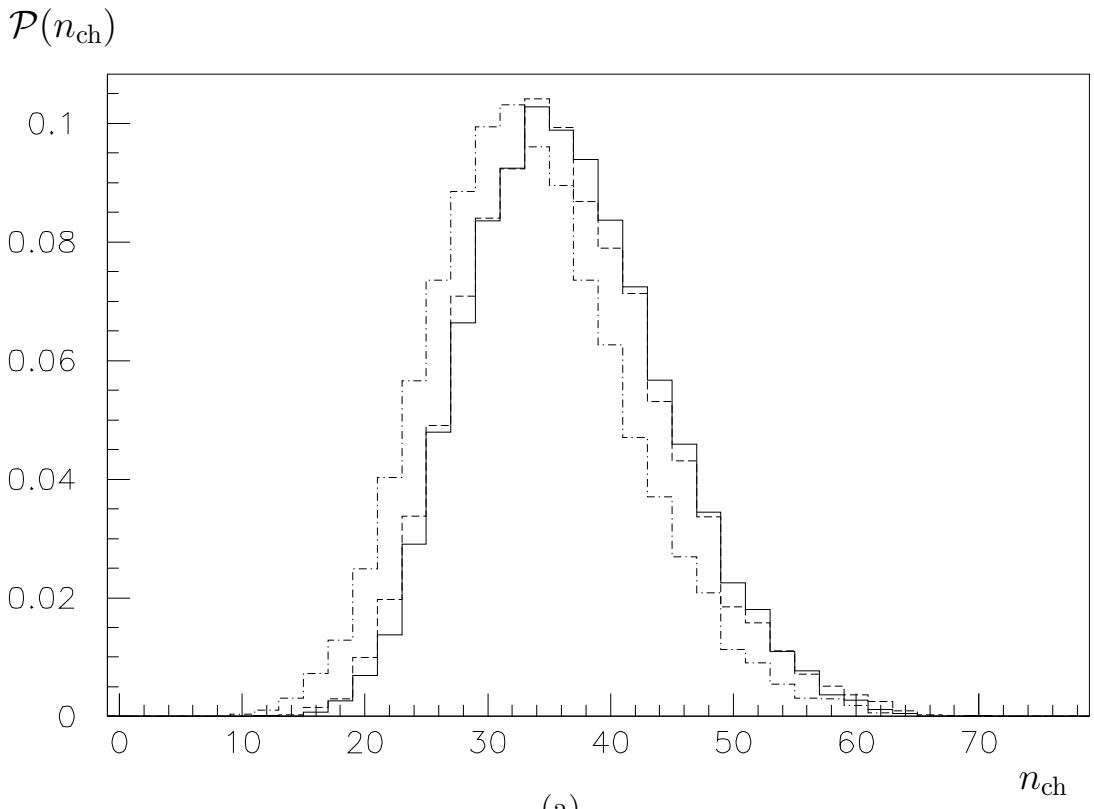
$\mathcal{P}(n_{\rm ch})$
0.1
0.08
0.06
0.04
0.02
0
0
10
20
30
40
50
60
70
$n_{\rm ch}$

(a)

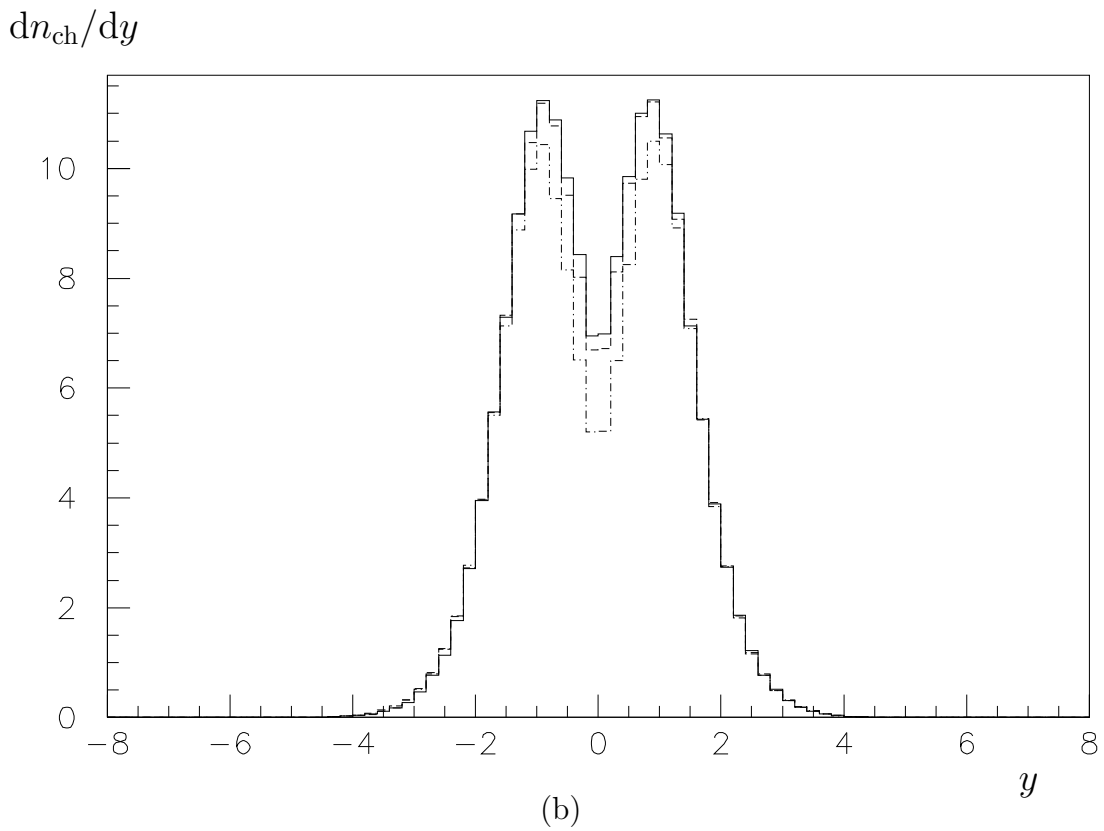
$\mathrm{d}n_{\rm ch}/\mathrm{d}y$
10
8
6
4
2
0
−8
−6
−4
−2
0
2
4
6
8
y

(b)

Fig. 3

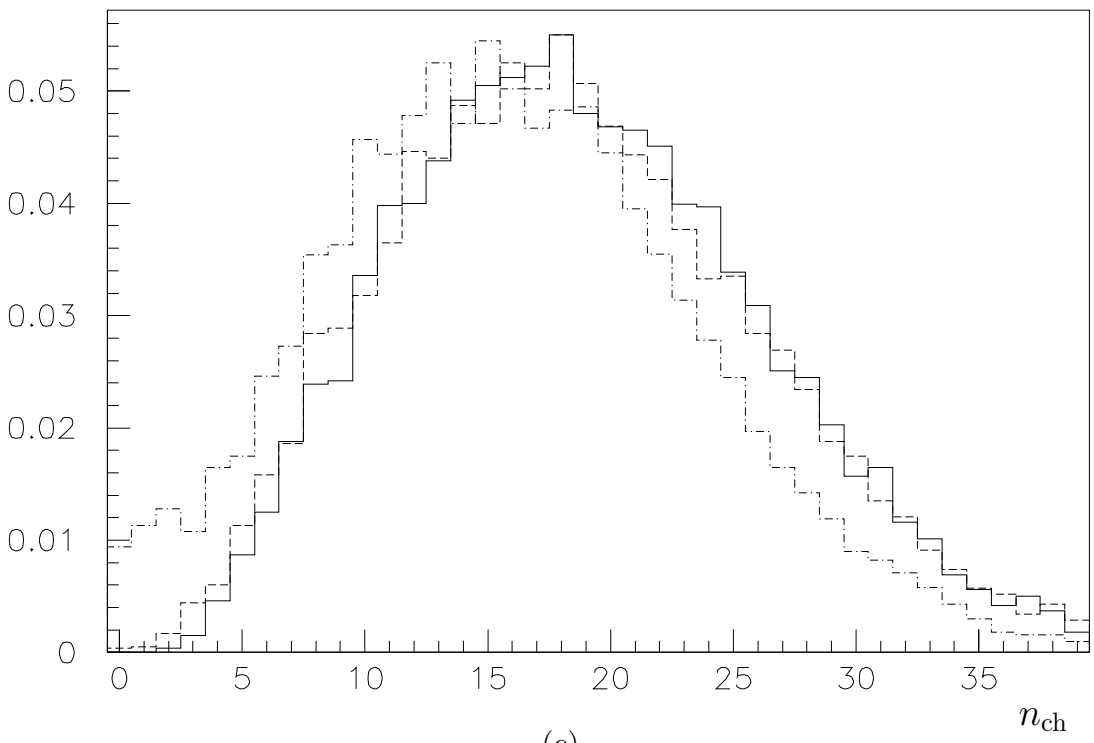
$\mathcal{P}(n_{\rm ch}$ in $|y| < 1)$
0.05
0.04
0.03
0.02
0.01
0
0
5
10
15
20
25
30
35
$n_{\rm ch}$

(c)

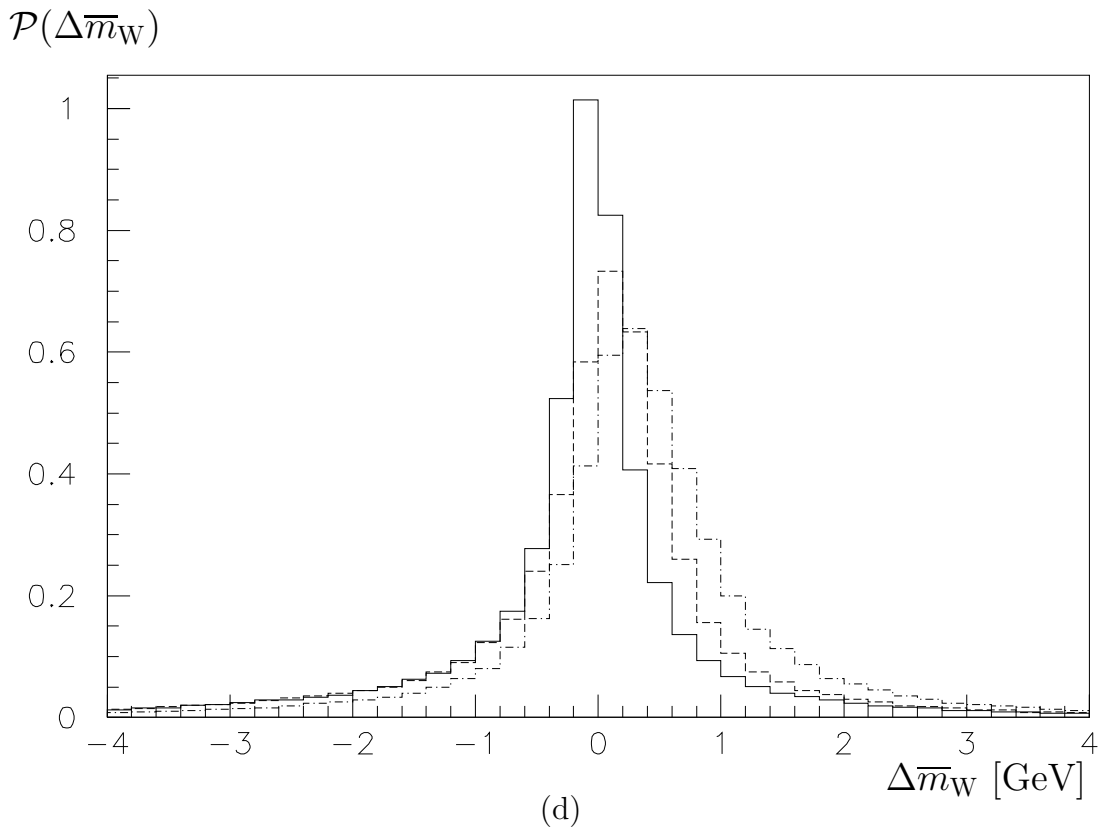
$\mathcal{P}(\Delta\overline{m}_{\rm W})$
1
0.8
0.6
0.4
0.2
0
−4
−3
−2
−1
0
1
2
3
4
$\Delta\overline{m}_{\rm W}$ [GeV]

(d)

Fig. 3

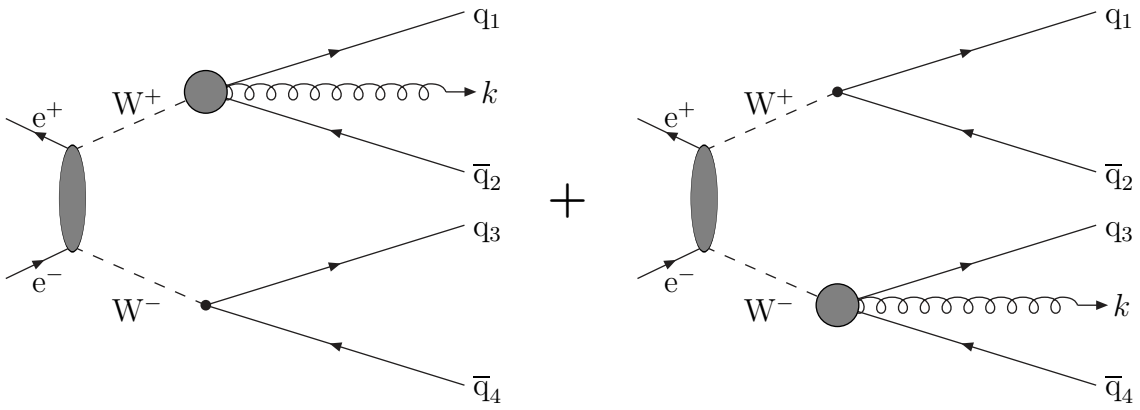

Fig. 4

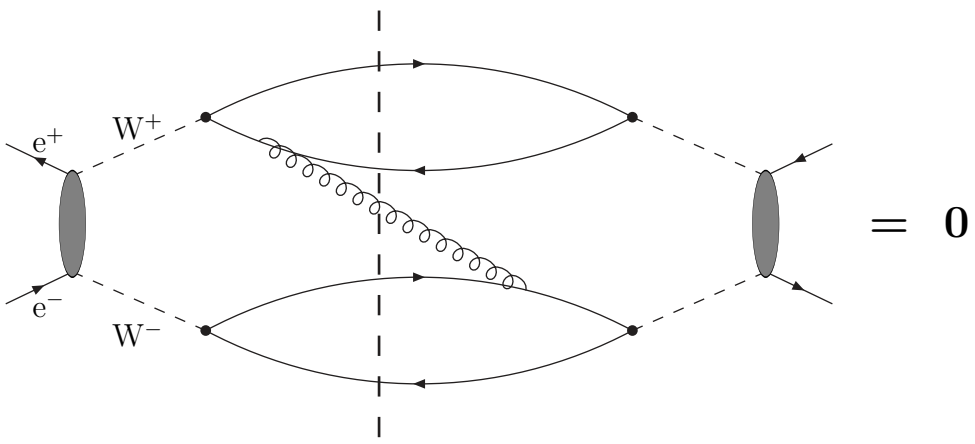

Fig. 5

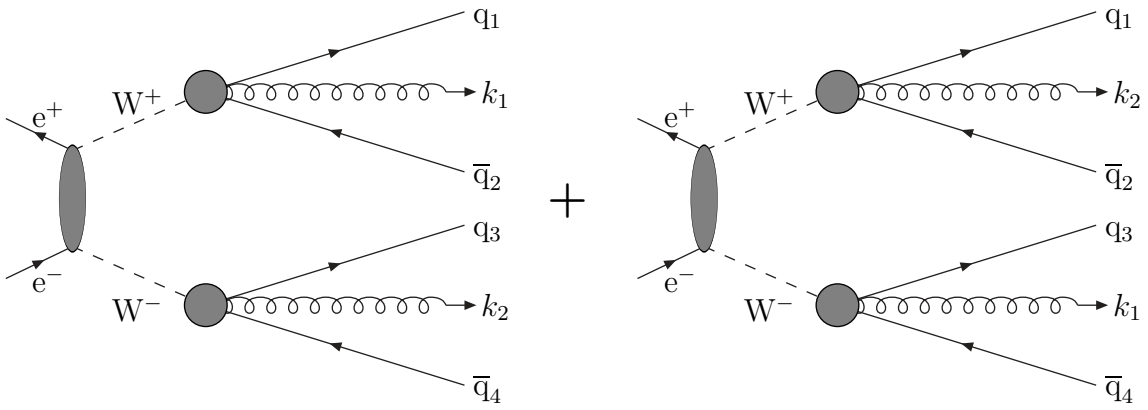
e+
e−
W+
W−
q1
k1
q2
q3
k2
q4
+
e+
e−
W+
W−
q1
k2
q2
q3
k1
q4

(a)

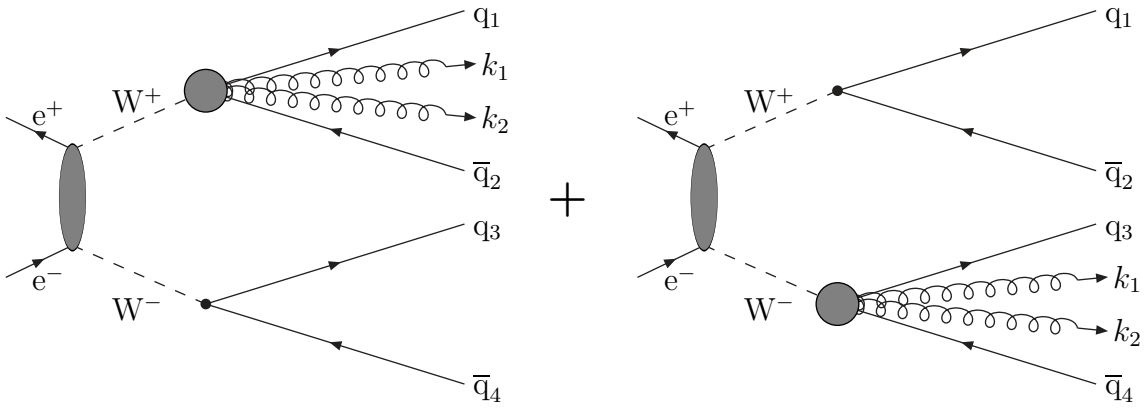
e+
e−
W+
W−
q1
k1
k2
q2
q3
q4
+
e+
e−
W+
W−
q1
q2
q3
k1
k2
q4

(b)

Fig. 6

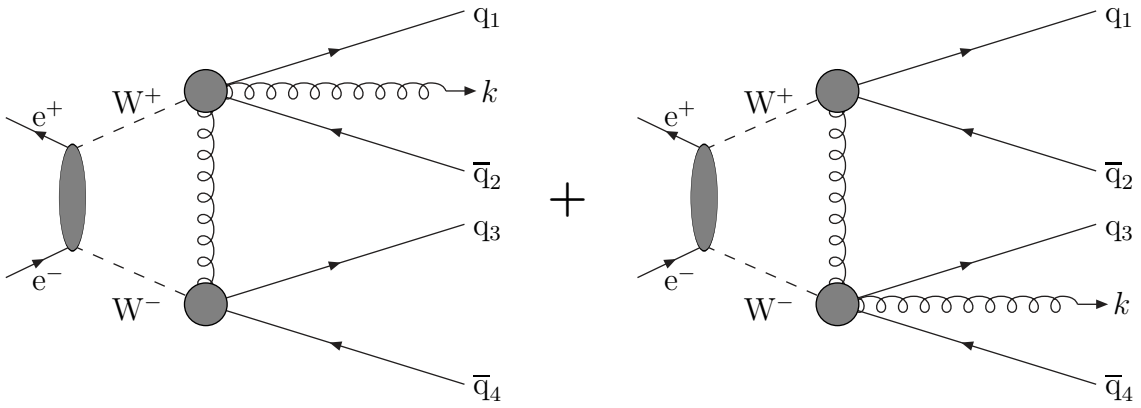

Fig. 7

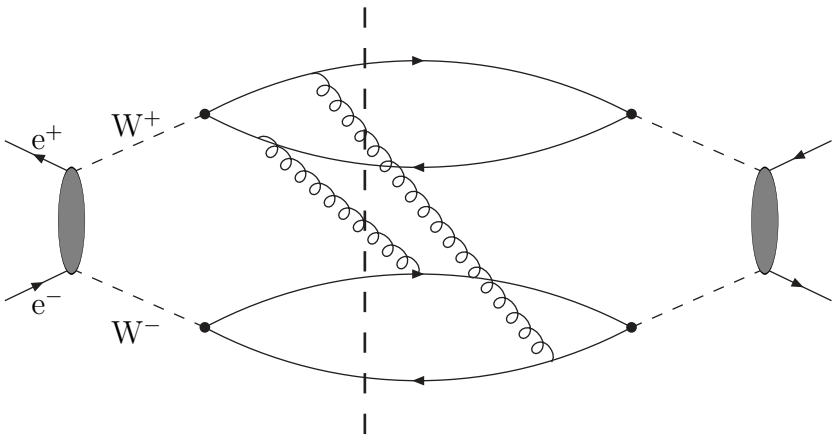

Fig. 8

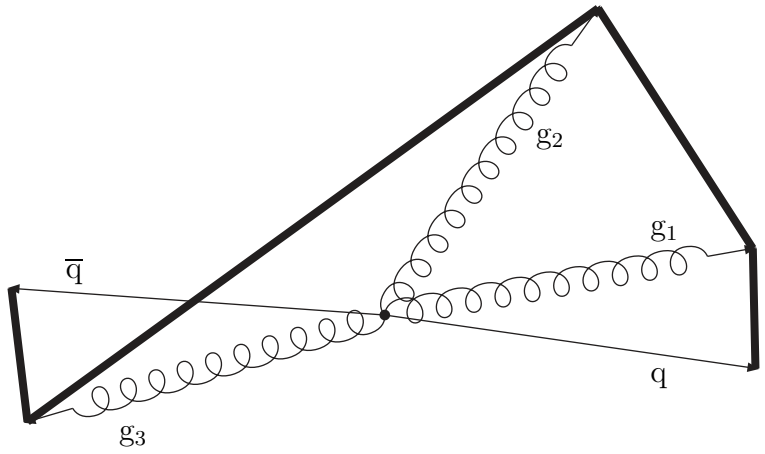

Fig. 9

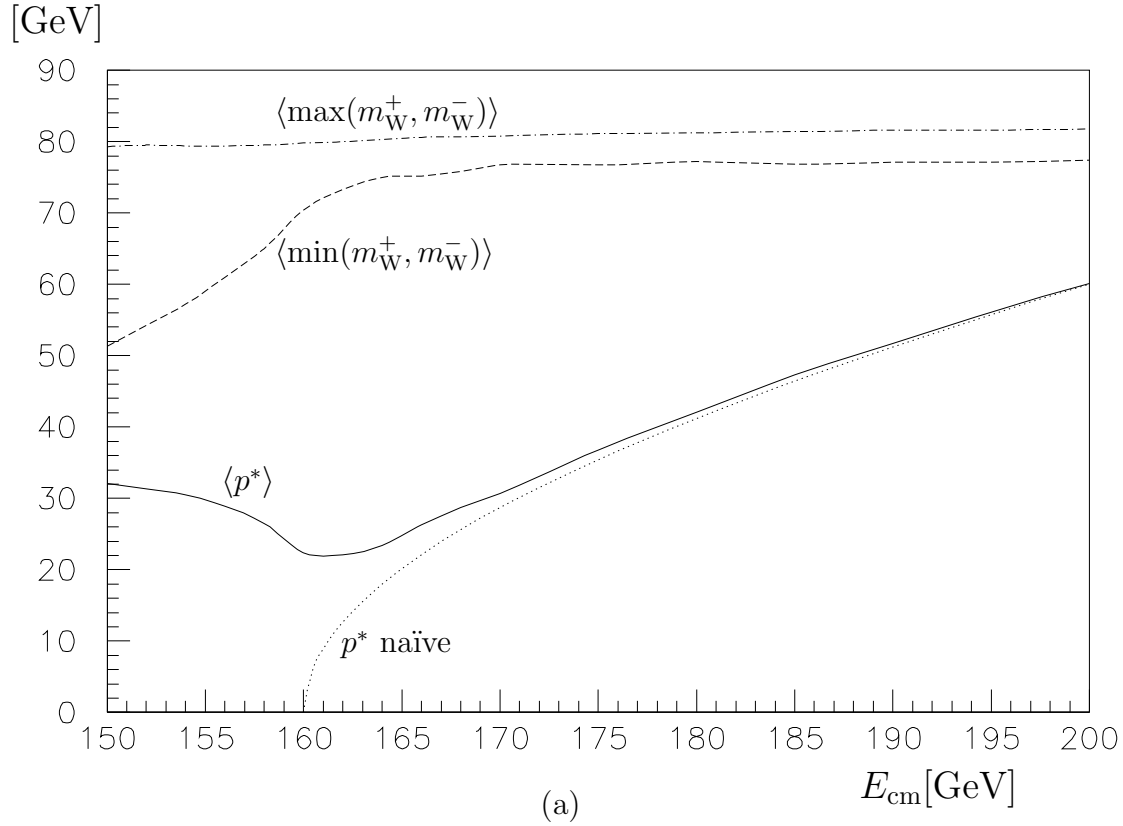
[GeV]
90
80
70
60
50
40
30
20
10
0
150
155
160
165
170
175
180
185
190
195
200
$\langle \max(m_{\mathrm{W}}^{+}, m_{\mathrm{W}}^{-}) \rangle$
$\langle \min(m_{\mathrm{W}}^{+}, m_{\mathrm{W}}^{-}) \rangle$
$\langle p^{*} \rangle$
p^{*} naïve
E_{cm}[GeV]

(a)

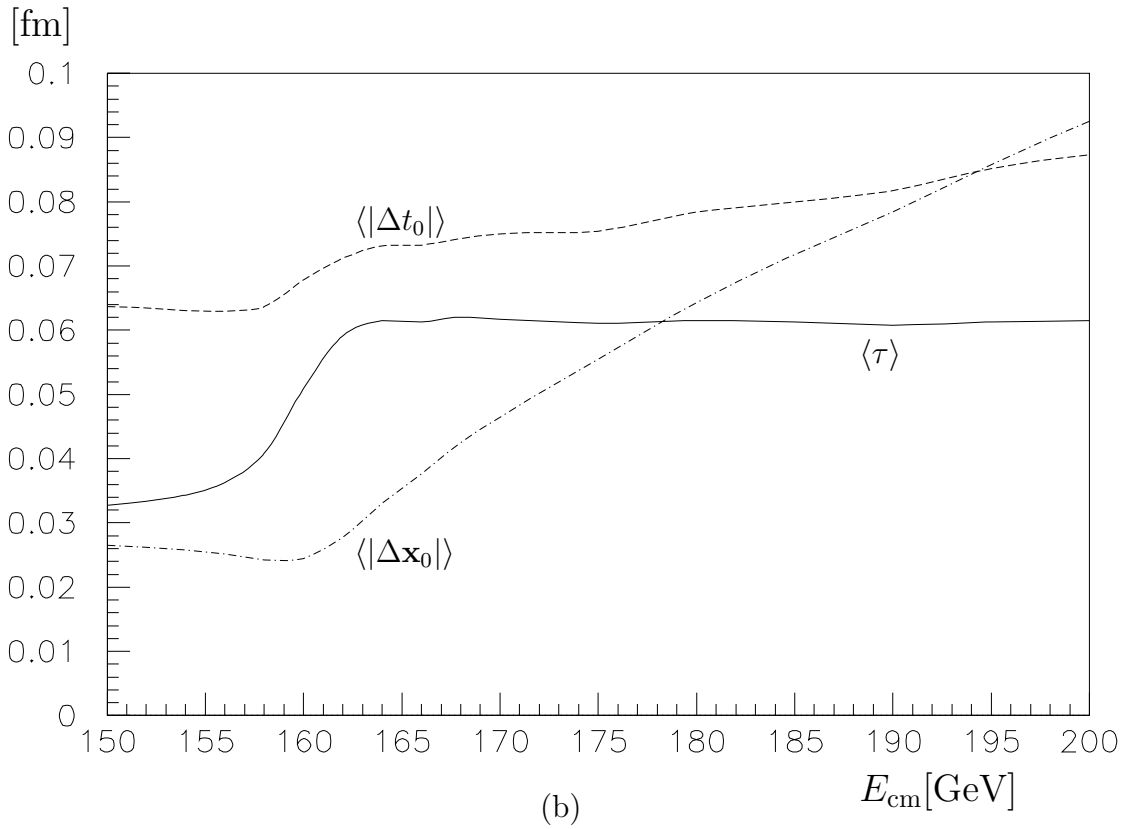
[fm]
0.1
0.09
0.08
0.07
0.06
0.05
0.04
0.03
0.02
0.01
0
150
155
160
165
170
175
180
185
190
195
200
$\langle |\Delta t_0| \rangle$
$\langle \tau \rangle$
$\langle |\Delta \mathbf{x}_0| \rangle$
E_{cm}[GeV]

(b)

Fig. 10

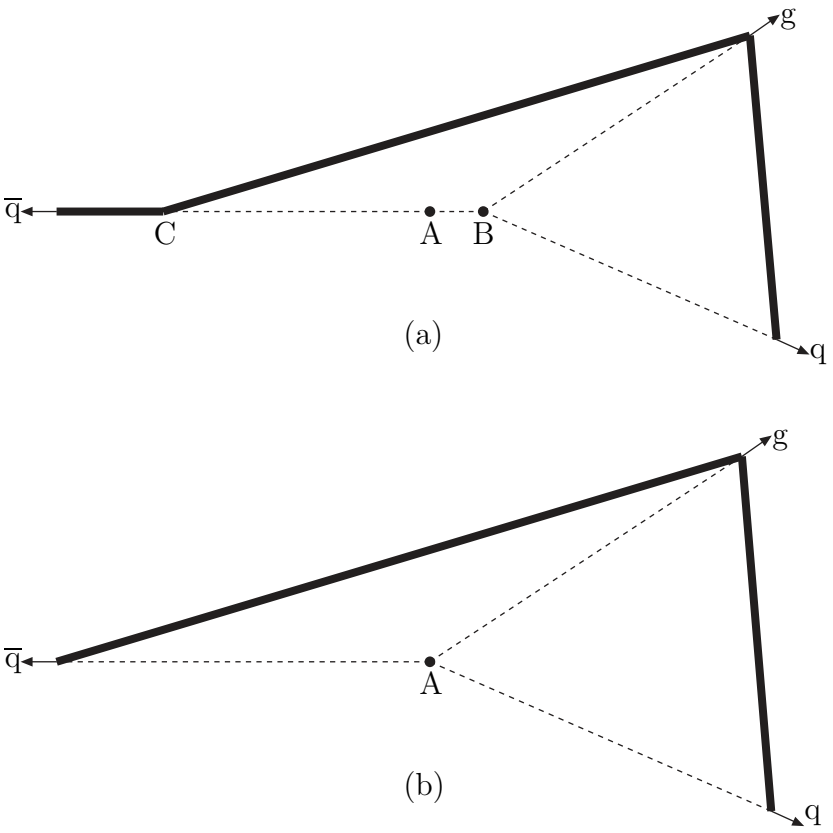

Fig. 11

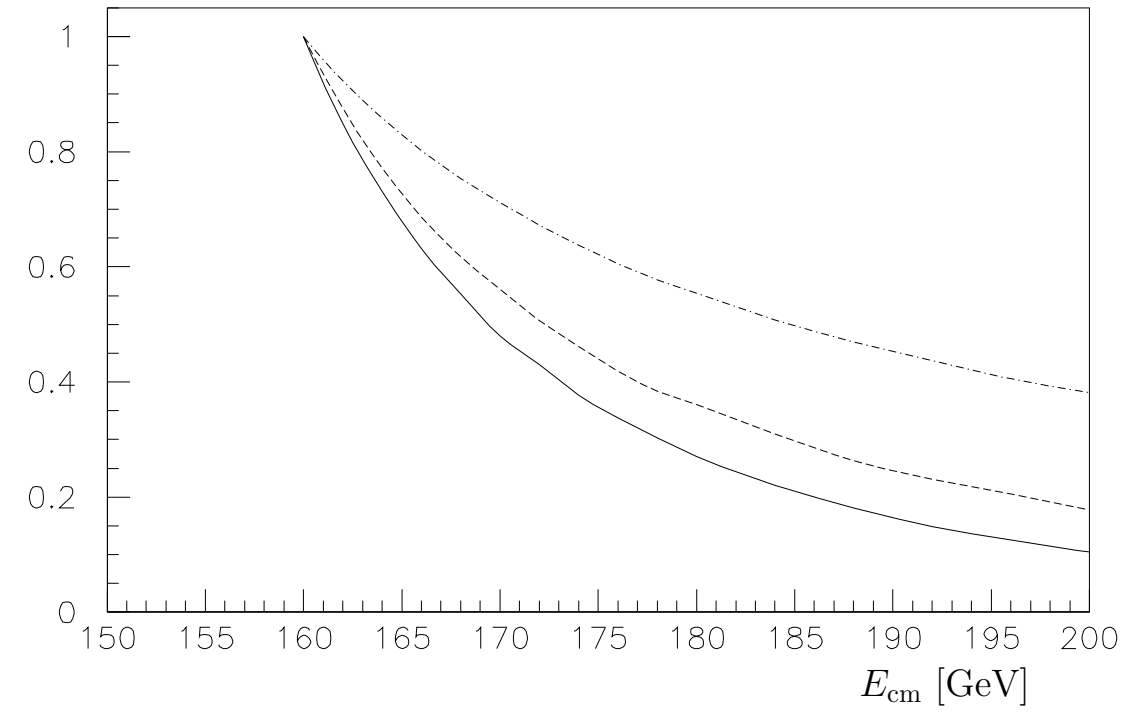
$\mathcal{I}(\beta)/\mathcal{I}(0)$
1
0.8
0.6
0.4
0.2
0
150
155
160
165
170
175
180
185
190
195
200
$E_{\rm cm}$ [GeV]

Fig. 12

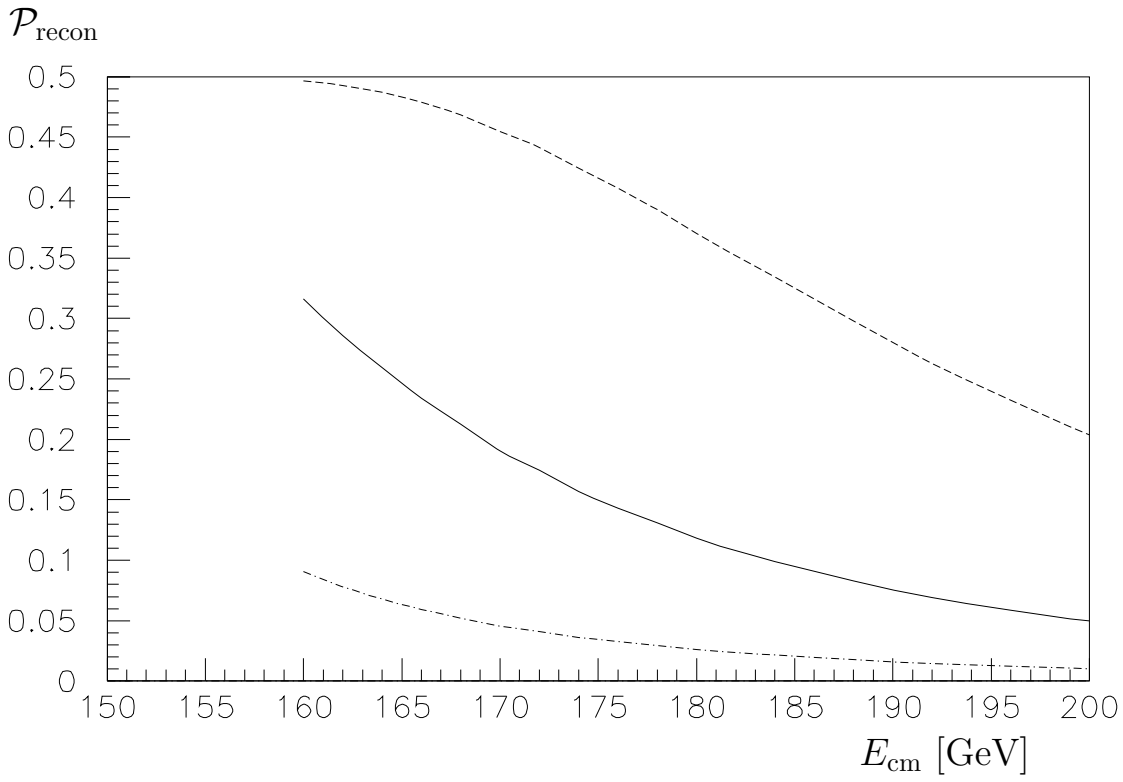
$\mathcal{P}_{\rm recon}$
0.5
0.45
0.4
0.35
0.3
0.25
0.2
0.15
0.1
0.05
0
150
155
160
165
170
175
180
185
190
195
200
$E_{\rm cm}$ [GeV]

Fig. 13

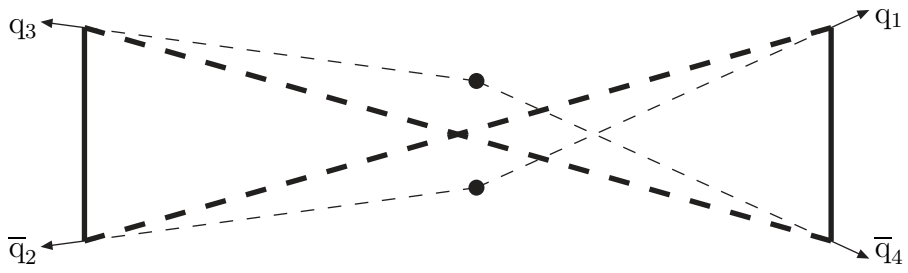
q_3
q_1
$\overline{q}_2$
$\overline{q}_4$

(a)

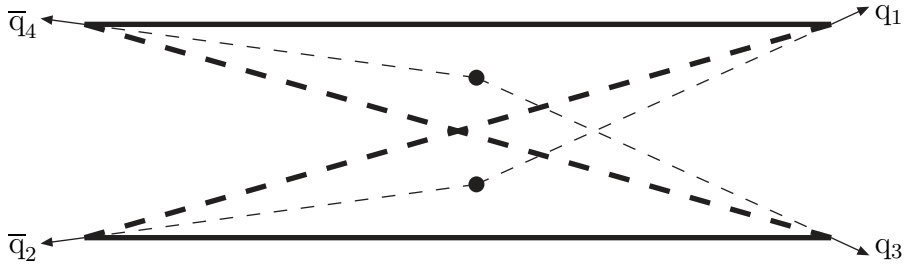
$\overline{q}_4$
q_1
$\overline{q}_2$
q_3

(b)

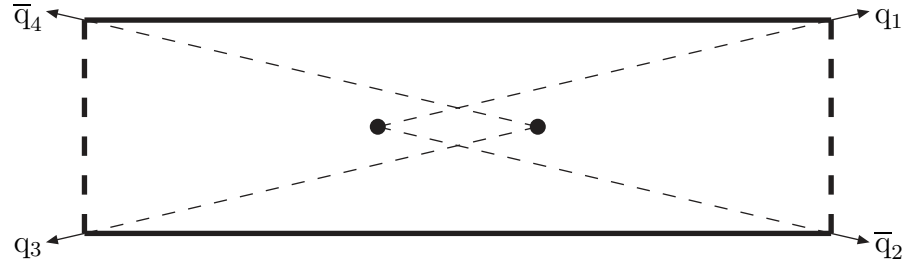
$\overline{q}_4$
q_1
q_3
$\overline{q}_2$

(c)

Fig. 14

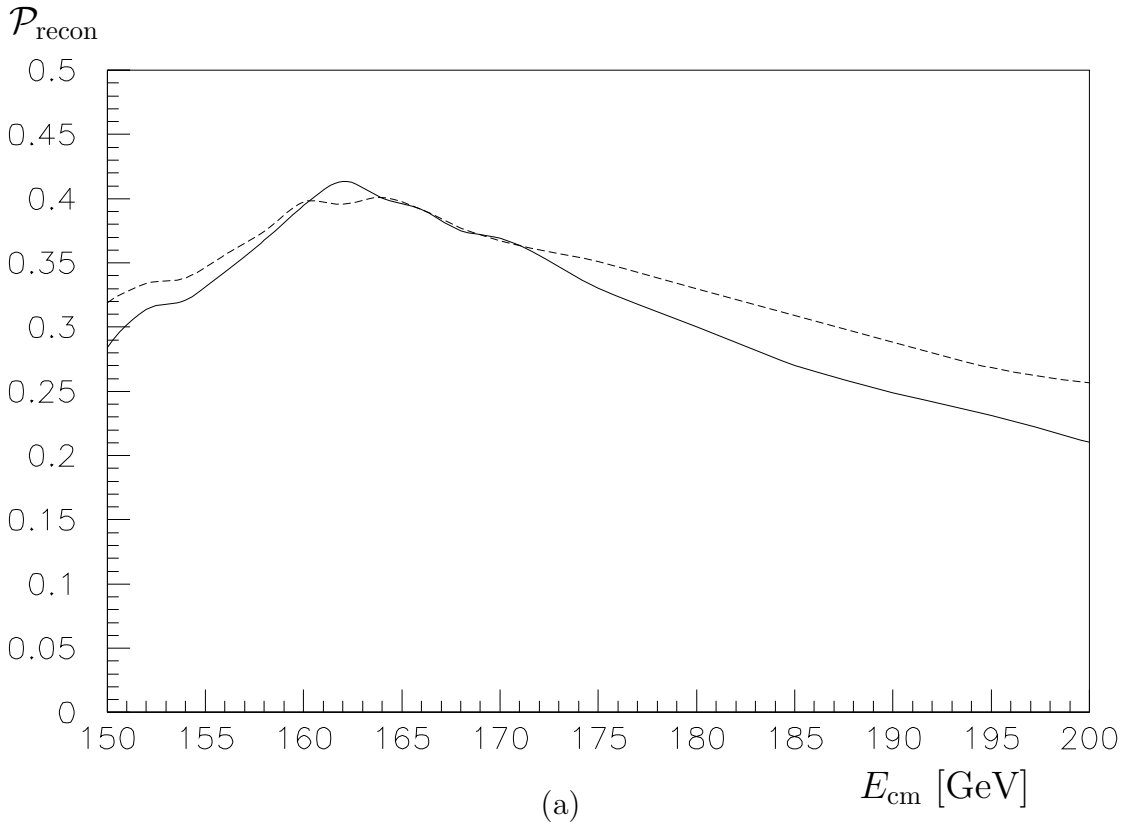
$\mathcal{P}_{\rm recon}$
0.5
0.45
0.4
0.35
0.3
0.25
0.2
0.15
0.1
0.05
0
150
155
160
165
170
175
180
185
190
195
200
$E_{\rm cm}$ [GeV]

(a)

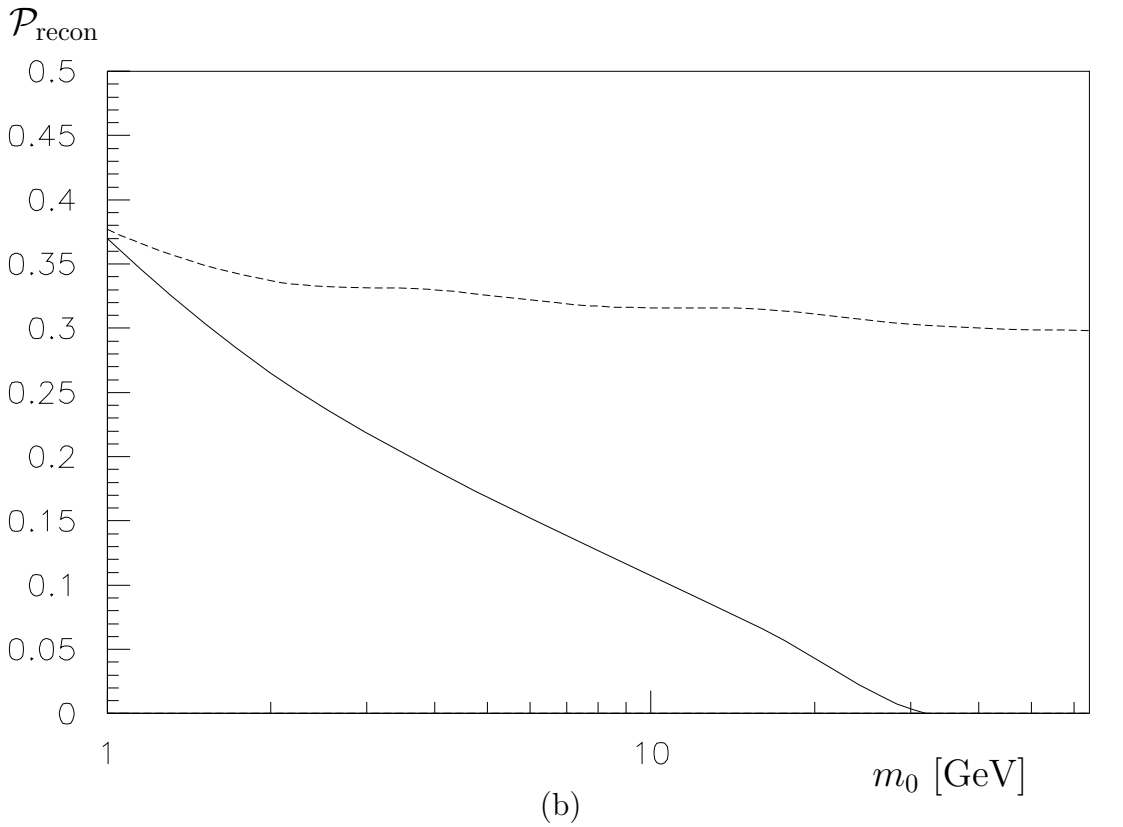
$\mathcal{P}_{\rm recon}$
0.5
0.45
0.4
0.35
0.3
0.25
0.2
0.15
0.1
0.05
0
1
10
m_0 [GeV]

(b)

Fig. 15

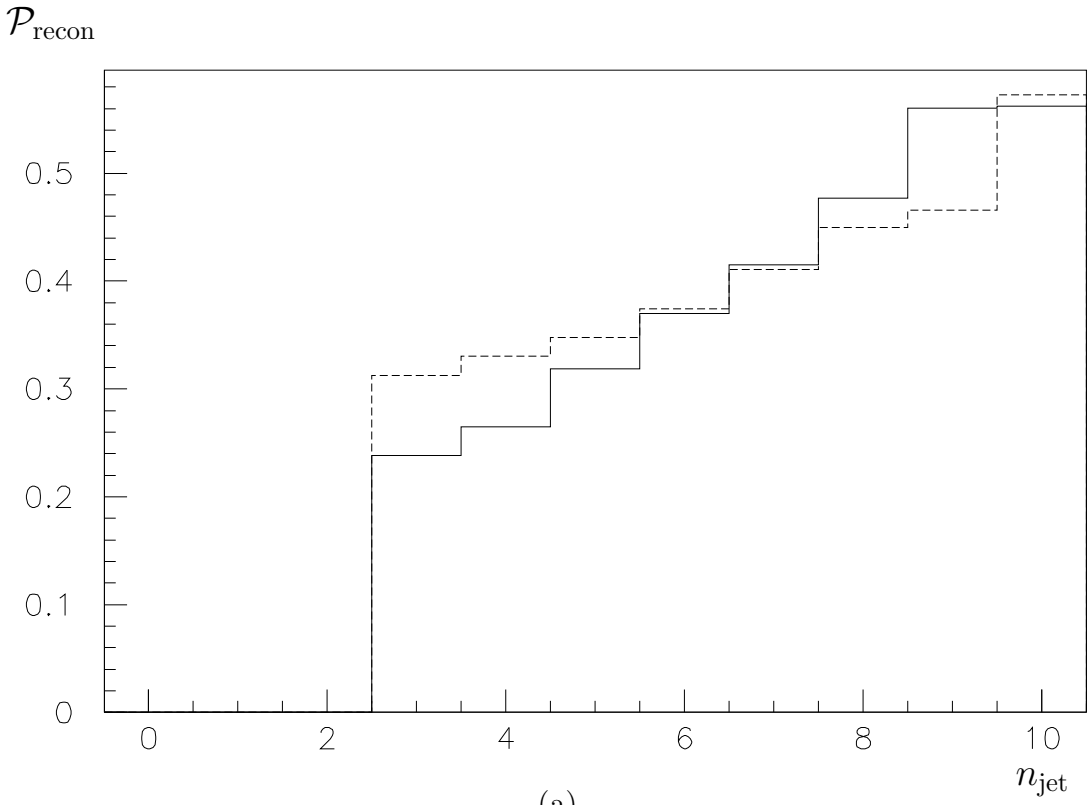
$\mathcal{P}_{\rm recon}$
0.5
0.4
0.3
0.2
0.1
0
0
2
4
6
8
10
$n_{\rm jet}$

(a)

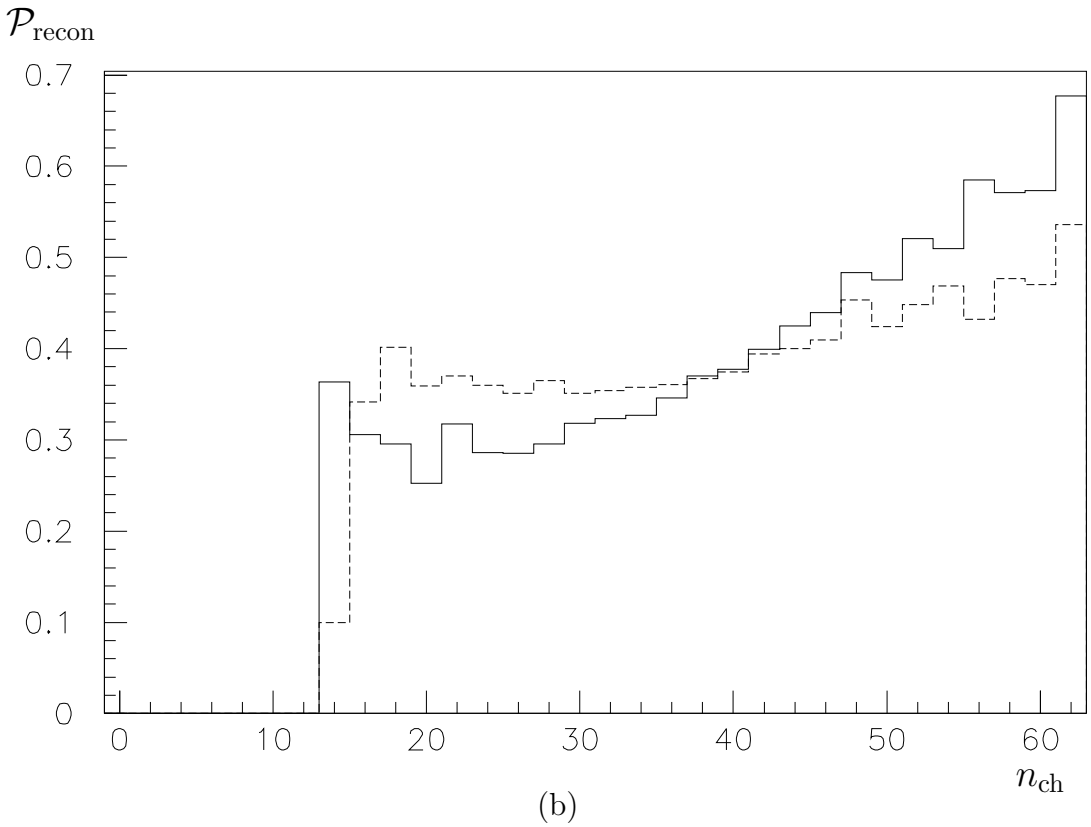
$\mathcal{P}_{\rm recon}$
0.7
0.6
0.5
0.4
0.3
0.2
0.1
0
0
10
20
30
40
50
60
$n_{\rm ch}$

(b)

Fig. 16

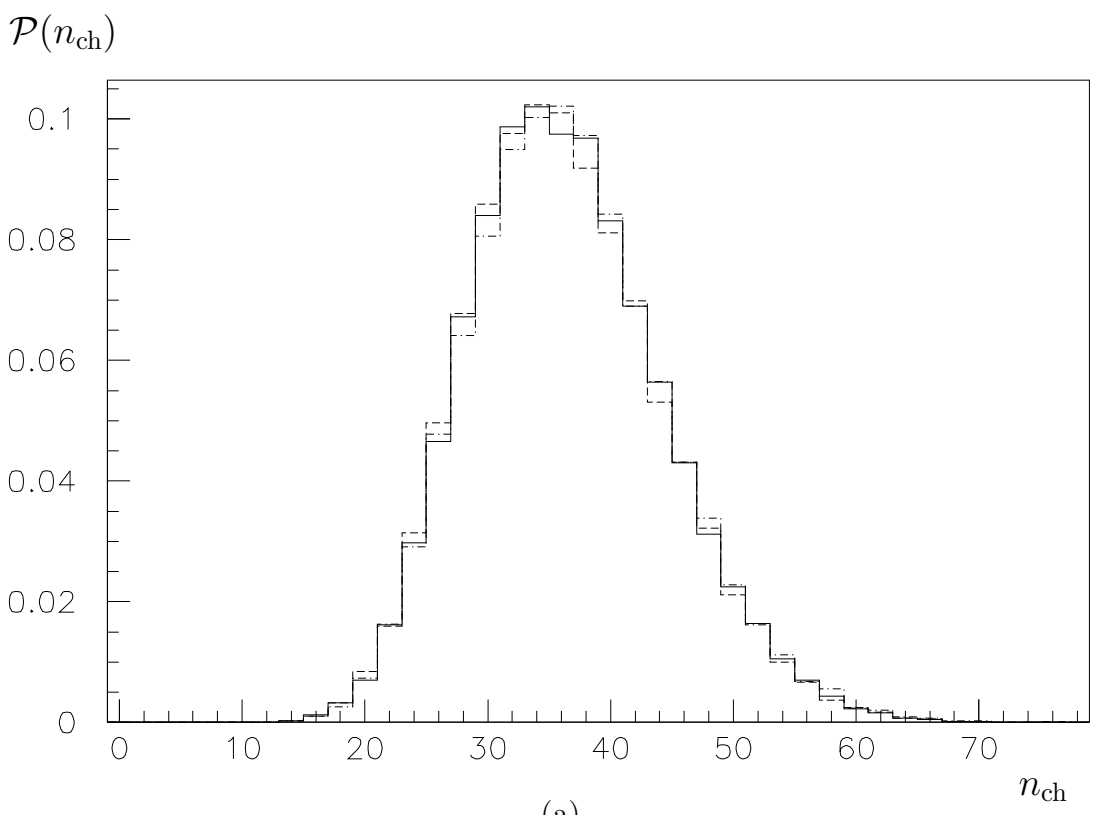
$\mathcal{P}(n_{\rm ch})$
0.1
0.08
0.06
0.04
0.02
0
0
10
20
30
40
50
60
70
$n_{\rm ch}$

(a)

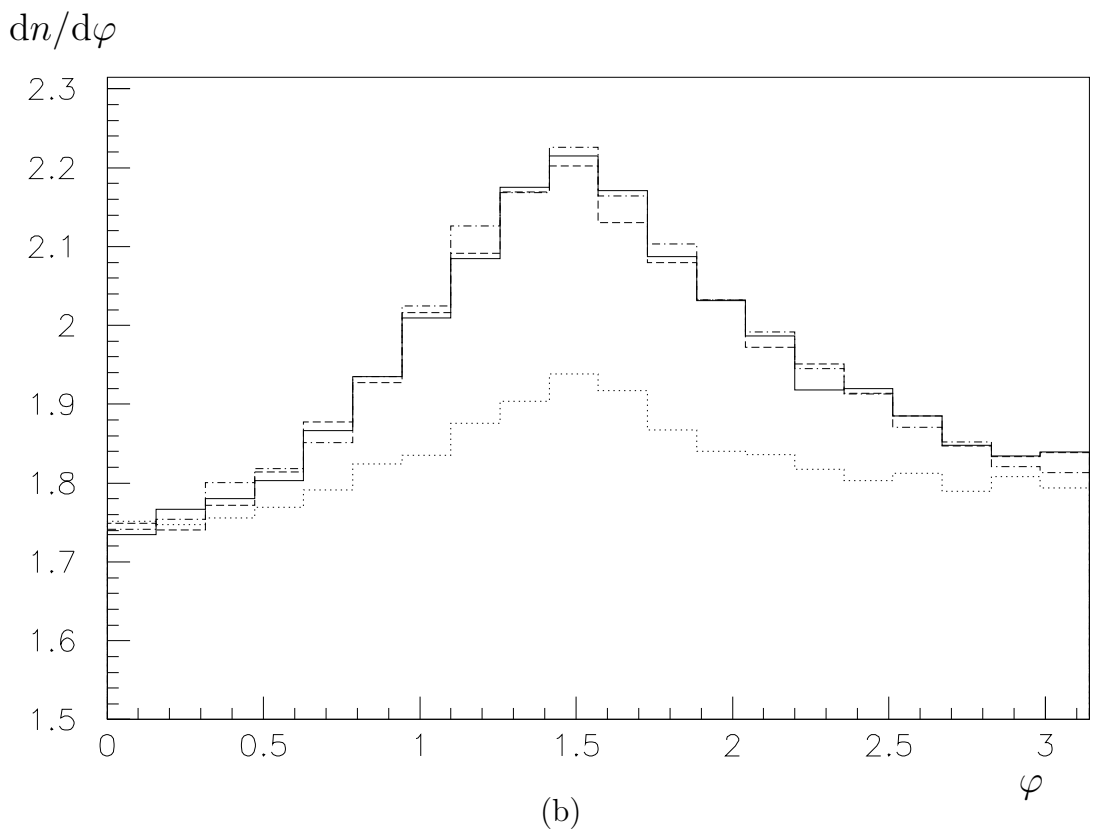
$\mathrm{d}n/\mathrm{d}\varphi$
2.3
2.2
2.1
2
1.9
1.8
1.7
1.6
1.5
0
0.5
1
1.5
2
2.5
3
φ

(b)

Fig. 17

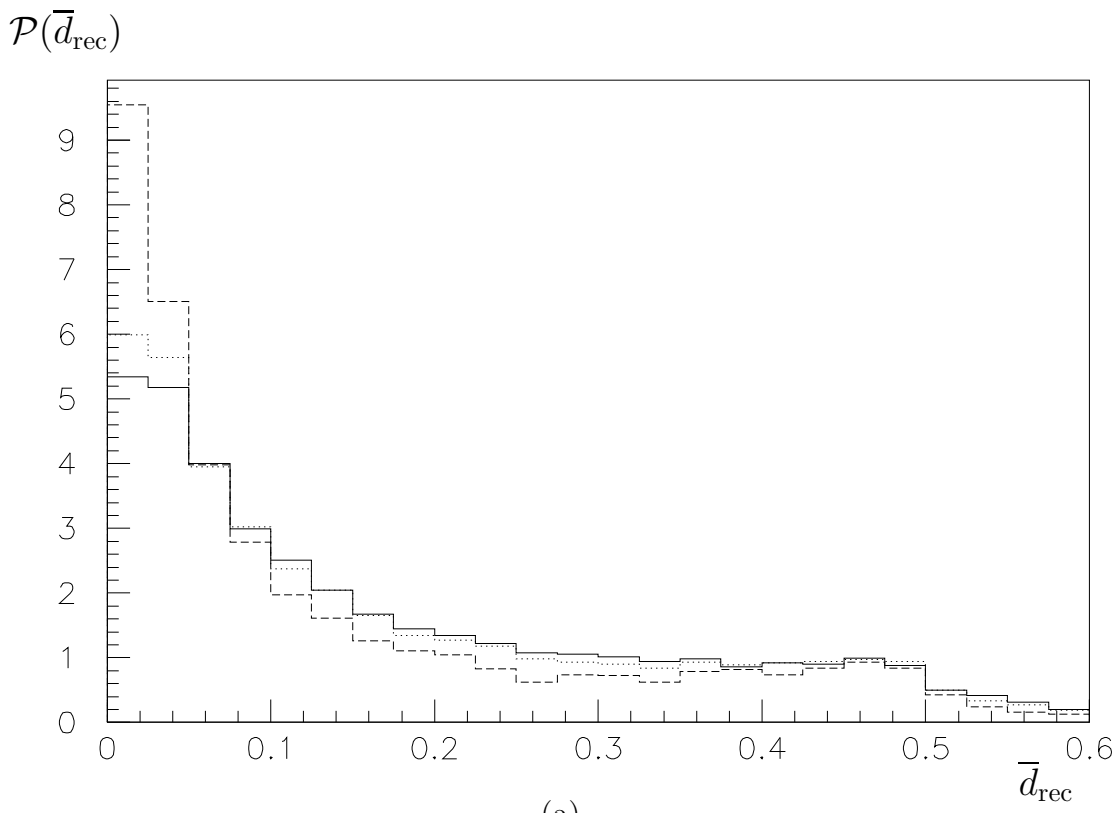
$\mathcal{P}(\overline{d}_{\rm rec})$
9
8
7
6
5
4
3
2
1
0
0
0.1
0.2
0.3
0.4
0.5
0.6
$\overline{d}_{\rm rec}$

(a)

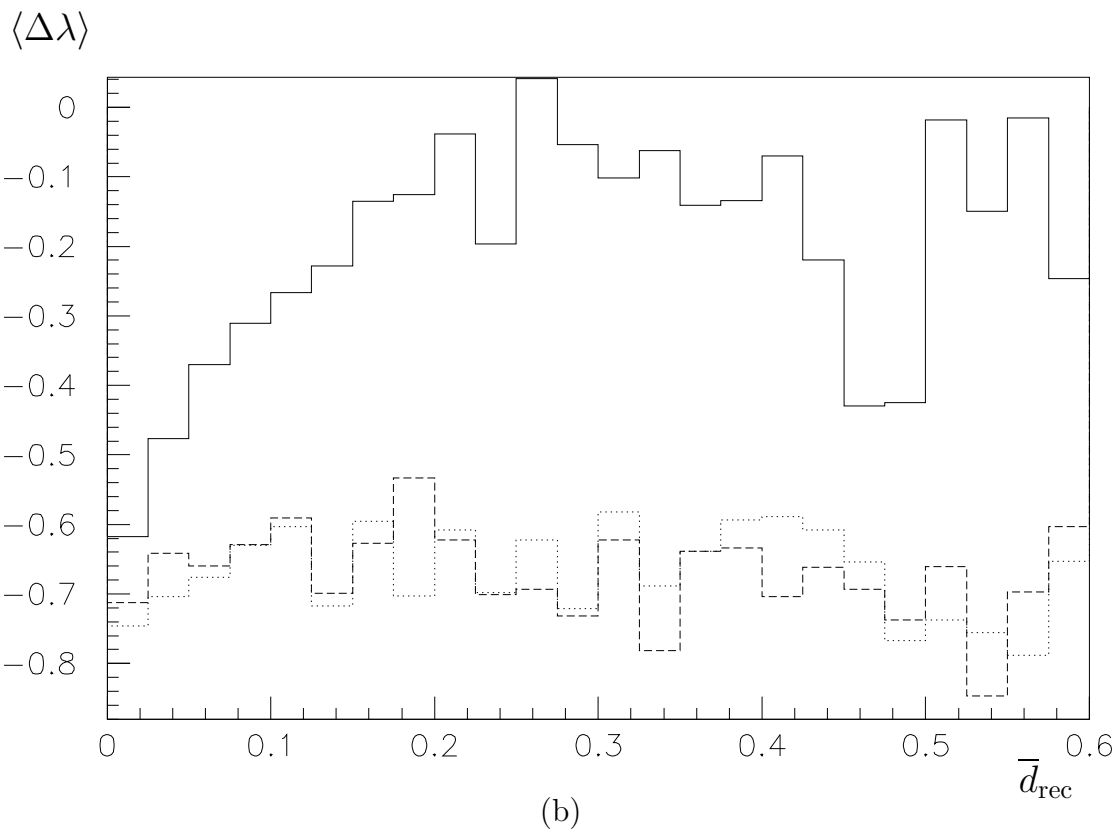
$\langle\Delta\lambda\rangle$
0
−0.1
−0.2
−0.3
−0.4
−0.5
−0.6
−0.7
−0.8
0
0.1
0.2
0.3
0.4
0.5
0.6
$\overline{d}_{\rm rec}$

(b)

Fig. 18

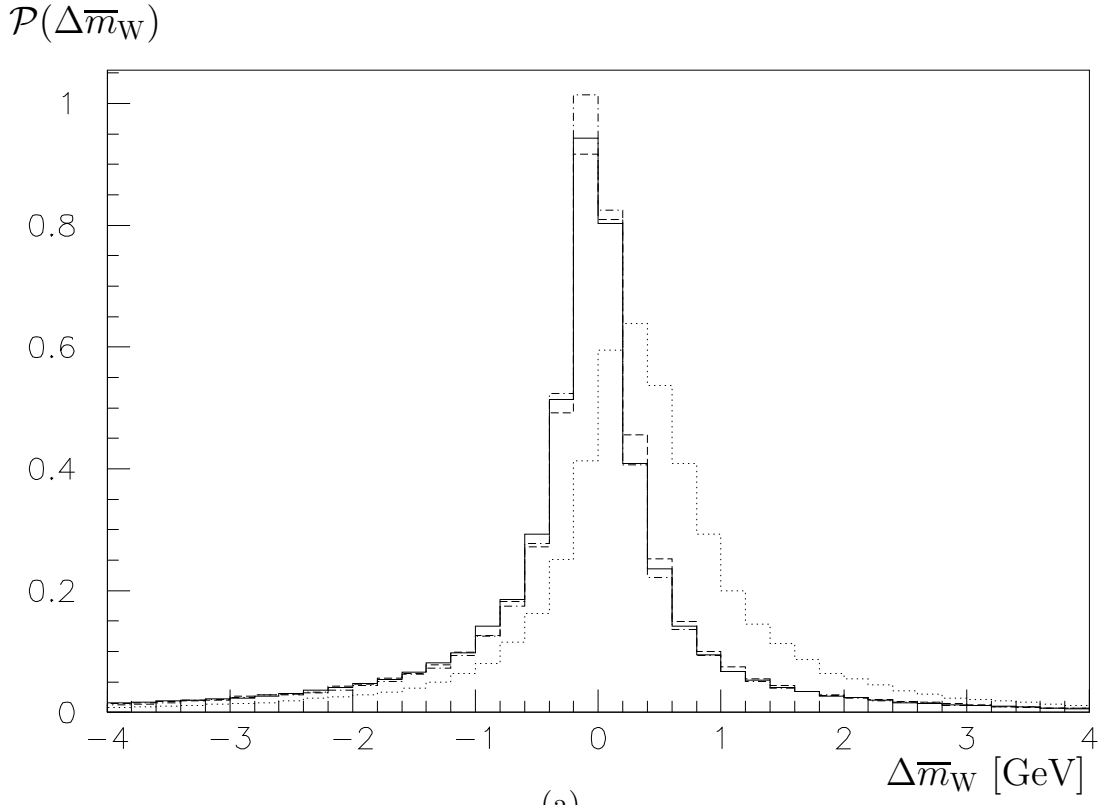
$\mathcal{P}(\Delta\overline{m}_{\mathrm{W}})$
1
0.8
0.6
0.4
0.2
0
−4
−3
−2
−1
0
1
2
3
4
$\Delta\overline{m}_{\mathrm{W}}$ [GeV]

(a)

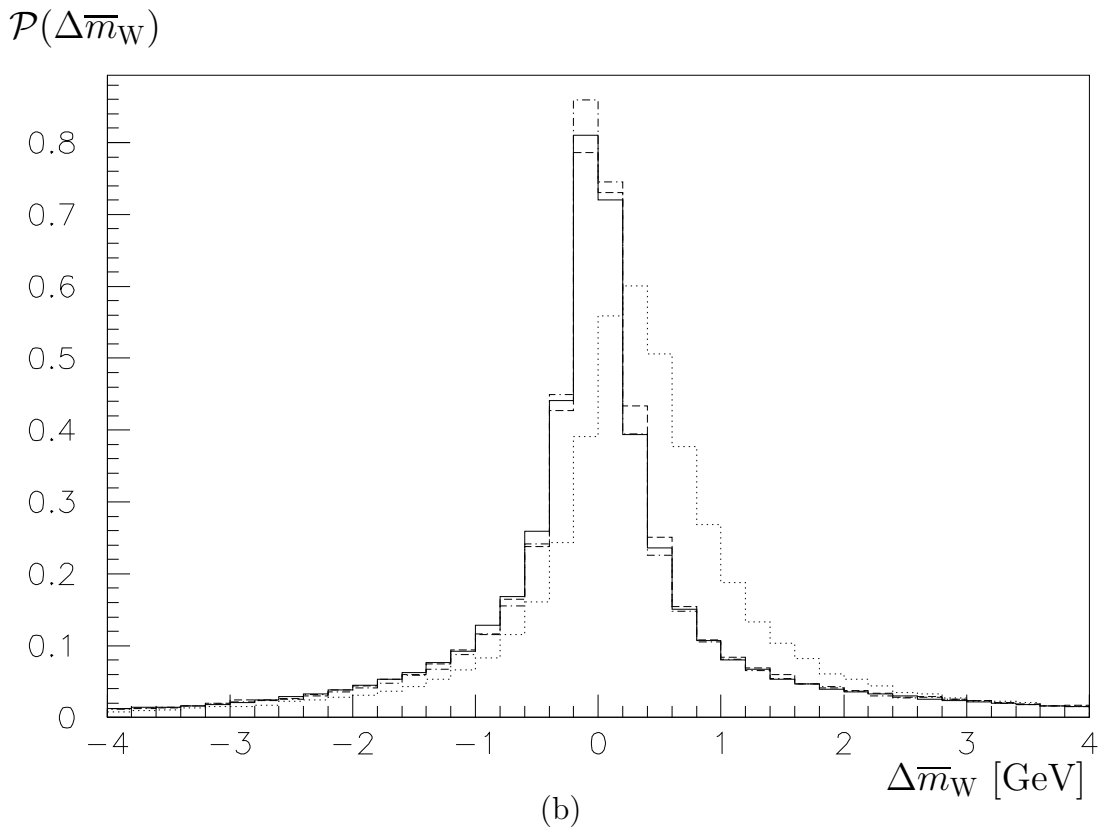
$\mathcal{P}(\Delta\overline{m}_{\mathrm{W}})$
0.8
0.7
0.6
0.5
0.4
0.3
0.2
0.1
0
−4
−3
−2
−1
0
1
2
3
4
$\Delta\overline{m}_{\mathrm{W}}$ [GeV]

(b)

Fig. 19

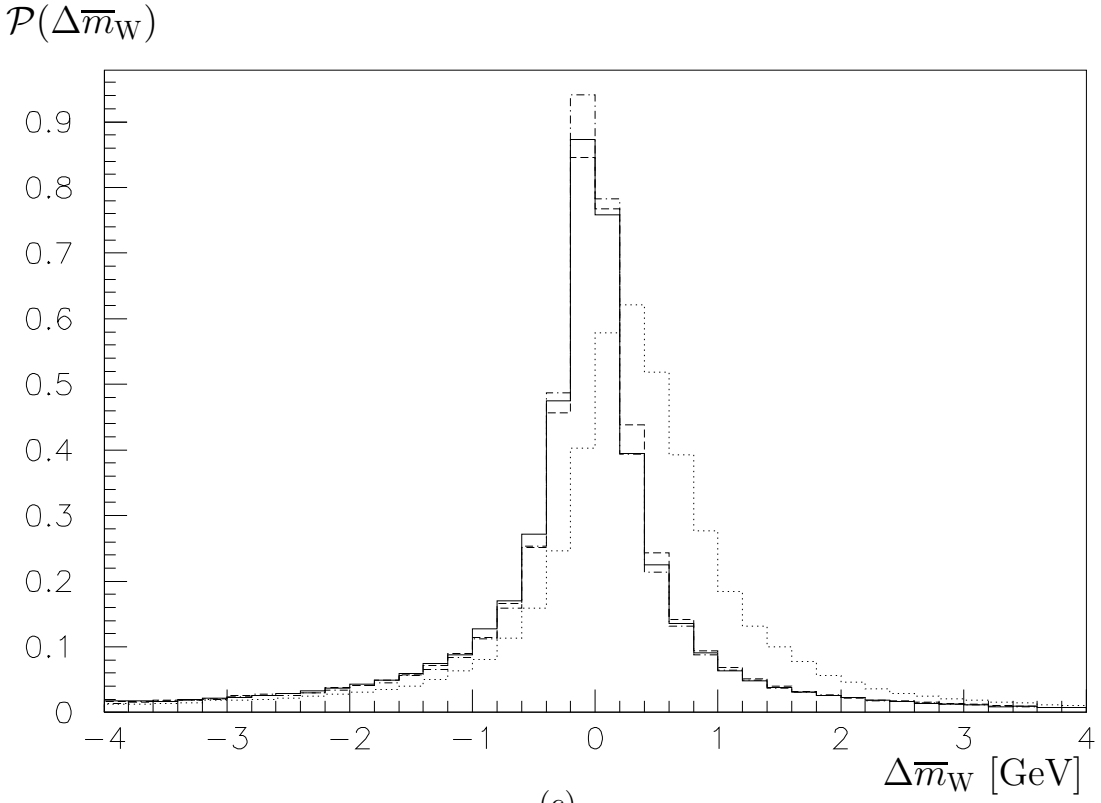
$\mathcal{P}(\Delta\overline{m}_{\mathrm{W}})$
0.9
0.8
0.7
0.6
0.5
0.4
0.3
0.2
0.1
0
−4
−3
−2
−1
0
1
2
3
4
$\Delta\overline{m}_{\mathrm{W}}$ [GeV]

(c)

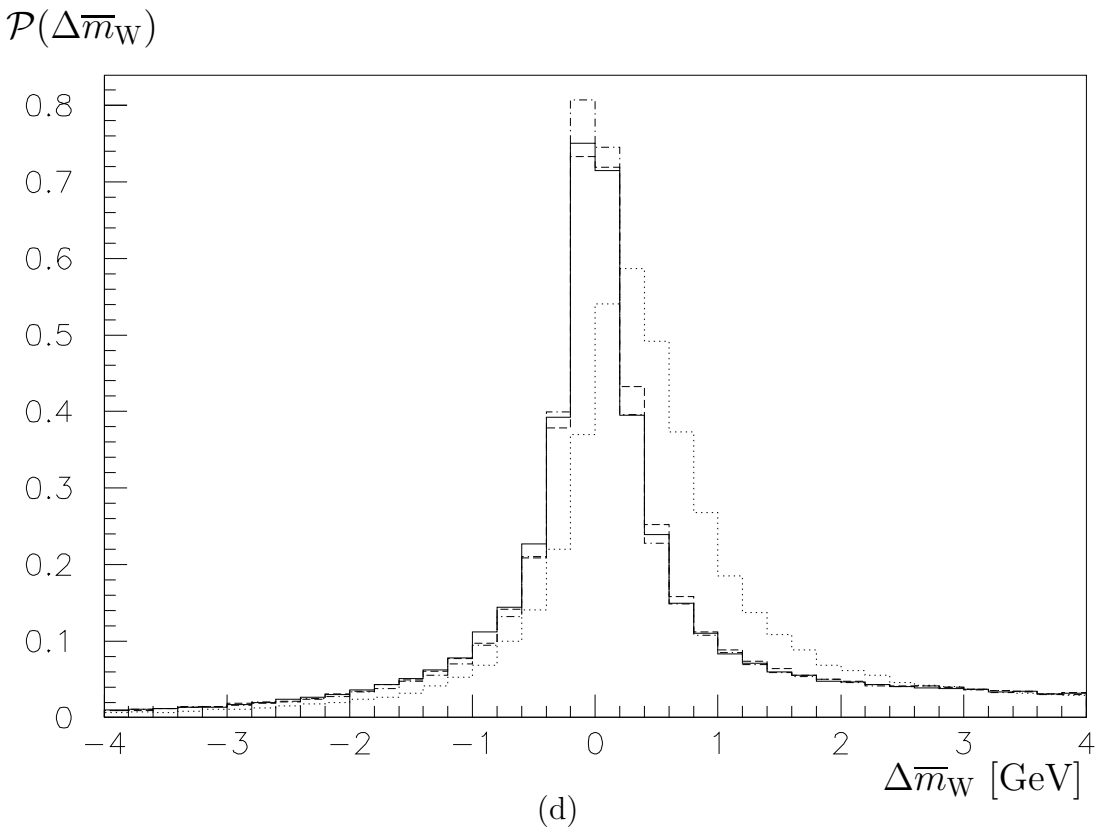
$\mathcal{P}(\Delta\overline{m}_{\mathrm{W}})$
0.8
0.7
0.6
0.5
0.4
0.3
0.2
0.1
0
−4
−3
−2
−1
0
1
2
3
4
$\Delta\overline{m}_{\mathrm{W}}$ [GeV]

(d)

Fig. 19